Density Matrix Analysis and Simulation of Electronic Excitations in Conjugated and Aggregated Molecules

Sergei Tretiak*

Theoretical Division, Los Alamos National Laboratory, Los Alamos, New Mexico 87545

Shaul Mukamel*

Department of Chemistry and Department of Physics & Astronomy, University of Rochester, P. O. RC Box 270216, Rochester, New York 14627-0216

Received May 23, 2001

Contents

I. Introduction

Predicting the electronic structure of extended organic molecules constitutes an important fundamental task of modern chemistry. Studies of electronic excitations, charge-transfer, energy-transfer, and isomerization of conjugated systems form the basis for our understanding of the photophysics and photochemistry of complex molecules[1−3] as well as organic nanostructures and supramolecular assemblies.[4,5] Photosynthesis and other photochemical biological processes that constitute the basis of life on Earth involve assemblies of conjugated chromophores such as porphyrins, chlorophylls, and carotenoids.[6−8] Apart from the fundamental interest, these studies are also closely connected to numerous important technological applications.[9] Conjugated polymers are primary candidates for new organic optical materials with large nonlinear polarizabilities.[10−19] Potential applications include electroluminescence, light emitting diodes, ultrafast switches, photodetectors, biosensors, and optical limiting materials.[20−27]

Optical spectroscopy which allows chemists and physicists to probe the dynamics of vibrations and electronic excitations of molecules and solids is a powerful tool for the study of molecular electronic structure. The theoretical techniques used for describing spectra of isolated small molecules are usually quite different from those of molecular crystals, and many intermediate size systems, such as clusters and polymers, are not readily described by the methods developed for either of these limiting cases.[28]

* Corresponding author. E-mail: serg@lanl.gov (S.T.); mukamel@chem.rochester.edu (S.M.).

10.1021/cr0101252 CCC: $39.75
Published on Web 08/24/2002

Sergei Tretiak is currently a Technical Staff Member at Los Alamos National Laboratory (LANL). He received his M.Sc. (highest honors, 1994) from Moscow Institute of Physics and Technology (Russia) and his Ph.D. in 1998 from the University of Rochester where he worked with Prof. Shaul Mukamel. He was then a LANL Director-funded Postdoctoral Fellow in T-11/CNLS. His research interests include development of modern computational methods for molecular optical properties and establishing structure/optical response relations in electronic materials, such as donor–acceptor oligomers, photoluminescent polymers, porphyrins, semiconductor nanoparticles, etc., promising for device applications. He is also developing effective exciton Hamiltonian models for treating charge and energy transfer phenomena in molecular superstructures such as biological antenna complexes, dendrimer nanostructures, and semiconductor quantum dots assemblies.

Shaul Mukamel, who is currently the C. E. Kenneth Mees Professor of Chemistry at the University of Rochester, received his Ph.D. in 1976 from Tel Aviv University, followed by postdoctoral appointments at MIT and the University of California at Berkeley and faculty positions at the Weizmann Institute and at Rice University. He has been the recipient of the Sloan, Dreyfus, Guggenheim, and Alexander von Humboldt Senior Scientist awards. His research interests in theoretical chemical physics and biophysics include: developing a density matrix Liouville-space approach to femtosecond spectroscopy and to many body theory of electronic and vibrational excitations of molecules and semiconductors; multidimensional coherent spectroscopies of structure and folding dynamics of proteins; nonlinear X-ray and single molecule spectroscopy; electron transfer and energy funneling in photosynthetic complexes and Dendrimers. He is the author of over 400 publications in scientific journals and of the textbook, *Principles of Nonlinear Optical Spectroscopy* (Oxford University Press), 1995.

Solving the many-electron problem required for the prediction and interpretation of spectroscopic signals involves an extensive numerical effort that grows very fast with molecular size. Two broad classes of techniques are generally employed in the calculation of molecular response functions. Off-resonant optical polarizabilities can be calculated most readily by a variational/perturbative treatment of the ground state in the presence of a static electric field by expanding the Stark energy in powers of electric field. The coupled perturbed Hartree−Fock (CPHF) procedure computes the polarizabilities by evaluating energy derivatives of the molecular Hamiltonian. It usually involves expensive ab initio calculations with basis sets including diffuse and polarized functions, that are substantially larger than those necessary for computing ground-state properties.[14]

The second approach starts with exact expressions for optical response functions derived using time-dependent perturbation theory, which relate the optical response to the properties of the excited states. It applies to resonant as well as off-resonant response. Its implementation involves calculations of both the ground state and excited-state wave functions and the transition dipole moments between them.[29,30] The configuration-interaction/sum-over-states (CI/SOS) method[15,31] is an example for this class of methods. Despite the straightforward implementation of the procedure and the interpretation of the results in terms of quantum states (which is common in quantum chemistry), special care needs to be taken when choosing the right configurations. In addition, this method is not size-consistent,[32,33] and intrinsic interference effects resulting in a near cancellation of very large contributions further limit its accuracy and complicate the analysis of the size-scaling of the optical response. The SOS approach has been widely applied using semiempirical Hamiltonians (e.g., simple tight-binding or Hückel, π-electron Pariser−Parr−Pople (PPP), valence effective Hamiltonians (VEH), complete neglect of differential overlap (CNDO), and intermediate neglect of differential Overlap (INDO) models).[14,15,34−39] The global eigenstates carry too much information on many-electron correlations, making it hard to use them effectively for the interpretation of optical response and the prediction of various trends.

A completely different viewpoint is adopted in calculations of infinite periodic structures (molecular crystals, semiconductors, large polymers). Band structure approaches that focus on the dynamics of electron−hole pairs are then used.[40−44] Band theories may not describe molecular systems with significant disorder and deviations from periodicity, and because they are formulated in momentum (k) space they do not lend themselves very easily to real-space chemical intuition. The connection between the molecular and the band structure pictures is an important theoretical challenge.[45]

To formulate a unified formulation that bridges the gap between the chemical and semiconductor points of view, we must retain only reduced information about the many-electronic system necessary to calculate the optical response. Certainly, the complete information on the optical response of a quantum system is contained in its set of many-electron eigenstates $|\nu\rangle$, $|\eta\rangle$, ... and energies ϵ_ν, ϵ_η, ...[29] Using the many-electron wave functions, it is possible to calculate all n-body quantities and correlations. Most of this information is, however, rarely used in the calculation of common observables (energies, dipole moments, spectra, etc.) which only depend on the

expectation values of a few (typically one- and two-) electron quantities. In addition, since even in practical computations with a finite basis set, the number of molecular many-electron states increases exponentially with the number of electrons, exact calculations become prohibitively expensive even for fairly small molecules with a few atoms. A reduced description that only keeps a small amount of relevant information is called for. A remarkably successful example of such a method is density-functional theory (DFT),[46−51] which only retains the ground-state charge density profile. The charge density of the nth orbital is

$$\bar{\rho}_{nn} = \langle g|c_n^\dagger c_n|g\rangle \tag{1.1}$$

where $|g\rangle$ denotes the ground-state many-electron wave function and $c_n^\dagger$ (c_n) are the Fermi annihilation (creation) operators for the nth basis set orbital, when the overlap between basis set functions is neglected, the molecular charge density depends on ρ_{nn}. Hohenberg and Kohn's theorem proves that the ground-state energy is a unique and a universal functional of the charge density,[52,53] making it possible in principle to compute self-consistently the charge distribution and the ground-state energy.

The single-electron density matrix[54−60] given by

$$\rho_{nm}^{\nu\eta} \equiv \langle \nu|c_n^\dagger c_m|\eta\rangle \tag{1.2}$$

is a natural generalization of the ground-state charge density (eq 1.1). Here $|\nu\rangle$ and $|\eta\rangle$ represent global electronic states, whereas n and m denote the atomic basis functions. $\rho^{\nu\nu}$ is the *reduced single-electron density matrix* of state ν. For $\nu \neq \eta$ $\rho^{\nu\eta}$ is the density-matrix associated with the transition between ν and η. These quantities carry much more information than $\bar{\rho}_{nn} \equiv \rho_{nn}^{gg}$ (For brevity, the ground-state density matrix ρ^{gg} will be donoted $\bar{\rho}$ throughout this review), yet considerably less than the complete set of eigenstates.[51,61−66]

Density functional theory has been extended to include current (in addition to charge) density.[67] The current density can be readily obtained from the near diagonal elements of the density matrix in real space. The current is thus related to short range coherence, whereas the density matrix includes short as well as long range coherence. The single electron density matrix is the lowest order in a systematic hierarchy. Higher order density matrices (2 electron, etc.) have been used as well in quantum chemistry. They retain successively higher levels of information.[68−73] Green function techniques provide an alternative type of reduced description.[74,75]

The wave function of a the system driven by an optical field is a coherent superposition of states

$$\Psi(t) = \sum_\nu a_\nu(t)|\nu\rangle \tag{1.3}$$

and its density matrix is given by

$$\rho_{\mathrm{nm}}(t) \equiv \langle \Psi(t)|c_n^\dagger c_m|\Psi(t)\rangle = \sum_{\nu\eta} a_\nu^*(t)a_\eta(t)\rho_{nm}^{\nu\eta} \tag{1.4}$$

$\rho_{nm}^{\nu\eta}$ are thus the building blocks for the time-dependent single-electron density matrix $\rho_{mn}(t)$.

The greatly reduced information about the global eigenstates contained in the matrices $\rho^{\nu\eta}$ is sufficient to compute the optical response. To illustrate this, let us consider the frequency-dependent linear polarizability $\alpha(\omega)$ (see Appendix F3).

$$\alpha(\omega) = \sum_\nu \frac{2\Omega_\nu \mu_{g\nu}\mu_{g\nu}^*}{\Omega_\nu^2 - (\omega + i\Gamma)^2} \tag{1.5}$$

where $\mu_{g\nu} \equiv \langle g|\mu|\nu\rangle$ are the transition dipoles, and $\Omega_\nu \equiv \epsilon_\nu - \epsilon_g$ are the transition frequencies. Γ is a phemenological dephasing rate which accounts for both homogeneous (e.g., an interaction with bath) and inhomogeneous (e.g., static distribution of molecular transition frequencies) mechanisms of line broadening (for a review see ref 76).

The molecular dipole μ is a single-electron operator that may be expanded in the form

$$\mu = \sum_{nm} \mu_{mn} c_n^\dagger c_m \tag{1.6}$$

We therefore have

$$\mu_{g\nu} = \sum_{nm} \mu_{mn}\rho_{nm}^{g\nu} \tag{1.7}$$

The matrices $\rho^{g\nu}$ and the corresponding frequencies Ω_ν thus contain all necessary information for calculating the linear optical response. Complete expressions for higher order polarizabilities up to third order and other spectroscopic observables are given in Appendix F.

Equation 1.2 apparently implies that one first needs to calculate the eigenstates $|\nu\rangle$ and $|g\rangle$ and then use them to compute the matrix elements $\rho^{g\nu}$. If that was the case, no computational saving is obtained by using the density matrix. However, its great power is derived from the ability to compute the electronic response directly, totally avoiding the explicit calculation of excited states: the time-dependent variational principle (TDVP)[64,65,77,78] and time-dependent density-functional theory (TDDFT)[49,50,79,80] in the Kohn−Sham (KS) form[52,53] are two widely used approaches of this type. In either case, one follows the dynamics of a certain reduced set of parameters representing the system driven by an external field. In the TDVP, these parameters describe a trial many-electron wave function, whereas in TDDFT they represent a set of KS orbitals. The time-dependent Hartree−Fock (TDHF) equations are based on the TDVP where the trial wave function is assumed to belong to the space of single Slater determinants.[77,81]

Both TDHF and the TDDFT follow the dynamics of a similar quantity: a single Slater determinant that can be uniquely described by an idempotent single-electron density matrix ρ (with $\rho^2 = \rho$).[62,63,77,78] However, they yield different equations of motion for $\rho(t)$, stemming from the different interpretation of $\rho(t)$. In the TDHF, $\rho(t)$ is viewed as an approximation for the actual single-electron density matrix,[77] whereas in TDDFT $\rho(t)$ is an auxiliary quantity constrained

to merely reproduce the correct electronic charge distribution at all times.[52,53] TDDFT is formally exact. However, in practice it yields approximate results since exact expressions for the exchange-correlation energy $E_{xc}[n(\mathbf{r})]$ and the corresponding potential $v_{xc}(\mathbf{r}, [n])$ in the KS scheme are not available and are introduced semiempirically. A close resemblance between TDHF and TDDFT (especially its adiabatic version) may be established by formulating KS density functional theory (DFT) in terms of the density matrix ρ rather than on the KS orbitals.[78] This formal similarity makes it possible to apply the same algorithms for solving the equations for the matrices $\rho^{g\nu} \equiv \xi_\nu$ (Abbreviated notation ξ_ν for the family of single-electron density matrices $\rho^{g\nu}$ will be used throughout this review) and frequencies Ω_ν, directly avoiding the tedious calculations of global eigenstates in both cases.

This review focuses on the TDHF method,[77,82−88] which combined with a semiempirical model Hamiltonian provides a powerful tool for studying the optical response of large conjugated molecules and chromophore aggregates.[81,89−96] The accuracy of this combination is determined by the approximations involved in closing the TDHF equations and by the semiempirical models. The TDDFT approach is on the other hand usually based on the ab initio Hamiltonians,[49,50,79,80,97,98] making these computations significantly more expensive and limited to smaller molecular systems than TDHF/semiempirical technique. $\rho(t)$ computed in the TDHF approach provides the variation of electron charge distribution (diagonal elements) and the optically induced coherences, i.e., changes in chemical bond orders, (off-diagonal elements) caused by an external field. The latter are essential for understanding optical properties of conjugated molecules and for the first-principles derivation of simple models for photoinduced dynamics in molecular aggregates (e.g., the Frenkel-exciton model).[90]

The TDHF equation of motion for the single-electron density matrix (eq A4 in Appendix A) was first proposed by Dirac in 1930.[99] This equation has been introduced and explicitly applied in nuclear physics by Ferrel.[100] The TDHF description was widely used in nuclear physics in the 50−60s.[101−104,83,84] The random phase approximation (RPA) was first introduced into many-body theory by Pines and Bohm.[105] This approximation was shown to be equivalent to the TDHF for the linear optical response of many-electron systems by Lindhard.[106] (See, for example, Chapter 8.5 in ref 83. The electronic modes are identical to the transition densities of the RPA eigenvalue equation.) The textbook of D. J. Thouless[82] contains a good overview of Hartree−Fock and TDHF theory.

The RPA approach was subsequently introduced into molecular structure calculations and was extensively studied in 60th and 70th as an alternative to the CI approach for solving many-electron problems. The RPA theory was developed based on the particle-hole propagators or two-electronic Green's functions technique[74] employing a direct decoupling of equations of motion[107,108] or perturbative approach.[109,110] In this language, the RPA procedure corresponds to the summation of ring diagrams to infinite order.[82,104] The RPA approach in combination with the Pariser-Par-Pople (PPP) Hamiltonian[111,112] was used to study low-lying excited states of ethylene and formaldehyde by Dunning and McKoy in 1967.[113,114] This investigation concluded that the RPA results are superior to single-electron transition approximation and are very similar to CI Singles (the latter coincides with the Tamm-Dancoff approximation). Subsequent computations of small molecules,[107,108,115−121] such as benzene,[107] free radicals[118] diatomics and triatomics,[117] showed high promise of RPA for molecular excitation energies. However, it was found that the first-order RPA yields inaccurate results for triplet states[113,119] and impractical for unstable HF ground state.[122−126] This happens when electronic correlations (doubles and higher orders) are significant for the ground-state wave function, and the Hartree−Fock reference state becomes a poor approximation for the true ground state wave function. For example, large contributions from doubly excited configurations lead to imaginary RPA energies of triplet states in both ethylene and formaldehyde.[113,114] Several improved schemes that take into account correlations beyond the first-order RPA have been suggested[120,127−133] to avoid these difficulties. Subsequently, RPA-based methods have been applied to calculate dynamics polarizabilities of small molecules using an analytical propagator approach.[134−137] We refer readers to reviews[104,74,138,75] for further details of this early development of RPA approaches.

Zerner and co-workers had subsequently attempted to use RPA as an alternative to Singles CI for computing molecular electronic spectra with ZINDO code.[139−141] However, historically, these early RPA advances did not develop into standard quantum chemical software. Modern computational packages[142−145] usually offer extensive CI codes but not propagator-based techniques for handling the electronic correlations. However, current studies of propagator techniques[146,147] will be gradually incorporated into quantum-chemical software.

Faster computers and development of better numerical algorithms have created the possibility to apply RPA in combination with semiempirical Hamiltonian models to large molecular systems. Sekino and Bartlett[85,86,148,36] derived the TDHF expressions for frequency-dependent off-resonant optical polarizabilities using a perturbative expansion of the HF equation (eq 2.8) in powers of external field. This approach was further applied to conjugated polymer chains. The equations of motion for the time-dependent density matrix of a polyenic chain were first derived and solved in refs 149 and 150. The TDHF approach based on the PPP Hamiltonian[111,112] was subsequently applied to linear and nonlinear optical response of neutral polyenes (up to 40 repeat units)[151,152] and PPV (up to 10 repeat units).[153−155] The electronic oscillators (We shall refer to eigenmodes of the linearized TDHF eq ξ_ν with eigenfrequencies Ω_ν as *electronic oscillators* since they represent collective motions of electrons and holes (see Section II))

contributing to the response were identified, and the size-scaling of optical susceptibilities were analyzed. Further development of the classical TDHF representation and algebra of electronic oscillators[77,156−158] reduced the number of independent variables to electron−hole oscillators representing occupied−unoccupied orbital pairs. These developments evolved into the collective electronic oscillator (CEO) approach for molecular electronic structure.

In this article, we review the basic ideas and recent developments in the CEO framework for computing the optical excitations of large conjugated systems and connecting them directly with the motions of electron−hole pairs in real space. The CEO approach solves the TDHF equations to generate the *electronic normal modes*; quasiparticles which represent the dynamics of the optically driven reduced single electron density matrix. Fast Krylov-space based algorithms for the required diagonalization of large Hamiltonian matrices are used to calculate excited-state structure of organic molecular systems with hundreds of heavy atoms with only moderate computational effort.

A real space analysis of electronic normal modes (transition densities) results in a systematic procedure for identifying the *electronic coherence sizes* which control the scaling and saturation of spectroscopic observables with molecular size. Localization of these density matrices is further used to simplify the description of the optical response of large molecules by dissecting them into coupled chromophores. Illustrative examples are presented, including linear polyenes, donor/acceptor substituted oligomers, poly-phenylenevinylene (PPV) oligomers, chlorophylls, naphthalene and PPV dimers, phenylacetylene dendrimers, and photosynthetic light-harvesting antenna complexes.

In Section II, we describe the CEO computational approach combined with semiempirical molecular Hamiltonian. Section III presents a real space analysis of electronic excitations and optical response of different conjugated molecules. In Section IV, we compute interchromophore interactions to derive an effective Frenkel exciton Hamiltonian for molecular aggregates. Finally, summary and discussion are presented in Section V.

II. The CEO Formalism

The CEO computation of electronic structure[81,89] starts with molecular geometry, optimized using standard quantum chemical methods,[142−144] or obtained from experimental X-ray diffraction or NMR data. For excited-state calculations, we usually use the INDO/S semiempirical Hamiltonian model (Section IIA) generated by the ZINDO code;[145,159−163] however, other model Hamiltonians may be employed as well. The next step is to calculate the Hartree−Fock (HF) ground state density matrix. This density matrix and the Hamiltonian are the input into the CEO calculation. Solving the TDHF equation of motion (Appendix A) involves the diagonalization of the Liouville operator (Section IIB) which is efficiently performed using Krylov-space techniques: e.g., IDSMA (Appendix C), Lanczos (Appendix D), or Davidson's (Appendix E) algorithms. A two-dimensional real space representation of the resulting transition density matrices is convenient for an analysis and visualization of each electronic transition and the molecular optical response in terms of excited-state charge distribution and motions of electrons and holes (Section IIC). Finally, the computed vertical excitation energies and transition densities may be used to calculate molecular spectroscopic observables such as transition dipoles, oscillator strengths, linear absorption, and static and frequency-dependent nonlinear response (Appendix F). The overall scaling of these computations does not exceed $\sim K^3$ in time and $\sim K^2$ in memory (K being the basis set size) for both ground and excited-state (per state) calculations. Typically, direct diagonalization of the Liouville operator L or CI Singles matrix A without invoking Krylov-space methods increases the computational cost to $\sim K^6$ in time and $\sim K^4$ in memory for the excited states. The cost is even higher ($\sim K^{8-12}$) for methods taking into account higher order electronic correlations, such as higher order CI, coupled cluster and CAS−SCF.[60]

A. Electronic Hamiltonian and Ground State Calculations

The general Hamiltonian of a molecule interacting with an external field in second quantization form reads[60]

$$\hat{H} = \sum_{mn\sigma} t_{mn} c^{\dagger}_{m\sigma} c_{n\sigma} + \sum_{\substack{mnkl \\ \sigma\sigma'}} \langle nm|kl\rangle c^{\dagger}_{m\sigma}\, c^{\dagger}_{n\sigma'} c_{k\sigma'} c_{l\sigma} - \mathcal{E}(t) \sum_{mn\sigma} \mu_{mn} c^{\dagger}_{m\sigma} c_{n\sigma}, \quad (2.1)$$

where the subscripts m, n, k, l run over known atomic basis functions $\{\chi_n\}$ and σ,σ' label spin components. These atomic orbitals are assumed to be orthogonal

$$\langle n|m\rangle \equiv \int d\mathbf{r}_1 \chi^{\star}_{n}(1)\chi_m(1) = \delta_{nm} \quad (2.2)$$

$c^{\dagger}_{n\sigma}(c_{n\sigma})$ are the creation (annihilation) operators which satisfy the Fermi anticommutation relations

$$c_{m\sigma} c^{\dagger}_{n\sigma'} + c^{\dagger}_{n\sigma'} c_{m\sigma} = \delta_{mn}\delta_{\sigma\sigma'} \quad (2.3)$$

and all other anticommutators of $c^{\dagger}$ and c vanish.

The first term in eq 2.1 is the core single-body Hamiltonian describing the kinetic energy and nuclear attraction of an electron

$$t_{nm} = \left\langle n \left| -\frac{1}{2}\nabla_1^2 - \sum_A \frac{Z_A}{|\boldsymbol{r}_1 - \boldsymbol{R}_A|} \right| m \right\rangle \equiv \int d\mathbf{r}_1 \chi^{\star}_n(1) \left(-\frac{1}{2}\nabla_1^2 - \sum_A \frac{Z_A}{|\mathbf{r}_1 - \mathbf{R}_A|} \right) \chi_m(1) \quad (2.4)$$

where $\mathbf{R}_A$ is the nuclear coordinate of atom A. The second two-body term represents electron−electron Coulomb interactions where

$$\langle nm|kl\rangle \equiv \int d\mathbf{r}_1 d\mathbf{r}_2 \chi^{\star}_n(1)\chi^{\star}_m(2)\frac{1}{r_{12}}\chi_k(1)\chi_l(2) \quad (2.5)$$

are the two-electron integrals. The interaction between the electrons and the external electric field $\mathcal{E}(t)$ polarized along the chosen z-axis is given by the last term in eq 2.1, μ being the dipole operator

$$\mu_{nm} = \langle n|\mu_z|m\rangle \equiv \int d\mathbf{r}_1 \chi_n^\star(1) z_1 \chi_m(1) \qquad (2.6)$$

To simplify the notation, we hereafter focus on closed-shell molecules and exclude spin variables assuming that N electron pairs occupy K ($N \le K$) spatial atomic orbitals. Generalization to the unrestricted opened-shell case and nonorthogonal basis set is possible.[60] The ground state is obtained by solving the Schrödinger equation $\hat{H}\Psi = E\Psi$ for the ground-state assuming the simplest antisymmetric wave function, i.e., a single Slater determinant $\Psi = |\phi_1(1)\phi_2(2)...\phi_N(2N)\rangle$[60] (HF approximation). Here $\{\phi_\alpha\}$ are the molecular orbitals (MO). Following Roothaan's procedure,[60,164] they are expanded as linear combinations of localized atomic basis functions $\{\chi_n\}$

$$\phi_\alpha = \sum_i^K C_{\alpha i}\chi_i \qquad (2.7)$$

The HF approximation maps the complex many-body problem onto an effective one-electron problem in which electron−electron repulsion is treated in an average (mean field) way. Even though the resulting ground state is uncorrelated, this approximation works reasonable well for majority of extended molecular systems. However, the HF solution is not always stable, in particular, for opened-shell[124−126] and near degenerate cases (e.g., conical intersections[165,166]).

The HF eigenvalue equation is derived by minimizing the ground-state energy with respect to the choice of MOs

$$FC = C\epsilon \qquad (2.8)$$

This equation may be recast using the density matrix in the form

$$[F(\bar{\rho}), \bar{\rho}] = 0 \qquad (2.9)$$

For closed-shells, the ground-state density matrix is related to the MO expansion coefficients (eq 2.7) as

$$\bar{\rho}_{nm} = 2\sum_a^{N_{occ}} C_{na}C_{ma}^\star = 2\sum_a^N C_{na}C_{ma}^\star \qquad (2.10)$$

$F(\bar{\rho})$ is the Fock matrix with matrix elements

$$F_{nm}(\bar{\rho}) = t_{nm} + V_{nm}(\bar{\rho}) \qquad (2.11)$$

and the matrix representation of the Coulomb electronic operator V in the atomic basis set $\{\chi_n\}$ is

$$V(\bar{\rho})_{mn} = \sum_{k,l}^K \bar{\rho}_{kl}\left[\langle ml|nk\rangle - \frac{1}{2}\langle ml|kn\rangle\right] \qquad (2.12)$$

The HF eq 2.9 for $\bar{\rho}$ is nonlinear and may be readily solved iteratively using the self-consistent field (SCF) procedure.[60]

In all computations presented below, we use a semiempirical (INDO/S) parametrization of the Hamiltonian (2.1) that was fitted to reproduce the spectra of simple molecules at the singly excited CI level. The INDO approximation[159−163] limits the basis set to valence orbitals of Slater type. Exchange terms in the two-electron interaction are permitted only among orbitals located on the same atom

$$\langle \chi_n^A \chi_k^B|\chi_m^A \chi_l^B\rangle = \begin{cases} \langle \chi_n^A \chi_k^A|\chi_m^A \chi_l^A\rangle & A = B, \\ \langle \chi_n^A \chi_k^B|\chi_n^A \chi_k^B\rangle \delta_{nm}\delta_{kl}, & A \neq B, \end{cases} \qquad (2.13)$$

where χ_n^A belongs to atom A and χ_n^B to atom B. The tetradic matrix $\langle \chi_n\chi_k|\chi_m\chi_l\rangle$ thus becomes block-diagonal in two dimensions. Thus, this approximation limits the number of computed Coulomb matrix elements and allows the storing of all of them in memory instead of recalculating them when needed as is commonly done in ab initio computations, making semiempirical techniques significantly easier and faster.

The parameters of the INDO/S Hamiltonian are given in refs 159−163. This widely used model first introduced by Pople[159,160] and later carefully parametrized by Zerner and collaborators to reproduce UV-visible spectra of small organic chromophores at CI single level.[161−163,167−172] The INDO/S parameters were initially available for the main group elements[161,162] and subsequently for transition metals,[163,168,173−175] actinides,[176] and lanthanides.[177,178] Special attention was paid to reproduce triplet states.[167] INDO/CIS calculations have been successfully applied to studies of electronically excited states in a wide variety of chromophores,[179,180] and this model is currently widely used in optical response computations.[14,15,181] The ZINDO code[145] developed by Zerner and co-workers serves as a convenient platform for these calculations. In addition to the CIS calculations, they have investigated how INDO works with RPA approximation for molecular excited states[139−141] using conventional diagonalization of the RPA matrix (see Section IIB). These studies concluded that the INDO/RPA excited-state energies are close to INDO/CIS where both show some red-shifts compared to experiment. However, RPA shows better accuracy for the oscillator strengths and for molecular systems with fine splittings in the spectrum such as free base porphins.[140] We also found that the TDHF (RPA) combined with the INDO/S Hamiltonian works extremely well for many molecules without further reparametrization and thus provides an alternative approach for computing their optical properties.[182,183] Typically, this method reproduces vertical excitation energies with accuracy of 0.1−0.3 eV, whereas transition dipoles and nonlinear polarizabilities agree with experimental data within 10% and 20−30%, respectively.[182,183]

Effects of the surrounding media (e.g., solvent) may be readily incorporated using the self-consistent reaction field (SCRF) approach,[184,185] whereby the interaction energy between a solute and the solvent is added to the HF energy of an isolated molecule, and the total energy of the system is then minimized self-consistently. The SCRF method is based on

classical ideas originally introduced by Onsager[186] and Kirkwood.[187]

For electrically neutral solutes, only the dipolar interactions contribute to the solvation energy. In the Onsager's spherical cavity model, the Fock operator F_{mn} is then modified by adding the response of a dielectric medium, resulting in

$$F_{mn} = F^0_{mn} - \frac{\epsilon - 1}{2\epsilon + 1} \frac{\vec{\mu}_g \cdot \vec{\mu}_{mn}}{a_o^3} \qquad (2.14)$$

where F^0_{mn} is the isolated complex Fock operator, $\vec{\mu}_g$ is the ground-state dipole moment, ϵ is the dielectric constant, and a_o is a cavity radius. The second Onsager dipolar term in eq 2.14 has been derived[188,185] assuming that the solute is separated from the solvent by a sphere of radius a_o. The Gaussian 98 package[142] provides a reasonable estimate for a cavity radius.

Onsager's SCRF is the simplest method for taking dielectric medium effects into account and more accurate approaches have been developed such as polarizable continuum modes,[189,190] continuum dielectric solvation models,[191,192] explicit-solvent dynamic-dielectric screening model,[193,194] and conductor-like screening model (COSMO).[195] Extensive refinements of the SCRF method (spherical, elliptical,[188] multicavity models) in conjunction with INDO/CIS were introduced by Zerner and co-workers[185,196−202] as well.

The shape of the cavity has some effect on the molecular polarizabilities;[203,204] however, the methods taking into account "real" molecular shapes are computationally expensive and are most appropriately utilized with accurate ab initio or density functional theory (DFT) approaches.[205,206] Even though spherical cavity is a crude approximation for most molecules, the predicted trends usually agree well with experiment and with the results of much more sophisticated and expensive methods.[182,185,200]

B. Computation of Electronic Oscillators

Using the ground-state density matrix as an input, the CEO procedure[81,89] computes vertical transition energies Ω_ν and the relevant transition density matrices (denoted *electronic normal modes* $(\xi_\nu)_{mn} = \langle g|c^\dagger_m c_n|\nu\rangle$), which connect the optical response with the underlying electronic motions. Each electronic transition between the ground state $|g\rangle$ and an electronically excited state $|\nu\rangle$ is described by a mode which is represented by $K \times K$ matrix. These modes are computed directly as eigenmodes of the linearized time-dependent Hartree−Fock equations of motion for the density matrix (eq A4) of the molecule driven by the optical field.

$$L\xi_\nu = \Omega_\nu \xi_\nu \qquad L\xi^\dagger_\nu = -\Omega_\nu \xi^\dagger_\nu \qquad \nu = 1, ..., K^2/2 \qquad (2.15)$$

where L is a linear Liouville space operator (i.e., superoperator) whose eigenvectors are the transition densities ξ_ν.[81,89] The electronic modes obey normalization conditions (see Section B)

$$\mathrm{Tr}(\bar{\rho}[\xi^\dagger_\alpha, \xi_\beta]) = \delta_{\alpha\beta} \qquad (2.16)$$

$$\mathrm{Tr}(\bar{\rho}[\xi^\dagger_\alpha, \xi^\dagger_\beta]) = \mathrm{Tr}(\bar{\rho}[\xi_\alpha, \xi_\beta]) = 0 \qquad (2.17)$$

The complete set of density matrices (eq 1.2) may be subsequently calculated using the ξ_ν eigenvectors.[207]

Only particle-hole and hole-particle components of ξ_ν are computed in the restricted TDHF scheme[77] (Appendix A). Therefore, this non-Hermitian eigenvalue problem of dimension $2M \times 2M$, $M = N_{occ} \times N_{vir} = N \times (K - N)$ in the MO basis set representation may be recast in the form[82,74]

$$\begin{pmatrix} A & B \\ -B & -A \end{pmatrix} \begin{bmatrix} X \\ Y \end{bmatrix} = \Omega \begin{bmatrix} X \\ Y \end{bmatrix} \qquad (2.18)$$

This is known as the first-order RPA eigenvalue equation,[79,107,113,127,130,131,208] where X and Y are, respectively, the particle-hole and hole-particle components of the transition density $\xi = \left[\begin{smallmatrix} X \\ Y \end{smallmatrix}\right]$ in the MO representation.[77,79,80,113,120,208] In eq 2.18, the matrix A is Hermitian and identical to the CI Singles matrix, whereas the Hermitian matrix B represents higher order electronic correlations (double excitations) included in the TDHF approximation. We recall, however, that the TDHF uses the HF ground state (Section IIA) as a reference state. If this state is unstable (e.g., saddle point) near curve crossings or conical intersections, or if the second-order electronic correlations are large (the magnitudes of matrix B elements are comparable to that of matrix A), eq 2.18 may have imaginary eigenvalues (frequencies). In this case, the first-order RPA breaks down,[113,120] and higher order RPA are called for.[128−131,133,209] We note that the extended conjugated molecular systems considered in this review have stable HF ground state (closed shell), and the first-order RPA is well suited for computing their electronic excitations. We therefore restrict our subsequent discussion to this approximation.

The formal properties of operator L eq 2.18 (known as the symplectic structure[77]) allow the introduction of a variational principle eq D3,[210] a scalar product (eq B1), and ultimately to reduce the original non-Hermitian eigenvalue problem (eq 2.18) to the equivalent Hermitian problem which may be solved using standard numerical algorithms (Appendices B−E). For example, L^2 is a Hermitian operator. Löwdin's symmetric orthogonalization procedure[60,211,212] leads to the Hermitian eigenvalue problem as well (eq E5), which may be subsequently solved by Davidson's algorithm (Appendix E). The spectral transform Lanczos method developed by Ruhe and Ericsson[213] is another example of such transformation.

Direct diagonalization of the TDHF operator L or the CIS operator A in eq 2.18 is the computational bottleneck, requiring computational effort which scales as $\sim K^6$ in time and $\sim K^4$ in memory (for comparison, SCF ground-state calculations scales as $\sim K^3$ in time and $\sim K^2$ in memory) because we are working in the space of higher dimensionality (electron−hole pairs). Direct diagonalization of eq 2.18 should give the entire spectrum of excited states. The traditional quantum-chemical approach addresses

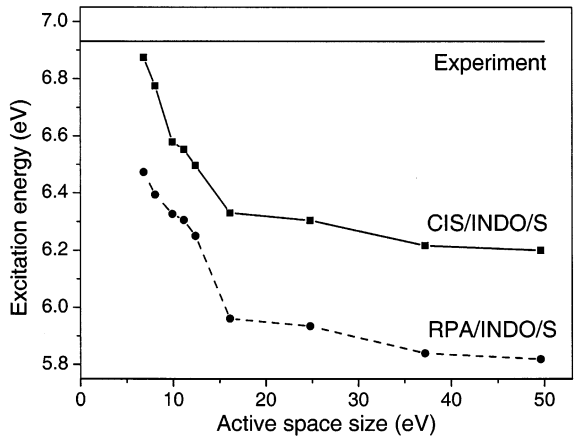

Figure 1. Benzene $^1E_{1u}$ transition as a function of active space calculated with CI Singles and RPA methods combined with INDO/S model. Adapted from Baker and Zerner ref 139.

this problem by limiting the total basis set size variables K to a few MOs which are "important" for visible-UV optical response. Indeed, most of the electronic states obtained by diagonalization of eq 2.18 lie in the X-ray spectral region and correspond to atomic-core type transitions. Visible−UV collective molecular excitations, on the other hand, could be adequately described by truncating an active space, taking into account only few MOs close to HOMO−LUMO energy gap. Although this approach works quite well and the ZINDO code[161,163,168] became very successful, truncating the active space is a complicated and somewhat arbitrary procedure. In addition, even truncated CI calculations are usually significantly more expensive than ground-state computations. The effects of size of the active space on the computed spectra of small molecules for CIS and RPA approximations have been studied by Zerner and Baker.[139] They showed that (i) even minimal configurational space (∼7 eV) provides qualitative description for lowest electronic transition, (ii) fairly large active space is required (∼10 eV) (The number of molecular orbitals and subsequently the CI expansion size grows very rapidly with the active space window size) to account for all essential configurations, and (iii) inaccuracy grows for higher lying electronic transitions. Figure 1 shows variation of energy of calculated $^1E_{1u}$ state of benzene (the third transition in electronic spectrum) as a function of active space size. These data are extracted from ref 139. Both CI Singles and RPA energies show considerable red-shift with increasing the active space size. It is interesting to note that CI Singles gives the closest agreement with experiment for the small active space size used for parametrizing the INDO/S model. This points out the need for a future reparametrization of the INDO/S Hamiltonian to account for the entire active space.

An alternative solution to this problem is provided by fast Krylov-space algorithms.[214,215] These techniques construct a small subspace of orthogonal vectors which contains a good approximation to the true eigenvector. This Krylov subspace $Sp\{\xi, L\xi, L^2\xi, ..., L^j\xi\}$, $j \ll M$, spans the sequence of vectors generated by the power method (the multiple action of the RPA operator L on some initial vector ξ). These methods find several eigenvalues and eigenvectors of a large matrix L using only matrix-vector operations.[214,215] Indeed, usually only a small fraction of eigenstates of L (∼100) lie in the UV-visible region and are of interest for optical spectroscopy. In addition, the action of the TDHF operator L on an arbitrary single electron matrix ξ, which only contains particle-hole and hole-particle components is given by

$$L\xi = [F(\bar{\rho}),\xi] + [V(\xi), \bar{\rho}] \qquad (2.19)$$

This product may therefore be calculated on the fly without constructing and storing the full matrix L in memory.[77,79−81,89,208] The action of the CIS operator A on an arbitrary matrix ξ can be also computed directly[216,217] (e.g., using eq 2.19 by setting the hole-particle component of ξ to zero). The cost of such operation in Hilbert ($K \times K$) space scales as $\sim K^3$ in time and $\sim K^2$ in memory with system size. Computing a single eigenvalue-eigenvector of matrix L which corresponds to molecular excited state thus requires a computational effort comparable to that of the ground state.

In Appendices D, E, and C, we outline three Krylov-space based algorithms. The original Lanczos algorithm computes effectively the lowest eigenvalue and the corresponding eigenvector of a large Hermitian matrix.[214,218] Since the matrices L that need to be diagonalized in the TDHF or adiabatic TDDFT approaches are non-Hermitian, a modified nonstandard Lanczos algorithm should be used[219−221] (Appendix D). Similarly, Davidson's algorithm originally formulated for the diagonalization of large Hermitian CI matrices[216] was further modified for the TDHF[208,222] and adiabatic TDDFT[49,50,79,80,97,217] methods. A third method for computing the lowest frequency eigenmode of a large Hamiltonian matrix is based on the iterative density matrix spectral moments algorithm (IDSMA).[81,89] All three algorithms show similar scaling of computational time, resulting from $K \times K$ matrix multiplications. However, the scaling prefactors are different. The Davidson type algorithms, especially the recently improved versions,[79,80,142] are extremely fast but I/O (input/output) intensive, since one needs to keep all the previous iterations for the eigenmodes throughout the iteration procedure. Consider, for example, the computation of the lowest eigenmode of a matrix using the Davidson iteration in a 200 dimension Krylov space (default maximum dimension in the Gaussian 98). To improve the accuracy, we need to calculate the 201st trial Krylov vector, which should be orthogonal to all others. This requires storing of all previous 200 vectors! On the other hand, to compute the 201st vector in the Lanczos procedure we only need the 200th and the 199th vectors: by orthogonalizing the 201st to the 200th and 199th, it automatically becomes orthogonal to all previous vectors. The need to store only two vectors, rather than 200, constitutes a substantial improvement in memory requirements of Lanczos over Davidson's. However, the Lanczos method usually requires larger Krylov-space dimension to obtain an approximate eigenvalue with the same accuracy as Davidson's. The latter thus converges faster and

generally involves lower computational effort compared to Lanczos. This fast convergence is ensured by Davidson's preconditioning (Appendix E), which assumes that the matrices L (or A) are dominated by their diagonal elements.[216] In practice, the Lanczos is 2−4 times faster than the IDSMA; however, the IDSMA has low memory requirements and allows to compute both "exact" and "effective" eigenstates. The latter may represent the overall contribution from several electronic states to the optical response by a single effective state,[89,81] providing an approximation for the spectrum in terms of very few variables.[91] There is no clear single method of choice and different algorithms may be preferable for specific applications.

All algorithms converge to the lowest eigenmode, and higher eigenmodes can be successively obtained (Appendix D) by finding the lowest mode in the subspace orthogonal to that spanned by the lower modes already found. This orthogonalization procedure is not always stable, leading to the accumulation of numerical error for the higher modes. A deflection procedure[214,219,223] that involves the antisymmetric scalar product eq B1 may be alternatively used to solve this problem. There is a whole arsenal of other related algorithms, such as Chebyshev's polynomial[224,225] and Arnoldi's[226−228] which may be used as well. These are included in standard packages such as Matlab.

These outlined numerical methods are commonly used in quantum-chemical computations and became a part of standard quantum-chemical packages.[142−144] However, new developments in computational techniques may offer even faster and more dependable numerical algorithms (such as "the rational Krylov algorithm for nonsymmetric eigenvalue problems" proposed by Ruhe[229−232]) which will undoubtedly find their place in the future quantum-chemical codes.

C. Real Space Analysis of Electronic Response

Each calculated transition density matrix $\rho^{gv} \equiv \xi_v$ with the corresponding frequency Ω_v enters the TDHF equations of motion as an electronic oscillator. Density matrices establish a natural connection between electronic structure and the molecular optical response. The ground-state density matrix $\bar{\rho}_{mn} \equiv \langle g|c_m^\dagger c_n|g\rangle$ is widely used in the description of the ground-state properties.[54,55,233−235] Its diagonal elements $\bar{\rho}_{nn}$ are used in various types of population analysis[56,59,233,234,236] to prescribe a charge to specific atoms and are commonly visualized using contour charge density maps. The off-diagonal elements, $m \neq n$, known as bond orders represent the bonding structure associated with a pair of atomic orbitals and are useful for interpreting the chemical bonding pattern across the molecule.[57−60,233,234]

In complete analogy with $\bar{\rho}$, the diagonal elements of $(\xi_v)_{nn}$ represent the net charge induced on the nth atomic orbital when the molecule undergoes the g to v electronic transition, whereas $(\xi_v)_{mn}$ $n \neq m$ is the *dynamical bond-order* representing the joint amplitude of finding an extra electron on orbital m and a hole on orbital n. The electronic modes thus directly show the flow of optically induced charges and electronic coherences. To display these modes, we need to coarse grain them over the various orbitals belonging to each atom. The INDO/S Hamiltonian uses from one to nine atomic orbitals (s, p, and d type) for each atom. In practice, the hydrogen atoms that weakly participate in the delocalized electronic excitations (such as π-type) are usually omitted. For other atoms, we use the following contraction: the total induced charge on each atom A is given by the diagonal elements

$$(\xi_v)_A = \left|\sum_{n_A} (\xi_v)_{n_A n_A}\right| \tag{2.20}$$

whereas an average over all the off-diagonal elements represents the effective *electronic coherence* between atoms A and B

$$(\xi_v)_{AB} = \sqrt{\sum_{n_A m_B} [(\xi_v)_{n_A m_B}]^2} \tag{2.21}$$

Here the indices n_A and m_B run over all atomic orbitals localized on atoms A and B, respectively. The size of the matrix $(\xi_v)_{AB}$ is now equal to the number of heavy atoms. (For planar molecules it is sufficient to include the π-electron contributions perpendicular to the molecular plane to represent π-excitations since σ contributions are usually negligible.) The resulting two-dimensional representation of the electronic modes $(\xi_v)_{AB}$ is useful for interpreting and visualizing these collective electronic motions in terms of the electronic density matrix in real space.[81,90−92] This is illustrated schematically by Figure 2: the coordinate axes label atoms and indices A and B of matrix $(\xi_v)_{AB}$ run along the y and x axes, respectively.

Two types of characteristic size for the degree of localization of the mode (ξ_v) may be clearly identified. The diagonal size (L_d) reflects the number of atoms over which the optical excitation is spread, i.e., the width of the distribution of the electron hole pair center of mass. The off-diagonal size L_c measures the degree of coherence between electrons and holes at different sites, and control the scaling of molecular properties with size. It reflects the size of electron−hole pair created upon optical excitation, (i.e., the confinement of their relative motion). L_d and L_c can be calculated quantitatively as follows.[237] To introduce L_d, we first define a normalized probability distribution of the charge induced on the nth atom

$$P_n = \frac{|\xi_{nn}|}{\sum_j |\xi_{jj}|} \tag{2.22}$$

L_d is then defined as the *inverse participation ratio* associated with the distribution of populations:

$$L_d \equiv [\sum_n P_n^2]^{-1} \tag{2.23}$$

For a localized excitation on site k $P_n = \delta_{nk}$ and $L_d = 1$; For a delocalized excitation $P_n = 1/L$ and $L_d = L$.

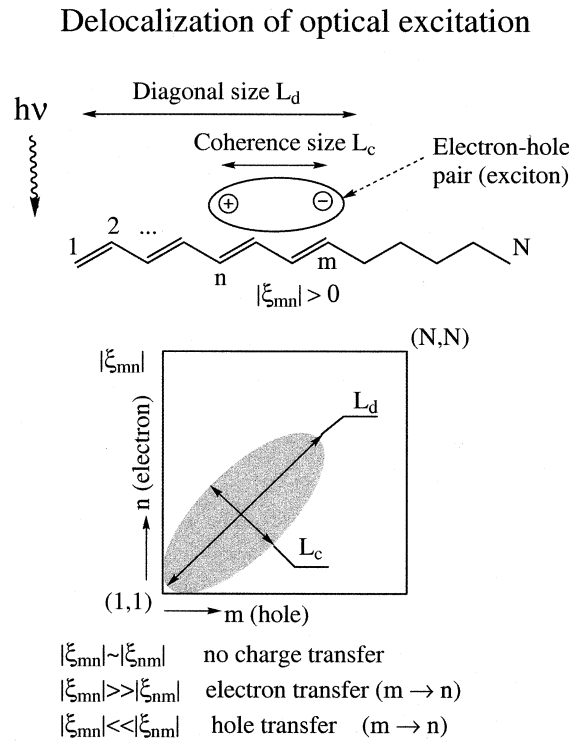

Figure 2. Two-dimensional representation and physical significance of electronic modes. Each mode ξ_ν is an $L \times L$ matrix, L being the number of atoms. The contour plot provides a direct real-space connection between the optical response and motions of charges in the molecule upon optical excitation. The x axis represents an extra electron on site n, and the y axis describes an extra hole on site m. The incident light moves an electron from some occupied to an unoccupied orbitals, creating an electron−hole pair (or exciton). The state of this pair can be characterized by two lengthscales: first, the distance between electron and hole (i.e., how far the electron can be separated apart from the hole). This coherence size L_c is the "width" of the density matrix along the antidiagonal direction. The second length L_d describes the exciton center of mass position (i.e., where the optical excitation resides within the molecule). L_d is the "width" of the mode along the diagonal antidiagonal direction. Charge-transfer processes can be characterized by the asymmetry of mode with respect to the diagonal symmetrical mode atom. $(\xi_\nu)_{mn} \sim (\xi_\nu)_{nm}$ means that there is no preferable direction of motion for electrons (or holes), whereas $(\xi_\nu)_{mn} > (\xi_\nu)_{nm}$ shows the transfer of electron from m to n.

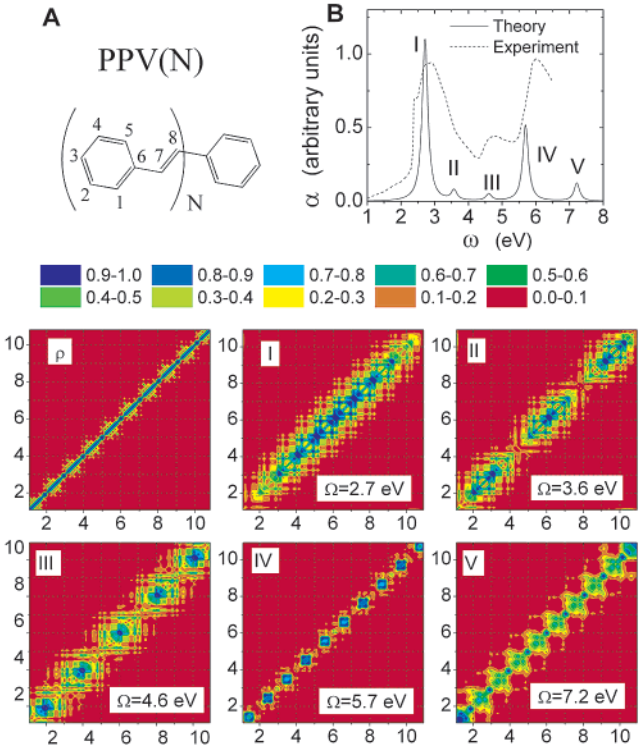

Figure 3. (A) Geometry and atom labeling of PPV oligomers. Molecular structure was optimized using the Austin model 1 (AM1) semiempirical model[492] in Gaussian 98 package;[142] (B) Absorption spectrum of PPV(10). Dashed line: experimental absorption of a PPV thin film.[243] Solid line: absorption line shape of PPV(10) obtained with 12 effective modes DSMA calculation with line width $\Gamma_\nu = 0.1$ eV; Contour plots of ground-state density matrix $\bar{\rho}$ and five electronic modes (I−V) which dominate the linear absorption of PPV(10). The sizes of plotted matrices are 78 × 78 (equal to the number of carbon atoms in PPV(10)). The axis are labeled by the repeat units. The color maps are given on the top of color plots. Reprinted with permission from ref 91. Copyright 1997 American Association for the Advancement of Science.

L_c can be defined in terms of coherence participation ratio.[237,238] At first, we introduce a normalized probability distribution of the density matrix elements

$$Q_{nm} = \frac{|\xi_{nm}|}{\sum_{ij}|\xi_{ij}|} \tag{2.24}$$

L_c is then defined as follows:

$$L_c \equiv [L_d \sum_{mn} Q_{nm}^2]^{-1} \tag{2.25}$$

For tightly bound e−h pairs $Q_{nm} = \delta_{nm}/L_d$ and $L_c = 1$; for loosely bound e−h pairs $Q_{nm} = 1/L_d^2$ and $L_c \sim L$. Both L_c and L_d thus vary between 1 and L, where L is the number of atoms. Unlike L_d, which only depends on the populations, L_c measures the degree of coherence and is sensitive to the off-diagonal elements of the density matrix. Both L_c, and L_d depend on the basis set.

Note, that L_d and L_c defined by eqs 2.23 and 2.25, respectively, represent a total number of atoms involved into electronic excitation, whereas coherence sizes obtained from the two-dimensional plots reflect the extent of the transition densities in real space. They may not be the same. For example, the exciton corresponding to the band-gap excitation in PPV (see Section IIIA) is extended over 5 repeat units (40 atoms) (Figure 3I). However, the coherence size L_c computed with eq 2.25 is only 26 atoms. This reflects uneven participation of phenyl and vinyl carbon atoms in the optical excitation. In remainder of the paper, we will be using two-dimensional plots to obtain necessary coherence sizes relevant to the delocalization of the transition densities in real space.

The significance of the CEO oscillators may be explained by drawing upon the analogy with the description of vibrational spectroscopy,[239] whereby the coherent motion of various atoms with well-defined amplitude and phase relations are represented by collective nuclear coordinates; the normal

modes. The normal modes provide a natural coordinate system and a highly intuitive classical oscillator real-space interpretation of infrared or Raman spectra,[240,241] which offers an alternative to the description in terms of transitions among specific vibrational states. The normal modes of nuclear vibrations are simply superpositions of the 3N nuclear displacements. In complete analogy, ξ_ν can be viewed as *collective coordinates* which represent not the individual electrons but the displacements of the electronic density matrix elements from their ground-state values $\bar{\rho}_{nm}$.

The electronic modes provide a direct real-space link between the structure of complex molecules such as organic oligomers with a delocalized π-electronic system and their optical properties. They clearly show how specific variations in molecular design, such as chain length or donor/acceptor substitutions, can impact their optical response. In the remainder of the paper, we apply this approach to various classes of molecules and to different types of optical response. The two-dimensional real space analysis of the transition densities (slices[16] or two-dimensional plots[181]) provides an attractive alternative to the traditional molecular orbital based quantum-chemical analysis of photoexcitation processes.

III. Electronic Coherence Sizes Underlying the Optical Response of Conjugated Molecules

A. Linear Optical Excitations of Poly(*p*-phenylene vinylene) Oligomers

In this section, we examine the electronic excitations of poly(*p*-phenylene vinylene) (PPV) oligomers (Figure 3A) and their scaling with molecular size.[91,96,95] Understanding the electronic structure and the overall electronic excitation processes in this photoluminescent polymer is needed to provide a consistent picture for the numerous experimental[242−250] and theoretical[16,95,149,153,251−253] studies of PPV.

The absorption spectrum of PPV(10) calculated using the CEO/DSMA algorithm combined with INDO/S Hamiltonian (Figure 3B, solid line)[91] is not inconsistent with the experimental spectrum of PPV thin film[243] (dashed line), which is typical for other PPV derivatives.[254,243,255] The experimental absorption has a fundamental band at 2.5 eV (I), two weak peaks at 3.7 eV (II) and 4.8 eV (III), and a strong band at 6.0 eV (IV). Peak II originates from electron correlations[247,253,255] and is missed by HF calculations.

Before analyzing the transition densities underlying each absorption peak, let us examine the ground-state density matrix. A contour plot of the absolute value of the matrix elements of $\bar{\rho}$ of PPV(10) is shown in Figure 3. The matrix size has been reduced according to contraction eqs 2.20 and 2.21. It is equal to the number of carbon atoms, and the axes are labeled by repeat units along the chain. $\bar{\rho}$ is dominated by the diagonal and near-diagonal elements, reflecting the bonds between nearest neighbors. The five oscillators denoted I−V which dominate the optical absorption are shown as well. All transition densities are almost symmetric with respect to the diagonal ($\xi_{mn} \approx \xi_{nm}$). This reflects the absence of charge separation for the lack of preferable direction of motion for electrons (or holes). Mode I is delocalized. The coherence size, L_c, that is the "width" of the density matrix along the antidiagonal section, where the coherences decrease to <10% of their maximum values, is 4−5 repeat units. Therefore, 10 repeat units already mimic the infinite chain as far as the optical spectrum is concerned.[91]

Mode II has a similar L_c as mode I, but a nonuniform diagonal space distribution. The molecule is dissected into three parts with diagonal size of 3, 4, and 3 repeat units with a very weak electronic coherence between them, and the molecule is effectively a trimer. The total contribution from the ends to the oscillator strength of this mode is very small, and only the middle region contributes.[81] This mode therefore only makes a weak contribution to the linear absorption. Mode III which also makes a weak contribution to the absorption spectrum has five noninteractive segments with off-diagonal and diagonal sizes of about 2 repeat units. Similar to mode II, only the middle region contribute to the oscillator strength of this transition. The middle frequency modes II and III thus have strong transition dipoles localized at the molecular ends which overall does not contribute to their oscillator strengths but could play an important role in charge separation processes, e.g., photoconductivity of PPV oligomers.[248,256]

Electronic modes (I−III) show an effective separation of molecule to segments with weak electronic coherence among them. The higher frequency modes tend to have more diagonal nodes.[91,81,89,96,95] The modes with odd number of nodes computed in ref 95 with the Lanczos algorithm do not contribute to the linear absorption and therefore do not show up in the DSMA computations. The nth mode (in order of increasing energy) thus has $n - 1$ nodes. Cancellation of the transition dipoles leads to vanishing oscillator strength of electronic modes with odd number of nodes, whereas the oscillator strength of electronic modes with even number of nodes scales as $\sim 1/n^2$. The connection to band theories could be drawn by associating an exciton with momentum n to the electronic mode with n nodes. For example, mode I corresponds to the band exciton with zero momentum. The energy difference between modes I−III stems from edge effects and vanishes in an infinite ideal chain. The appearance of these modes in the experimental spectrum may be attributed to structural disorder effects which limit the effective conjugation length of the polymer.

The higher frequency modes (IV) and (V) are completely localized on a single repeat unit. The optically induced coherences in the fourth peak (IV) only involves the phenylene ring carbon atoms 1, 2, 4, and 5, in agreement with earlier results obtained in refs 255 and 257 The high-frequency peak (V) corresponds to localized and weakly delocalized transitions involving the vinylene group atoms 7 and 8, and the phenylene ring atoms 3 and 6. These calculations further show that the frequencies of modes I, II, III are red-shifted and gradually saturate with increasing chain length, whereas the frequencies of

modes IV and V are not affected by size. These trends are consistent with the delocalized and localized nature, respectively, of the two groups of modes. One important consequence of this localization of optical excitations is that the Frenkel exciton model for molecular aggregates may be applied to high frequency spectral region in PPV, even though the chromophores are not separated spatially (see Section IV). Subsequent CI/INDO computations[16,253] which used the slices of transition density to study the coherence sizes and formulated an essential-state single-chain model to model linear and nonlinear response of PPV oligomers are in agreement with this analysis.

B. Linear Optical Excitations of Acceptor-Substituted Carotenoids

Substituted conjugated molecules have optical properties that reflect the interplay of the donor−acceptor strength and the type and the length of the connecting bridge.[1,2,12,13,18,31,259−261] The electronic spectra of a family of unsubstituted, neutral (N(n)) (and substituted with the strong acceptor polar) P(n) molecules shown in Figure 4A[17,262] were calculated using the CEO/INDO/S with IDSMA algorithm.[89,91,81] Our analysis shows the difficulties in disentangling the effects of donor acceptor and bridge in the spectroscopy of molecules with relatively short bridges. To obtain a clear picture of the optical response of acceptor-substituted molecules it is instructive to study the size-dependence of optical properties, starting with very long bridges, where the effects of the acceptor and the bridge regions can be clearly separated. Optical properties of acceptor-substituted molecules with shorter bridges can then be attributed to quantum confinement, which is important when the bridge size becomes comparable to the coherence length L_c.

We first consider the effect of the acceptor on the ground state by analyzing the bond-length alternation (BLA) parameter and relevant charge distributions. The BLA δl_j is defined as the difference between the single (l_{2j}) and the double (l_{2j-1}) bond lengths in the j'th repeat unit along the bridge:

$$\delta l_j = l_{2j} - l_{2j-1}, j = 1, ..., n \qquad (3.1)$$

The BLA is a signature of the uneven distribution of the π densities over the bonds (Peierls distortion), which has a well-established relation to molecular polarizabilities.[260,263−268] Figure 4B displays the BLA parameter and the variation of the total charge Q_A from the acceptor end

$$Q_A = Q_{acceptor} + \sum_{a=1}^{A} q_a \qquad (3.2)$$

where $Q_{acceptor} = 0.69e$ is the total electronic charge on the acceptor and q_a are the atomic charges. These calculations illustrate the roles of bridge and boundary (end) effects in electronic structure of conjugated molecules. The acceptor attracts electronic charge and attempts to convert the chain structure to zwitterionic. In response, the π-electronic system screens the acceptor influence by inducing a positive charge at the acceptor end. The electrons completely screen the acceptor over an effective length of about 10 double bonds leading to a saturation of the ground−state dipole moment at this molecular size. Other parts of the molecule are unaffected by the acceptor. δl_j and Q_A deviate again from their bulk values near the neutral end of the molecule (Figure 4B) due to boundary condition effects imposed by structure on the right molecular end.

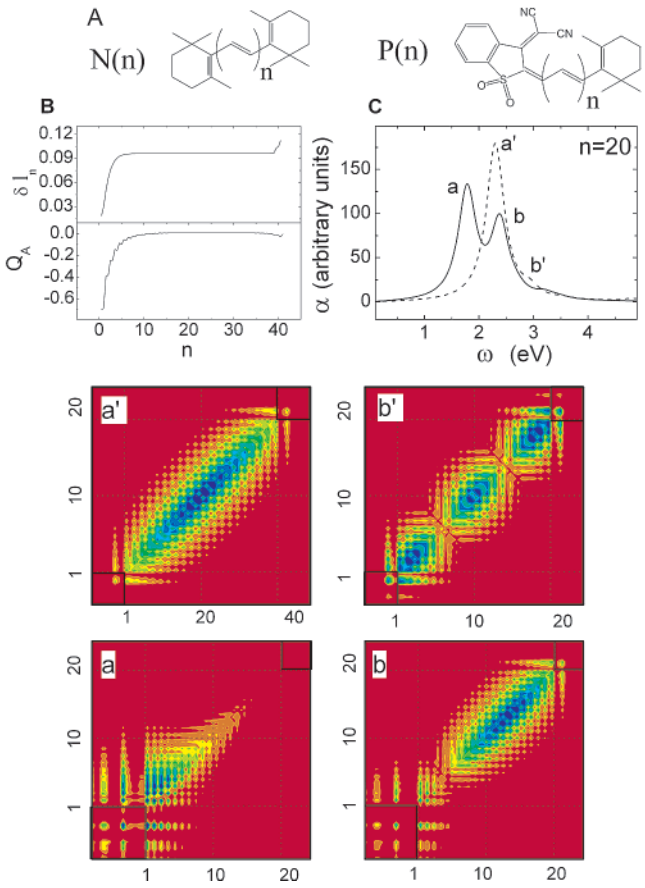

Figure 4. (A) Structures of the neutral N(n) and polar P(n) (substituted by the strongest acceptor) carotenoids. Molecular geometries were optimized using AM1 model[492] in Gaussian 98 package.[142] Calculations were done for chain lengths of n = 5, 10, 20, and 40 double bonds; (B) Variation of the bond-length alternation (top) and total charge Q_A (bottom) along the chain in polar P(40) molecule; (C) Linear absorption spectra calculated with line width $\Gamma = 0.2$ eV of the N(20) (dashed lines) and P(20) (solid lines) molecules; contour plots of electronic modes which dominate the absorption spectra of N(20) and P(20). Reprinted with permission from ref 81. Copyright 1997 American Chemical Society.

This effect of the acceptor substitution further strongly affects the absorption spectra:[17,81,262,269] The spectrum of the unsubstituted molecule N(20) is dominated by a single peak a, whereas in the acceptor molecule P(20) this resonance is red shifted and a second, weaker, peak b appears. These trends may be accounted for by inspecting the relevant transition densities. The electronic modes of N molecule (panels a′ and b′ in Figure 4) are almost symmetric with respect to the diagonal ($\xi_{mn} \approx \xi_{nm}$). This means that there is no preferable direction for the motion of

electrons (or holes). $\xi_{a'}$ is a *bulk mode* similar to the bulk transition in PPV (Figure 3(I)) with coherence size $L_c \sim 12$ double bonds.[81] The second oscillator $\xi_{b'}$ has a nonuniform diagonal spatial distribution, with three distinct contributions to the dipole moment, making a weak contribution to the linear absorption. The lowest feature (a) in P(20) Figure 4) is a *charge transfer* mode with diagonal size of $L_d \sim 17$ and coherence size $L_c \sim 12$ double bonds,[81] completely localized at the acceptor end. Its dipole moment is large and localized. This mode carries a strong oscillator strength in the optical response of small chains, which saturates in larger molecules ($n > 17$). The second mode (b) resembles the bulk mode of the neutral molecule (compared to a′). Its oscillator-strength for molecules with $\gtrsim 12$ grows linearly with n. The absorption spectra of small chains are therefore dominated by the charge-transfer mode (a) whereas the bulk mode (b) takes over with increasing molecular size. The distinct character of these modes is less apparent in chains shorter than the effective coherence size of 12 double bonds.[81]

The optical response of long donor/acceptor substituted molecules can thus be interpreted by dividing them into three effective regions: the acceptor (I) and the donor (III) boundary regions at the molecular ends, connected by the bridge (middle) region (II). The absence of electronic delocalization between these regions implies that the optical properties are additive and can be described in the same way as those of molecular aggregates.[270,271] Region II has the same properties as neutral molecule; it only shows odd order responses which scale linearly with size, whereas regions I and III have a fixed size determined by the screening length of the substituents. The ground and the excited states are zwitterionic. These effective regions are solely responsible for even-order optical responses. The odd-order responses for long chains are dominated by the contribution of region II, which is proportional to the size,[81] but regions I and III affect the response as well.

These acceptor substitution effects on the nonlinear response of carotenoid have been studied extensively. Experimental investigations[17,262] reveal that the substitution resulted in third-harmonic generation values up to 35 times higher than in β-carotene which corresponds to N(11) molecule. Subsequent CI/SOS quantum-chemical calculations[269] rationalized the origin of this enhancement and assessed the applicability of simple models to describe the evolution of the molecular polarizabilities. In particular, this study shows a steplike increase of the longitudinal component of the dipole moment with the applied external field, caused by charge-transfer toward the acceptor end leading to an enhanced nonlinear response.

C. Quantum Confinement and Size Scaling of Off-Resonant Polarizabilities of Polyenes

Conjugated polymers have large polarizabilities attributed to the delocalized nature of electronic excitations. Numerous experimental and theoretical studies have forged a pretty good understanding of their electronic and optical characteristics.[15,31] Pioneering theoretical investigations of NLO properties of polymers using solid-state physical concepts have been carried out by André, Champagne, and coworkers[272−276] These investigations utilized the sum over states[273] and the polarization propagator technique.[274,276] A similar study has been done by using a variational method for the time-dependent wave function.[277,278] Ab initio approach combined CPHF method has been applied to polyene oligomers of moderate sizes,[34,35] extrapolated to the infinite systems using the periodic boundary conditions,[279,280] and extended into finite frequency off-resonant regime.[280−282] It has been shown that vibrational contributions to the polarizability may be as important as their electronic counterparts.[283−289] These nuclear effects arise from geometry deformations induced by the external field π-electron delocalization and polymer nonrigid energy potential surface strongly enhances the vibrational contribution.

The variation of off-resonant optical polarizabilities of polyenes with molecular size may be described by the scaling law $\sim n^b$, n being the number of repeat units and b is a scaling exponent. In first (α) and third (γ) order responses the scaling exponents b vary considerably for short molecules: $1 < b_\alpha < 2$ and $2 < b_\gamma < 8$.[10,15,32,33,289−297] For elongated chains, the exponent b attains the limiting value 1, indicating that the polarizabilities become extensive properties. Recent theoretical studies suggest that this sets in at about 30−50 repeat units. An unusually large saturation length was reported experimentally in one case,[298] which was then corrected to yield a value of ~60 repeat units.[299])

Static electronic polarizabilities up to seventh order for polyacetylene oligomers with up to 300 carbon atoms were computed using the PPP Hamiltonian combined with the DSMA.[89,300] The polarizabilities are obtained by adding respective contributions from effective electronic modes calculated in the DSMA procedure.[89,300] These modes manifest themselves in the response with different effective oscillator strengths at each order. Typically, higher frequency modes make more significant contributions to the higher order responses. The ground state density matrix $\bar{\rho}$ (a) as well as the five dominant modes labeled b−f are depicted in Figure 5 for $N = 30$ (top two rows) and $N = 100$ (bottom two rows). As noted earlier, the delocalization of the off diagonal elements represents *electronic coherence* between different atoms. Figure 5 clearly shows how electronic coherence which is very limited for the almost diagonal $\bar{\rho}$ increases very rapidly for the higher modes in the case of longer oligomer ($N = 100$), whereas finite size (quantum confinement) effects are illustrated for $N = 30$. We note that modes a and b are hardly affected by reducing the size from 100 to 30. However, the more delocalized, higher modes, show significant confinement effects.

This coherence size directly controls the size-scaling behavior of nonlinear optical response. The calculated first- (α), third- (γ) and fifth-order (ε) static polarizabilities of polyacetylene chains with up to 200

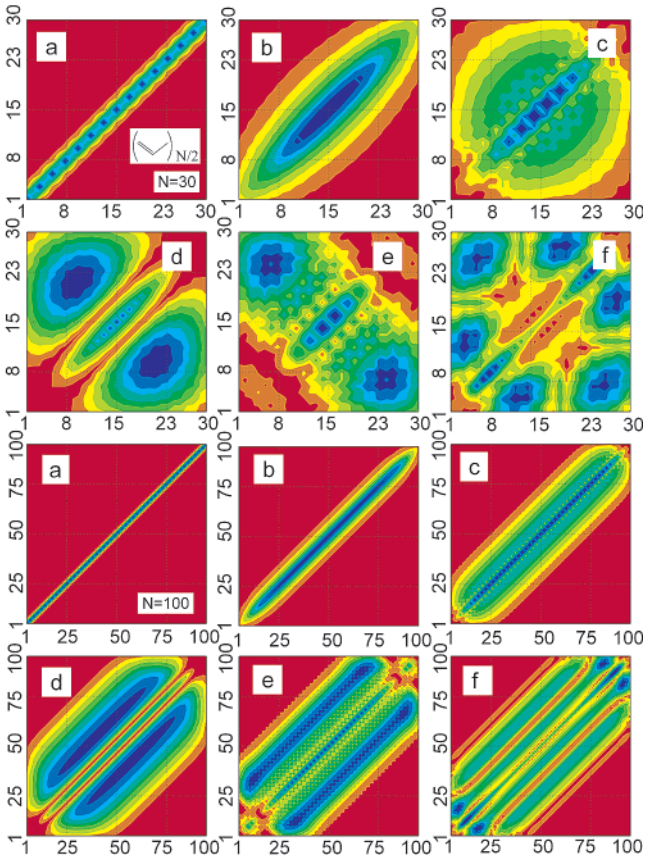

Figure 5. Top rows: Contour plots of $\bar{\rho}$ (a) and the dominant modes (b−f) that contribute to the responses up to the seventh order for polyacetylene oligomer with N = 30 carbon atoms. Shown are the absolute values of the density matrices averaged over four neighboring points to eliminate fast oscillations and to highlight the long range behavior. The axes are labeled by the carbon atoms along the chain. Exciton confinement effects are clearly seen in panels c, d, e, f. Frequencies of modes b−f are 2.6, 4.0, 4.8, 5.2, and 5.6 eV, respectively. Bottom rows: Same as A but for a longer chain (N = 100). Frequencies of b−f modes are 2.4, 3.9, 4.5, 4.7, and 5.1 eV, respectively. Reprinted with permission from ref 89. Copyright 1996 Elsevier Science.

carbon atoms are shown in the Figure 6A. Panel B shows their scaling exponents. We note that the variation with size is very rapid at small sizes but b eventually saturates, and attains the bulk value of 1. In general, higher frequency modes contribute more to the higher nonlinear response. Since the size of the mode grows with mode frequency (Figure 5), the crossover (coherence) size increases for higher orders nonlinearities (Figure 6A). The scaling and saturation sizes of static nonlinear polarizabilities in polyenes and other polyconjugated oligomers have been studied in detail using the CEO approach.[297,238] Simple analytical expressions for size and bond-length alternation dependence of off-resonant polarizabilities were derived[297] using a single-oscillator approximation. The relations between the magnitude of the saturation size L_c have been investigated for several families of molecules in ref 238. The size-scaling behavior of the second-order nonlinear response in conjugated oligomers substituted by donor and acceptor groups will be analyzed in Section IIID.[301,302]

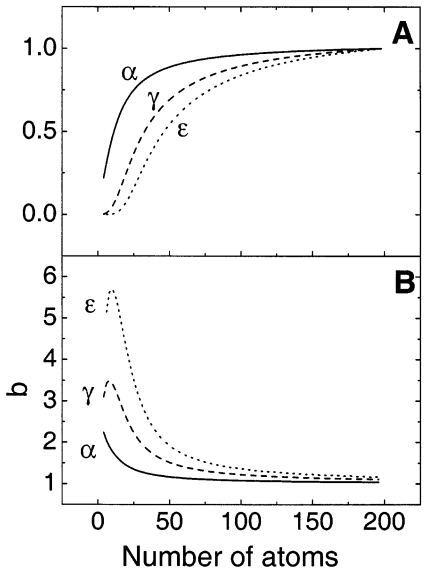

Figure 6. (A) Scaling and saturation of the lowest three nonvanishing static polarizabilities (α, γ, and ε) of polyacetylene chains with size; (B) variation of the scaling exponents $b \equiv d[ln\chi]]/d[lnN]$, $\chi = \alpha, \gamma, \varepsilon$ with size for the curves shown in panel A. Note how the exciton coherence size increases with the degree of nonlinearity. Reprinted with permission from ref 89. Copyright 1996 Elsevier Science.

D. Origin, Scaling, and Saturation of Off-Resonant Second Order Polarizabilities in Donor/Acceptor Polyenes

Donor/bridge/acceptor type molecules are not centrosymmetric and therefore possess even-order nonlinear polarizabilities. Experimental[12,13,18,19,303] and theoretical[14,304−310] studies have thoroughly investigated the variation of polarizabilities magnitudes with donor and acceptor strength, length, and type of the congugation bridge, and molecular conformations. A common approach for computing nonlinear polarizabilities is to use a perturbative expansion involving a summation over all molecular states. By restricting the summation to a single low-lying excited state and assuming that the charge-transfer transition is unidirectional, Oudar and Chemla[311,312] obtained the two-level expression commonly used for estimating the second-order polarizability

$$\beta \propto (\mu_{ee} - \mu_{gg})\frac{\mu_{ge}^2}{E_{ge}^2} \qquad (3.3)$$

where μ_{gg} and μ_{ee} are the ground and excited-state dipole moments, μ_{ge} is the transition dipole, and E_{ge} is the transition frequency. A superficial look at eq 3.3 suggests a rapid nonlinear scaling with n since the permanent dipole moments μ_{gg}, μ_{ee} and the transition dipole μ_{ee} are expected to grow with n. It is not clear from eq 3.3 precisely how should β scale with molecular size. Establishing the precise scaling law of β and its crossover to the bulk is an important issue. Experimental studies restricted by synthetic limitations to chain length of 15−20 repeat units show $1.4 < b_\beta < 3.2$,[14,18,13,12,19,313] whereas calculations performed with up to 22 repeat units yield $1.5 < b_\beta < 2$.[14,314]

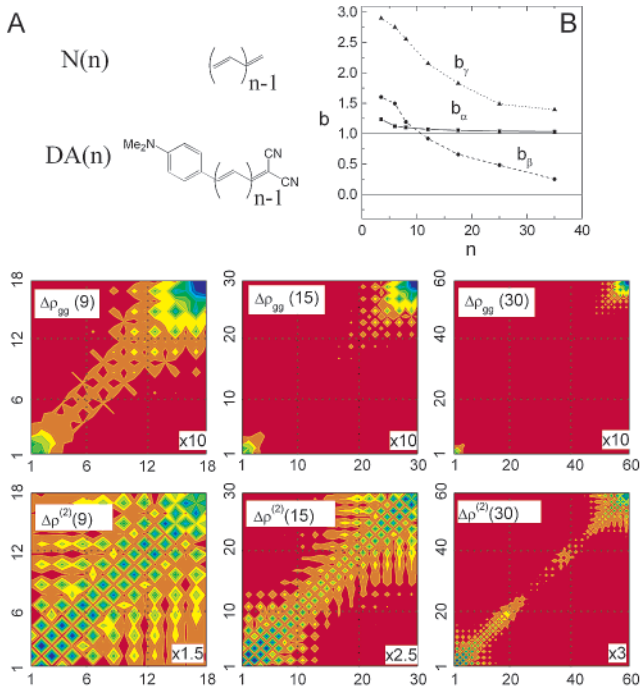

Figure 7. (A) Structures of the neutral N(n) and donor/acceptor DA(n) substituted molecules. Molecular geometries were optimized using AM1 model[492] in Gaussian 98 package.[142] Calculations were performed for bridges with $n = 5$, 10, 15, 20, 30, 40 double bonds; (B) Variation of the scaling exponents $b_\chi \equiv d[ln\chi]]/d[lnn]$, $\chi = \alpha, \beta, \gamma$ with size for DA(n). At large sizes b_α and b_γ tend to 1 whereas b_β approaches 0. These reflect the saturation of α/n, γ/n, and β; Contour plots of the ground state difference matrices $\Delta\bar{\rho} = \bar{\rho}_{DA} - \bar{\rho}_N$ for $n = 9$, 15, and 30 shown for the bridge part of the matrix. $\Delta\rho$ is magnified as indicated in each panel to use the same color code. Axes are labeled by the bridge carbon atoms with atom 1 on the donor side and atom $2n$ on the acceptor side. The second row displays the difference matrices to the second orders in the field $\Delta\rho^{(2)}$. Reprinted with permission from ref 301. Copyright 1998 Elsevier Science.

The CEO technique and our study of the linear response of elongated carotenoids described earlier provide a microscopic basis for predicting the size-scaling of β and pinpointing its origin. The calculated scaling exponents b_α, b_β, and b_γ of donor/acceptor substituted polyenes are displayed in Figure 7B.[301] As expected, b_α and b_γ reach the limiting value 1 at large sizes. b_β, however, is very different and vanishes at large sizes. This markedly different behavior of β can be explained by examining the differences $\Delta\rho^{(2)} \equiv \delta\rho^{(2)}_{DA} - \delta\rho^{(2)}_{N}$ between the induced density matrices in the substituted and the neutral molecules (Figure 7). This difference contributes to β. In complete analogy with the ground state where $\Delta\bar{\rho} \equiv \Delta\rho_{gg}$ (Figure 7) defines μ_{gg},[301,302] the donor/acceptor influence is screened by the π electrons and is confined to a finite section of the bridge with about 15−17 double bonds. For short chains ($\Delta\rho^{(2)}(9)$), the donor and acceptor communicate directly and significant electronic coherence then develops between them since their influence regions overlap spatially. However, for larger chains, $\Delta\rho^{(2)}(30)$ is block diagonal, and their effects are clearly separable. This is the reason β levels off to a constant with $b_\beta = 0$: only the ends of the molecule contribute to β, whereas the bridge is identical to that of neutral molecule and does not contribute to β.[301,302]

As noted earlier, unlike the present real-space analysis, the mechanism of saturation of β at large sizes is highly nontrivial in terms of the molecular eigenstates (eq 3.3). Since excited states are delocalized, it can be argued that $\mu^2_{ge} \sim n$ at large n in the two-level model.[297,300] This is necessary to guarantee that the linear scaling of the linear off-resonant polarizability with n: $\alpha \sim f_{ge}/E^2_{ge} = 2\mu^2_{ge}/E_{ge} \sim n$, where f_{ge} is the oscillator strength. μ_{gg}, μ_{ee}, and E_{ge} saturate with molecular size.[18,13,309,306] At first glance we thus expect $\beta \sim n$. This argument fails for the following reason: The difference $(\mu_{ee} - \mu_{gg})$ originates from charge redistribution upon electronic excitation. Figure 7 clearly shows that charge transfer which affects the permanent dipole only occurs in confined regions at the ends. Since the excited states are delocalized over the entire molecule, the difference $(\mu_{ee} - \mu_{gg})$ should scale as n^{-1}, which cancels the $\sim n$ scaling of μ^2_{ge}, resulting in an overall constant β, independent of n. Another way to state this is that both the ground state (μ_{gg}) and the excited-state (μ_{ee}) contributions to β scale as n, and the saturation of β originates from a delicate cancellation of these two $\sim n$ terms. It is interesting to note that similar cancellations have been observed in γ as well; individual contributions which scale as n^2 interfere and almost cancel, resulting in the overall $\sim n$ scaling.[31,14,15]

Defining and predicting the saturation size of optical properties is a key factor in developing synthetic strategies for optical materials. The two-dimensional CEO plots provide a highly intuitive yet quantitative tool for addressing this problem: the density matrix shows that the influence of the donor or the acceptor is limited to a few double bonds in its vicinity; the size of these coherence regions depends on the donor and the acceptor strength. Direct donor-to-acceptor communication and charge transfer do occur at short chains. However, when the molecular size is larger than the coherence size the donor and the acceptor are decoupled and their effects are additive; β itself (rather than β/n) then becomes size-independent.

E. Localized and Delocalized Electronic Excitations in Bacteriochlorophylls

Optical properties of chlorophylls and porphyrins have drawn considerable attention[315−326] because of their fundamental and biological relevance. We applied the CEO/INDO/S approach to study the electronic excitations of bacteriochlorophyll-*a* (Bchl-*a*)[93,94,327] from LH2 complex of photosynthetic bacteria *Rhodospirillum molischianum* (βB850).[328,318] The calculated properties of individual Bchl-*a*, both isolated and in a dielectric medium, are summarized in Table 1. This table reveals the significant impact of solvation on the linear absorption spectrum, reflecting the need for properly incorporating the dielectric environment in accurate computations.[94]

To trace the origin of the various resonances we had examined the corresponding collective electronic

Table 1. Calculated and Experimental Excitation Energies of Bchl-*a*[a]

state	CEO (ic)	CEO (dm)	experiment
$\mathbf{Q}_y$	1.20 (1.441)	1.61 (1.190)	1.6 (1.27,[d] 1.33[e])
$\mathbf{Q}_x$	2.13 (0.194)	2.26 (0.473)	2.16 (0.685)[d]
$\mathbf{B}_x$	3.12 (1.385)	3.19 (1.194)	3.17(∼1.11)[c]
Tx1	3.40 (0)	2.96 (0.073)	
Tx2	3.51 (0.068)	3.54 (0.095)	
Tx3	3.53 (0.117)	3.68 (0.355)	
$\mathbf{B}_y$	3.90 (1.152)	3.42 (0.883)	3.47 (∼0.96)[c]
N	4.21 (0.094)	4.05 (0.867)	

[a] CEO calculations were carried out for an isolated complex (ic) (ref 93) and in a dielectric medium (dm) with $\epsilon = 9$. The experimental transition energies correspond to Bchl-*a* monomers in ethyl ether solution (ref 494). Energies are in eV. Transition dipole moments (in eÅ) are given in parentheses. Reprinted with permission from ref 94. Copyright 2000 American Chemical Society. [c] Ref 184. [d] Ref 495. [e] Ref 390.[f] Ref 496. [g] Ref 497.

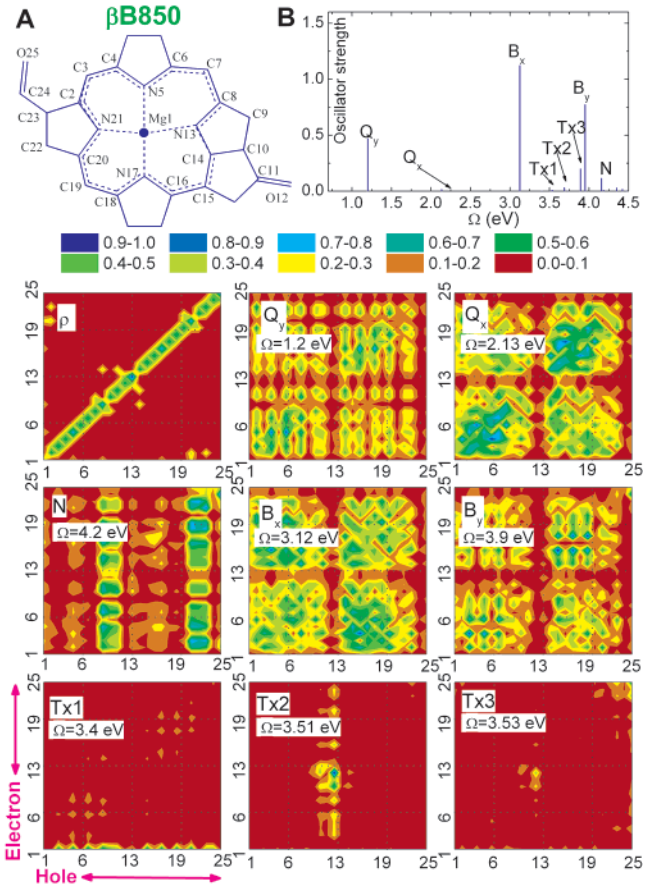

Figure 8. (A) Geometry and atom labeling of Bchl-*a* obtained from crystal structures of LH2 complex of *Rs. molischianum*[328] with added hydrogen atoms. Geometries of hydrogen atoms of the substructures were optimized by using the AM1 method.[492] (B) Calculated linear absorption spectrum of Bchl-*a*. Contour plots the electronic modes which dominate the optical absorption of Bchl-*a*. The axis labels represent the individual atoms as labeled in panel A. The panels indicate the electronic mode according to panel B. The color code is given in the top row. Mode frequencies are given in Table 1. Reprinted with permission from ref 93. Copyright 2000 American Chemical Society.

modes. Panel ρ in Figure 8 shows that the ground-state density matrix $\bar{\rho}$ of Bchl-*a* is essentially tri-diagonal, simply reflecting the nearest-neighbor chemical bonding in the ground state. The charge-distribution along the diagonal is not uniform: nitrogen and oxygen atoms (blue dots on the diagonal) have an excess electronic charge. Panel Q_y displays the electronic mode of the lowest absorption peak Q_y. This mode is delocalized across the entire molecule and is dominated by carbons 2−8 and 15−20. The coherences of the Q_x mode are distributed more uniformly across the molecule. The Soret B_x and B_y modes are very similar to the corresponding Q_x and Q_y transitions. Extensive delocalization and almost perfect symmetry with respect to the diagonal are common features of all Q and B modes. This reflects the absence of preferable direction of motion for holes or electrons. The Mg atom and both C═O groups do not participate in these excitations. The remaining excitations have distinct charge-transfer character that can be clearly identified by real-space analysis (see Section IIC and Figure 2). The Tx modes heavily involve Mg and C═O atoms. Panel Tx1 shows that the electron is transferred from the porphyrin to Mg(1) upon Tx1 excitation: the hole is delocalized (*x*-axis) and the electron is localized on the Mg (*y*-axis). This transition is forbidden for planar geometry and its intensity grows as the Mg atom is displaced out of the molecular plane. Panel Tx2 shows that the next Tx mode represents electron-transfer from the O12 oxygen mostly to C11 and to the rest of the molecule. As indicated earlier, oxygen is an electron acceptor, which attracts extra electronic charge in the ground state. In the Tx2 excited state the electron gains energy and becomes more "loose". Similarly, the Tx3 mode involves electron transfer from O25 to C24, with less electronic delocalization compared to Tx2. Finally, the N mode is localized on the two vertical strips and describes electron transfer from the pyrroles to the entire molecule. The Q, B, N, and Tx electronic modes are very similar to the corresponding transitions in Mg and free-base porphins.[329]

This analysis helps to predict energy transfer pathways and rates in light-harvesting complexes (Section IVD). It may further be used for rationalizing spectroscopic trends in porphyrin-base electronic materials in a search for an optimal chemical structure for optical limiting applications.[24,330,331]

IV. Optical Response of Chromophore Aggregates

Intermolecular interactions and bonding in chromophore aggregates may be directly probed by optical spectroscopy. Organic molecular crystals are typical examples of molecular assemblies whose electronic structure, polarization effects, and transport phenomena have been investigated for decades.[270,271,332] High-temperature superconductivity and lasing have been observed in high purity acene organic crystals.[25,333,334] In addition, extensive experimental and theoretical effort has been devoted to the studies of less ordered systems such as clusters in supersonic beams,[335−339] J-aggregates of cyanine dyes,[8] supramolecular structures,[4,340,341] and biological complexes (photosynthetic antennae and reaction centers).[315−324] Small aggregates may be treated as supermolecules employing standard quantum chemistry methods to calculate their electronic structure.[181,342−347] However,

the ability to relate the electronic states and spectra of aggregates to those of their monomeric building blocks[92,93,95,348] should provide a better microscopic insight into the nature of their electronic excitations and to predict qualitative features of complex large systems using simple, readily available information. Localization of optical excitations in certain regions of a molecule constitutes such a selection rule since it allows us to effectively break the molecule into a subset of coupled chromophores.

The problem is simplified considerably for chromophores, spatially well-separated, whose interactions are purely Coulombic (electron-exchange is negligible).[270,271] Each chromophore then retains its own electrons and the aggregate may be described using the Frenkel exciton Hamiltonian for an assembly of two-level systems:[349−352]

$$H = \sum_n \Omega_n B_n^\dagger B_n + \sum_{n \neq m} J_{nm} B_m^\dagger B_n \qquad (4.1)$$

Here B_n ($B_n^\dagger$) is the annihilation (creation) operator of an excitation localized on the nth chromophore, and Ω_n represents the transition energy from the ground state to the excited state. They satisfy the Pauli commutation rules $[B_n, B_m^\dagger] = \delta_{nm}(1 - B_n^\dagger B_n)$. The interaction between chromophores is described by the hopping parameters J_{nm}. Equation 3.1 is the simplest form of an exciton Hamiltonian. Other terms including high products of B, $B^\dagger$ can generally be included. For spatially well-separated chromophores, this interaction is purely electrostatic.[353−356,181] However, at closer proximity, intermolecular electron exchange processes become allowed,[92,93,181,251,342] making additional contributions to the chromophore couplings. These distinct Coulombic and electron exchange interactions are known as the Förster and the Dexter couplings, respectively. Calculations of optical excitations become considerably more complex when the electronic states are delocalized among the chromophores. This strong intermolecular interaction leads to formation of dynamic excited-state complexes (excimers and exciplexes) which have clear spectroscopic signatures.[357,358] The interplay between the Förster and the Dexter interactions have been extensively studies theoretically using "supermolecular" approach.[92,93,97,251,342] For example, quantum-chemical studies of co-facial PPV chains[251,359,95] reveal the dramatic effect of intermolecular electron exchange processes onto aggregate electronic structure at upon bringing monomer chains into close proximity (3−4 Å). A good review on intermolecular interactions in conjugated materials has been published recently.[181]

The real space CEO analysis provides a practical scheme for dissecting large molecular aggregates into a set of weakly interacting chromophores which do not necessary represent separate molecules.[90] The electronic couplings can be obtained from these computations without invoking the point-dipole[93,316,360] or similar approximations.

A. Excitonic Couplings and Electronic Coherence in Bridged Naphthalene Dimers

We first illustrate the CEO description of the molecular aggregates by analyzing the absorption

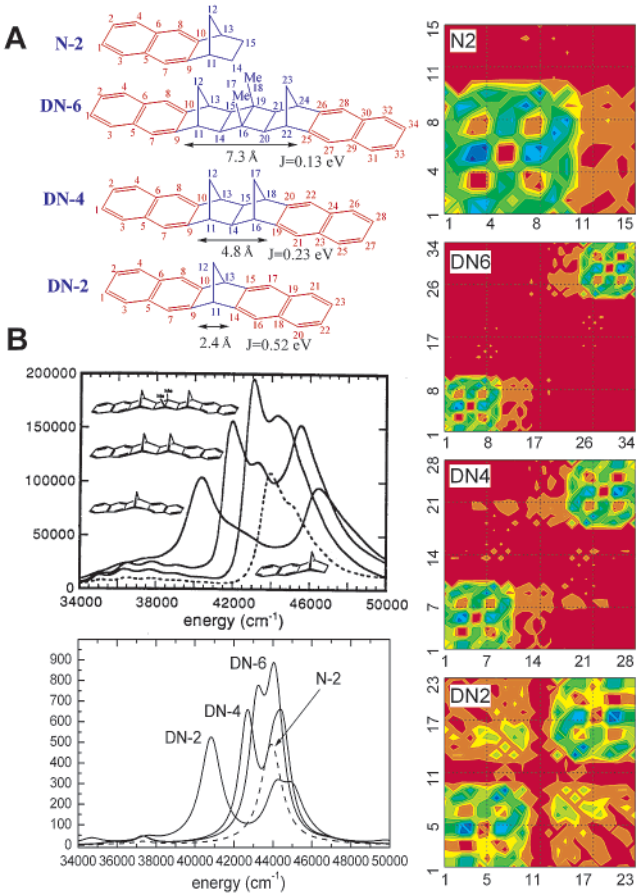

Figure 9. (A) Structures and atom labeling of naphthalene and bridged naphthalene dimer molecules. Molecular geometries were optimized using AM1 model[492] in Gaussian 98 package;[142] (B) UV absorption spectra of the DN-n series. Top: experiment.[361] Bottom: linear absorption profile calculated with line width $\Gamma_\nu = 0.2eV$. Computed absorption spectra are shown in arbitrary units; Contour plots of electronic modes which dominate the absorption spectra of DN-n. The axis labels represent the individual carbon atoms as labeled in the molecular templates (A). Reprinted with permission from ref 342. Copyright 1999 National Academy of Sciences, U.S.A.

spectra of naphthalene and a family of naphthalene−bridge−naphthalene systems DN-2, DN-4, and DN-6 shown in Figure 9A.[361,362] These molecules are essentially dimers where pairs of naphthalene chromophores are held at fixed distances and orientations by a rigid polynorbornyl-type bridge of variable length (two, four, or six σ bonds, respectively). Naphthalene is the smallest molecule in acene family. The UV spectra and radiative decay rates of these dimers have been measured by Scholes and coworkers,[343,344,361,362] and interpreted using a simple exciton model,[350,363] whereby each excited state of the monomer generates two states in the dimer. The interaction between two monomers results in a Davydov splitting of the two dimer states.[349] The estimated splitting using the exciton model was found to be very small compared with the observed value. This discrepancy was attributed to the through-bond interaction mechanism.[343,344,361,362] The exciton model[350] is based on the assumption that the interaction between chromophores is purely electrostatic and could be approximated by dipole−dipole coupling. All

interchromophores charge-transfer processes are neglected.

The CEO/INDO/S approach and Lanczos algorithm were applied to compute the excited-state electronic structure of DN-*n* molecules.[342] Figure 9B compares the calculated UV spectra with low-resolution experimental absorption of N-2 and DN-*n*. The computed trends are consistent with experiment.[342] The dimeric splitting resulting from the major naphthalene absorption band $^1A_g \rightarrow 2^1B_{3u}$ electronic transition of 5.62 eV is clearly observed. With decreasing the bridge length (from DN-6 to DN-2) the coupling between naphthalenes shown in the molecular templates becomes larger and the two primary peaks get far apart. We note that the magnitude of the coupling increases abruptly for molecule with the shortest bridge (DN-2) compared to the other two dimers.

This behavior may be easily rationalized by examining the relevant transition densities corresponding to one component of the Davydov's pair (usually the other component is very similar to the first.[342]) The mode of N-2 molecule (naphthalene with the bridge) shows that the excited electron−hole pair is delocalized over the naphthalene. As expected, the bridge does not participate in the optical excitation since it has no π-bonding network. Panels DN6 show one of the dimer state corresponding to the mode of N-2 where the corners represent the monomers. These are separated by the large bridge, and there is no off-diagonal coherences between monomers. The dimer states are therefore symmetric and antisymmetric combinations of the monomers excited states wave functions (compare to N-2 mode). The interaction between monomers is purely electrostatic and relatively weak, as can be seen from the absence of an off-diagonal block between them. The Frenkel exciton model (eq 4.1) is fully justified for this system.

Compared to DN-6, DN-4 shows a very weak long-range electronic coherence between monomers (off-diagonal blocks of the plot). The chromophores are closer and the dipole−dipole interaction is much stronger, leading to a larger splitting. In addition, weak exchange (Dexter) interaction starts to show up. The exciton model is therefore only marginally applicable to DN-4. Finally, DN-2 is drastically different from the other dimers. Bringing monomers to a close proximity results in large off-diagonal elements (coherences) which is a signature of electronic delocalization between chromophores (i.e., charge separation processes where the electron and hole reside on different monomers become allowed). This leads to a dramatic increase of the splitting and the exciton model completely breaks down for DN-2. These results agree well with experiments and computations of Scholes and co-workers:[343,344,361,362] the exciton model is adequate for excitations of DN-6, DN-4 dimers but is not suitable for DN-2 molecule where electron exchange "through-bond interaction" is dominant. The CEO real-space analysis which allows the separation of electrostatic and exchange interactions in molecular aggregates can therefore be used to establish when the Frenkel exciton model is applicable, and provides a simple algorithm for computing its parameters.

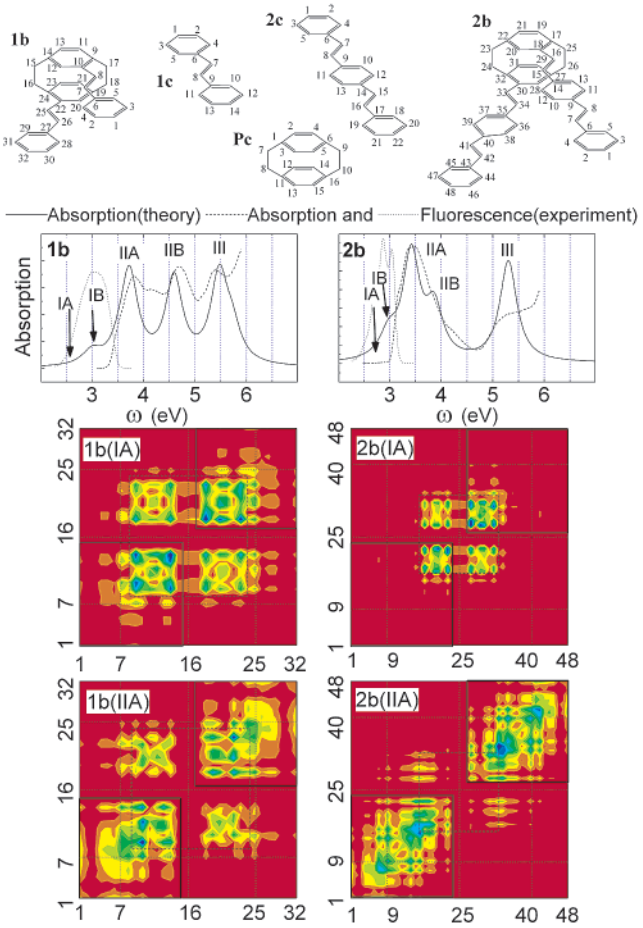

Figure 10. Structures and atom labeling of [2,2]paracyclophane (Pc), stilbenoid monomers (1c, 2c) and dimers (1b, 2b). Geometries were obtained from crystal structure data;[493] calculated (solid lines) and experimental (dashed lines) absorption spectra and experimental (dotted lines) fluorescence spectra of molecular dimers are shown in arbitrary units. Empirical line width $\Gamma_\nu = 0.2eV$ has been used to compute absorption profiles; contour plots of electronic modes which dominate the absorption spectra of 1b and 2b. The axis labels represent the individual carbon atoms as labeled in the molecular templates. Reprinted with permission from ref 92. Copyright 1998 American Chemical Society.

B. Electronic Excitations in Stilbenoid Aggregates

We next examine a more complex case: molecules with a significant through-space π-interaction.[92,359,364] A few members of a family of recently synthesized stilbenoid chromophore dimers with rigid geometry are shown in Figure 10. For reference, we have further considered the monomer units 1c, 2c, as well as [2,2]paracyclophane Pc, which is the central piece of all dimers studied.[348,365] These molecules with rigid structures are representative of chromophore aggregates in solids[353−356] and can be studied in the absence of interactions with other chromophores. They provide insights into chromophore−chromophore interactions which significantly affect the performance of organic optoelectronic materials.[249,366−368]

The CEO/INDO/S calculations combined with the IDSMA algorithm were carried out using geometries obtained from crystallographic X-ray diffraction.[92,359] Experimental absorption and fluorescence spectra of

1b and 2b[92] are displayed in Figure 10 (dashed and dotted lines). The calculated spectra (solid lines) reproduce the main features of the experiment.

To trace the origin of the various peaks, we examined the modes corresponding to these electronic excitations. The lowest-frequency electronic mode IA of 1b and 2b is essentially localized on the paracyclophane; it represents charge delocalization between monomers and has a vanishing oscillator strength. The optical spectrum of paracyclophane has similar transitions. Modes 1b(IIA) and 2b(IIA) resemble bulk modes of the corresponding monomers 1c and 2c (diagonal blocks). 1b(IIA) shows stronger electronic coherences between chromophores (off-diagonal blocks) compared with 2b(IIA). Thus charge delocalization is stronger for the shorter molecule 1b compared with 2b because in the former the electron−hole pair "spends more time" on the Pc unit, which promotes charge delocalization. The structures of 1b(IIB) and 2b(IIB) are similar to 1b(IIA) and 2b(IIB), respectively.[92] The coupling of the monomeric modes 1c(II) thus leads to a Davydov-like splitting resulting in modes IIA and IIB of the dimers.[349] This splitting reflects the exchange-dominated interaction strength between monomers. In contrast with the naphthalene dimers, the Frenkel exciton model is not applicable to these systems.

These electronic modes may be used to predict the observed trends of the experimental fluorescence spectra (dotted curves in Figure 10). Both monomer spectra show distinct vibronic structure and have a similar Stokes shift.[369,370] The fluorescence spectrum of 2b has virtually identical shape to the monomer (2c). In marked contrast, the spectrum of 1b is broad and featureless, shows no vibronic structure, and its shape resembles the fluorescence of Pc. These observations can be explained by assuming that in the short dimer (1b) the optically excited IIA state relaxes to the lower lying IA and IB states. The fluorescence originates from states IA and IB which are red-shifted by 0.93 and 0.8 eV with respect to IIA. The large Stokes shift is thus electronic in origin. In contrast, in the longer dimer (2b), the state IIA is significantly red-shifted since it is delocalized, whereas the states IA and IB do not shift. The separation between II and IA(IB) in the long dimer is only about 0.2 eV, and the emission originates primarily from the initially excited state. This picture is supported by calculations of the radiative decay rates of these molecules[92] which compare well with experiment. The CEO modes thus account for all observed trends in absorption spectra, fluorescence Stokes shift, and radiative lifetimes, and establish a clear connection between the optical response of aggregates and the monomers.

C. Localized Electronic Excitations in Phenylacetylene Dendrimers

Dendrimeric molecules with branched tree-like structures are an interesting novel class of polymers with well controlled structure and size[371−380] (Figure 11). Theoretical interest in these "Cayley trees" (also known as Bethe lattices) arises from their peculiar dimensionality: the connectivity between different sites is one-dimensional (there is only one path to go between two points). However, the number of atoms grows exponentially with generation, as in infinite-dimensional systems. This leads to unusual transport and optical properties. The dynamics of photophysical (electronic and vibrational energy transfer) as well as photochemical processes has been demonstrated to be strongly affected by geometric confinement. Calculating the electronic excitations of these systems, analyzing their nature, and predicting their scaling with molecular size is an open challenge.

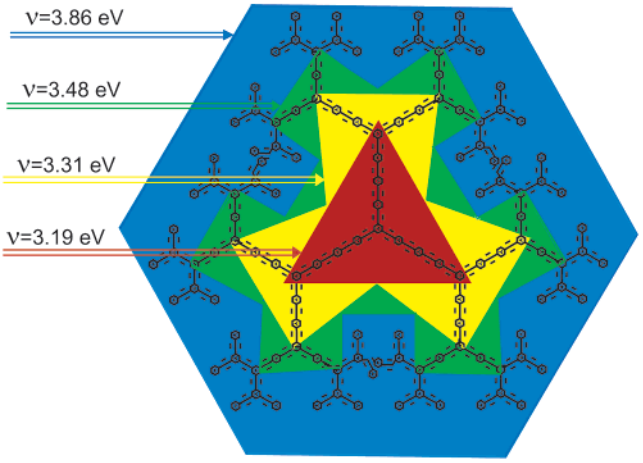

Figure 11. The generations (shown by different colors) in the extended family of phenylacetylene dendrimers have a varying linear segment length; their absorption frequency is therefore blue-shifted for higher generations.[90]

In this section, we discuss these interesting systems and show how they can be dissected into coupled chromophores. Below we present CEO analysis of the absorption spectra of two families of phenylacetylene dendrimers (Figure 12 A and B)[90] made out of phenylacetylene oligomer segments connected through *para*- or *meta*-substitutions of the phenyl rings, leading to linear or zigzag chains, respectively. These macromolecules have been suggested as artificial photonic antenna.[381−384] The construction of artificial light harvesting antennae which mimic the photosynthetic biological complexes has been a long standing goal. Antennae such as family B have an energy gradient that favors the migration of energy toward the center where a reactive site can be placed. The absorption spectra of family A which has the same segment (linear unit) length in the various generations are essentially unchanged with molecular size. Family B (Figure 12) has a varying segment length that decreases toward the periphery. Here the absorption spectra (dashed lines in Figure 12D) show new red-shifted features as the molecular size is increased. The CEO analysis[90] shows how these trends arise naturally from the localized electronic excitations in these systems. It is difficult to anticipate this localization by inspecting the molecular orbitals, since the system is conjugated and the orbitals are delocalized. Nevertheless, the electron−hole pairs which contribute to the elementary optical collective excitations are well localized.

Let us examine the linear (*para*-substituted) molecules (P-series) with $n = 1, 2, 3$ repeat units (triple bonds) and the M7 molecule which consists of linear

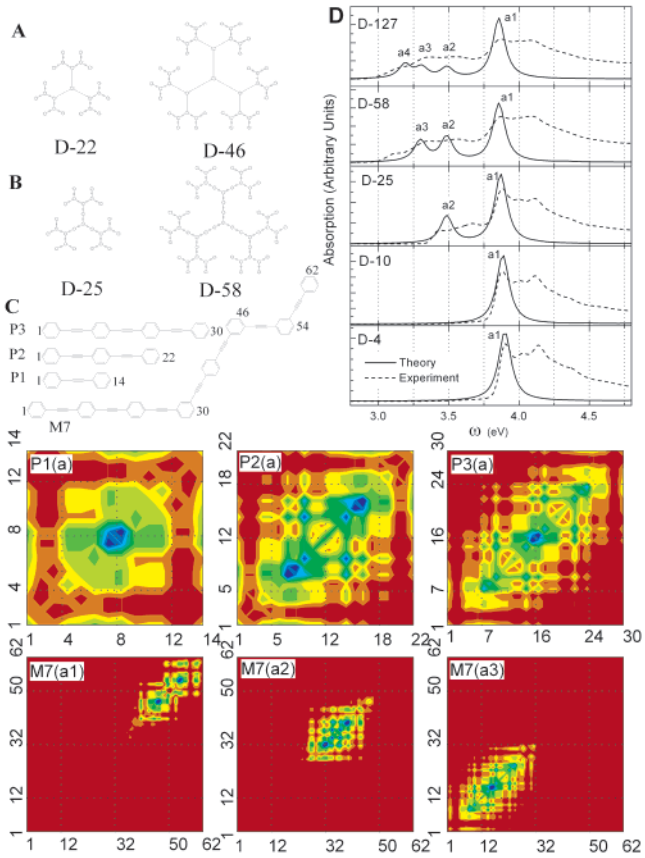

Figure 12. The compact dendrimers (A) are made of the same linear building block P1. The extended dendrimers (B) have a varying linear segment length which decreases for higher generations. **(**C) Structures and atom labeling of the linear *para*-oligomers *Pn* with $n = 1, 2, 3$ repeat units (triple bonds), and the M7 oligomer made of the P1, P2, P3 units conjugated at *meta*-position. (D) Calculated (solid lines) and experimental (dashed lines) absorption spectra of the dendrimers. Empirical line width $\Gamma_\nu = 0.1$ eV has been used to compute absorption profiles. Molecular geometries restricted to planar structures to avoid twisting around the tripple bonds were optimized using AM1 model[492] in Gaussian 98 package;[142] contour plots of the electronic modes which dominate the absorption spectra of the oligomers shown in panel C. The axes represent the carbon atoms. The spectrum of M7 is a sum of P1 + P2 + P3 spectra. Reprinted with permission from ref 90. Copyright 1998 American Chemical Society.

P1, P2, P3 segments connected at the *meta*-position with overall $n = 7$ repeat units and represents a branch of the dendrimers (see Figure 12C).[90] The calculated linear absorption spectra of the P-oligomers have a single low-lying absorption peak (the band-gap transition (a)) which is significantly red-shifted with increasing chain length, similar to peak I of PPV oligomers (Figure 3(I)). The spectrum of M7 is markedly different; the single (a) line is split into three low-frequency transitions (a1, a2, and a3) which have the same frequencies as the band-gap transitions of its building linear blocks: the P1, P2, and P3 oligomers.

The corresponding CEO modes are displayed in Figure 12. The top row of color plots shows the lowest frequency mode (a) of the *para*-oligomers. P1(a) centered at the triple bond shows maximum coherences and is delocalized over the entire molecule. The mode clearly shows that *meta*-carbons 2, 3, 12, and 13 have vanishing electronic coherences with other carbon atoms. This is shown by the "ring" around the plot with small coherences. Analogous patterns can be seen in mode (a) of longer linear oligomers P2, and P3.[90] The mode saturates with size and is no longer confined by the molecular ends. These plots clearly illustrate the two characteristic length-scales corresponding to the variation of the density matrix along the "antidiagonal" L_c and the "diagonal" directions L_d. We found that the coherence size is 5 repeat units similar to that in PPV oligomers (Figure 3). The boundary *meta*-atoms have vanishing coherences in all P-oligomers.

The bottom row of color plots in Figure 12 displays the electronic modes of M7. Mode (a3) is localized at the P3 linear segment of M7 and is virtually identical to mode P3 (a). Similarly, M7(a2) and M7(a1) resemble P2(a) and P1(a), respectively. The absence of coherence across *meta*-substitutions shown in this figure is remarkable; the optical excitations are clearly confined to the various segments. *meta*-conjugation makes a clear barrier for excitonic motion whereas *para*-conjugation is transparent to electronic coherences. This difference does not show up in the ground state, which is very similar for P7 and M7.

Meta-substituents are known to be much less effective in changing reaction rates compared with their *para*-counterparts.[2,3] This can be understood using resonant structures commonly used in organic chemistry which show that charges injected into the system by an nucleophilic or an electrophilic substituent are delocalized only at the *ortho*- and *para*-positions. The CEO modes establish the same trend for electron−hole pairs created by light and provide a direct link between spectroscopy and the well-established Hammet rules for chemical reactivity.[385]

The lack of electronic coherence across *meta*-substitutions suggests that we can describe the optical excitations of dendrimers by dividing them into chromophores with purely Coulombic (no exchange) interactions. In zero-order, we can neglect the interactions among chromophores altogether; the *meta*-conjugated dendrimer behaves as a collection of its linear *para*-conjugated segments which interact with light independently. We modeled the absorption spectra of family A as a collection of P1 chromophores. The spectra thus only show a single low frequency peak. The experimental and the modeled spectra of D-4 and D-10 members of family A are displayed in Figure 12D. The spectra of other generations are very similar.[383] The absorption spectra of family B were calculated similarly by simply adding the spectra of its segments. The resulting calculated and experimental spectra displayed in Figure 12 show that this procedure can reproduce the experimental band edge red-shift trend (see Figure 12) as well as the relative peak intensities in these macromolecules. Subsequent CEO calculations of couplings among chromophores generated an effective Frenkel exciton Hamiltonian which was then used to model the one and two exciton spectra.[237,360,386,387]

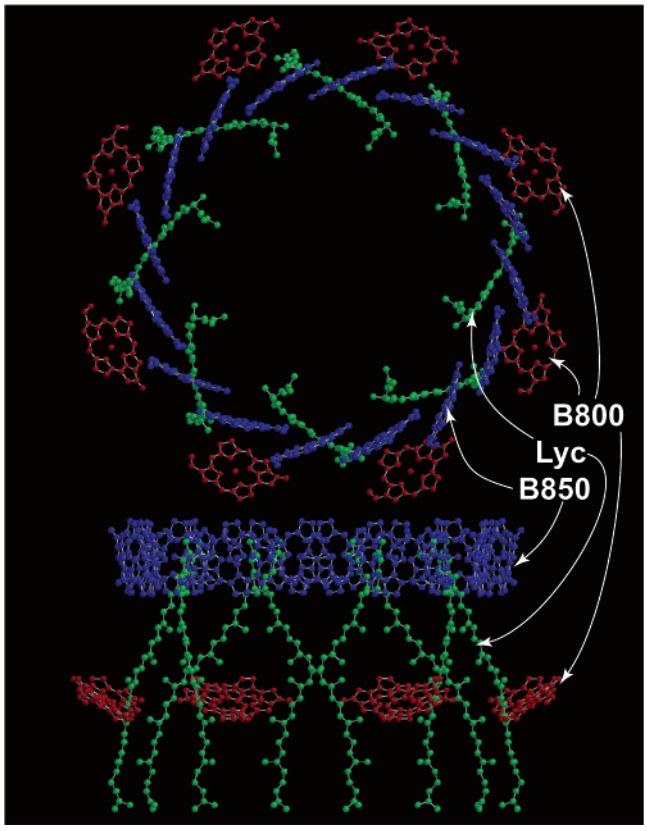

Figure 13. Top and side view of pigments in the light harvesting complex 2 (LH2) of *Rs. molischianum*. The aggregate is made of the upper ring of 16 Bchls-*a* (blue) paired in 8 $\alpha\beta$ heterodimers or intrasubunits (B850 molecules), lower ring of 8 Bchl-*a* (red) (B800 molecules), and ring of 8 lycopenes (carotenoids) (green). Reprinted with permission from ref 94. Copyright 2000 American Chemical Society.

D. Exciton-Coupling for the LH2 Antenna Complex of Purple Bacteria

The primary processes of photosynthesis, the capture of sunlight, and its subsequent conversion into chemical energy, constitute the very basis of all life.[6,7] The photosynthetic unit (PSU) of purple bacteria is the most studied and the best characterized among the known photosynthetic systems.[315−322] The 2.5 Å resolution structure of the *Rs. molischianum* LH2 complex[328] shows 24 bacteriochlorophyll-*a* (Bchl-*a*) monomers arranged in two rings: nine weakly coupled molecules form the outer ring which is responsible for the higher energetic B800 band, while 18 strongly interacting Bchl-*a* of the inner ring form the lower energetic B850 band. A circle of eight carotenoids bridges the B850 and B800 rings (see Figure 13). This high circular symmetry simplifies the computation of intermolecular interaction parameters. Numerous spectroscopic optical measurements which probe for the organization and functionality of the PSU were carried out. Energy-migration in the antenna complexes depends primarily on electronic coupling between the donor and acceptor chromophores.[315−319]

The electronic couplings between chromophores are key factors in determining the rates of energy transfer for weakly coupled B800−B800 and B800−B850 molecules. Energy transfer may be described[388,316] by the Förster incoherent hopping mechanism,[389] where the transfer rate (in ps^{-1}) is given by[390,316]

$$k = 1.18J^2\Theta \qquad (4.2)$$

Here J is the donor−acceptor electronic coupling (in cm^{-1}), and Θ is the overlap integral between donor fluorescence and acceptor absorption line shapes each normalized to a unit area on the cm^{-1} scale. On the other hand, B850−B850 couplings are stronger, exceeding the energetic disorder, and the molecular exciton picture needs to be used for the description of energy migration in the upper B850 ring.[391,392] A point dipole approximation (PDA) assumes that the chromophore sizes are small compared to their separation and the coupling is then given by the interaction between donor and acceptor transition dipole moments. The PDA which is routinely used for evaluating coupling constants does not hold for calculations of J between closely lying chromophores such as in the LH2 system since the chromophore sizes are not small compared to their separation. More accurate computational techniques have been developed.[388,393−397]

The CEO/INDO/S approach was applied toward the study of the electronic excitations of Bchl-*a* and carotenoid aggregates of LH2 complex of *Rs. molischianum*.[93,94,327] The electronic spectra of carotenoids and Bchl were analyzed in Sections IIIB and IIIE, respectively. Below we investigate the relevant electronic modes of the Bchl-*a* dimers, study the effects of aggregation in the LH2 complex, and compute interchromophore couplings. Figure 14A displays the $\alpha\beta$B850 heterodimer (intrasubunit) with atom labeling over β B850 first then over α B850, following the pattern of Figure 8A. The computed oscillator strengths f_ν are plotted vs transition frequencies Ω_ν in Figure 14B. The figure shows that each monomer peak splits into two transitions in the dimer spectra (e.g., $Q_y \rightarrow Q_y - 1$, $Q_y - 2$) showing J-type dimerizations.[270,271]

The ground-state density matrix of $\alpha\beta$B850 ρ is simply the sum of the monomeric ground states (compare to panel ρ in Figure 8), and both Bchls-*a* are clearly seen. The off-diagonal block between chromophores vanishes. Panels Q_y1 and Q_y2 show a pair of states corresponding to the Q_y mode. At the corners, we see the monomers which are separated by ∼9.2 Å Mg−Mg (3.7 Å between the closest atoms). The absence of off-diagonal coherences between Bchls implies that the interaction between chromophores is purely electrostatic, making the Frenkel exciton model applicable.[92,342,386] The 816 cm^{-1} splitting which is a measure of electronic coupling between chromophores provides the necessary information for constructing an effective Hamiltonian.[360,386] Compared with Q_y, the Q_x interaction is weak since the magnitude of Q_x transition dipole is very small. On the other hand, the strong transition dipoles of B_x result in the large coupling. Modes CT1 and CT2 are completely different from the Q and B dimer states. They are delocalized over the off-diagonal regions, reflecting the electronic coherence between chromophores, and have no intramonomer contributions (diagonal regions). The hole created by CT1 excitation

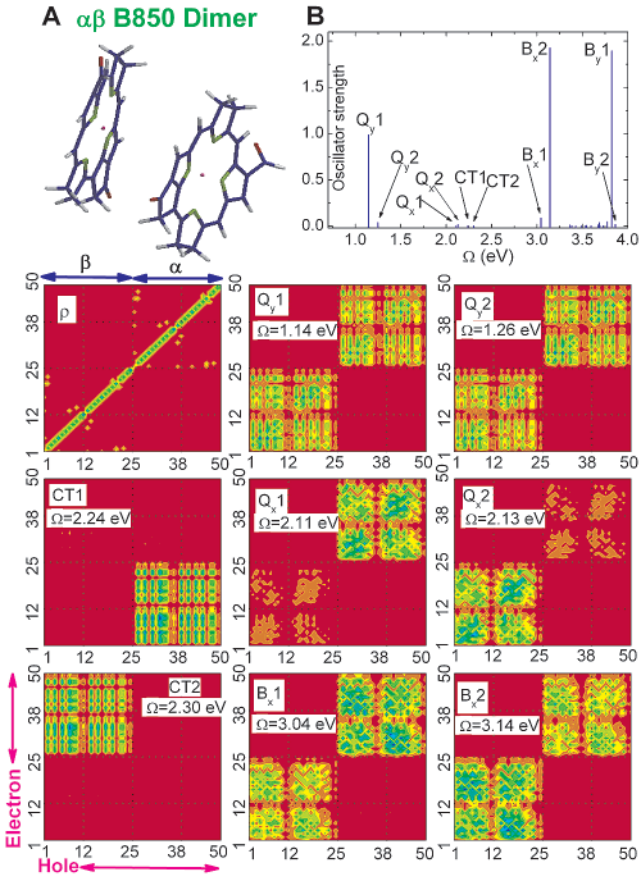

Figure 14. (A) Structure of the $\alpha\beta$ B850 dimer. **(**B) Calculated linear absorption spectrum of $\alpha\beta$ B850 dimer. Contour plots the electronic modes which dominate the optical absorption of B850 dimer. The axis labels represent the individual atoms. Atoms of each monomer are labeled according to panel A of Figure 8. The panels indicate the electronic mode according to panel B. Reprinted with permission from ref 93. Copyright 2000 American Chemical Society.

is localized on αB850 (*x*-axis), whereas the electron is transferred to *β*B850 (*y*-axis). On the other hand, state CT2 describes electron transfer from *β* to α. Thus, CT1 and CT2 correspond to intermolecular charge-transfer excitations. Even though the CT modes are essentially forbidden in linear absorption, they show up in nonlinear optical studies of these aggregates (e.g., electroabsorption).[398] The electronic excitations of other Bchls dimers and Bchl-carotenoid pairs have been similarly analyzed.[93,94]

Two techniques have been employed for calculating the electronic couplings: a spectroscopic procedure that is based on computing the Davydov's splitting in the dimer spectrum,[93,327] and a Coulombic method that computes the electrostatic interactions between transition densities of individual pigments.[93,356] Since the former takes both Coulomb and exchange interactions into account whereas the latter only incorporates the Coulomb interactions, comparison of the results allows the separation electrostatic (Förster) and electron exchange (Dexter) contributions to interchromophore couplings. Examination of the computed couplings[93,94,327] shows that it is essential to take into account dielectric medium effects in order to reproduce experimental transition dipoles of the

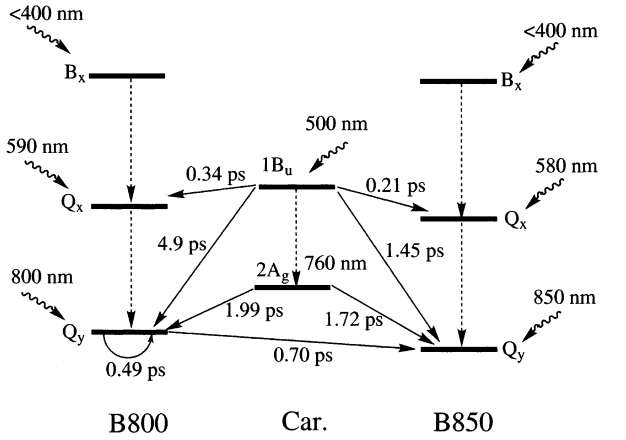

Figure 15. Electronic energy levels, major excitation funneling pathways, and their calculated transfer rates in LH2 of *Rs. molischianum*. Internal conversion is represented by dashed arrows whereas interpigment energy flows are shown by solid arrows. Wavy arrows point to the light-harvesting states. Reprinted with permission from ref 94. Copyright 2000 American Chemical Society.

chromophores (see Table 1) and intermolecular couplings. In general, protein environment screens interaction and reduces couplings up to 30%.[94] Dexter contributions account for approximately 10−15% of the interaction between nearest neighbor Bchls-*a* in the upper B850 ring and is negligible among all other pigments.

The calculated couplings could be immediately employed to estimate intermolecular Förster energy transfer time scales[389] in LH2 complex. Estimates of spectral overlaps in B800−B800, B800−B850, and Lyc-Bchl are available.[390,388] Transfer rates computed by substituting the calculated electronic couplings and spectral overlaps into eq 4.2 are summarized in Figure 15. The Bchl-Bchl time scales agree well with experiment, and the intermolecular Car-Bchl transfer rate from $1B_u$ is found to be comparable to the $1B_u - 2A_g$ internal conversion rate.

V. Discussion

The highly polarizable π-electron system of conjugated molecules forms the basis for their unique electronic and photophysical properties,[399] which are utilized in numerous biological phenomena and make them an important material for technology. The use of conjugated molecules for technological applications is rapidly becoming reality and organic-based devices may compete with traditional semiconductor and liquid crystal based approaches soon. Electronic phenomena traditionally studied in inorganic (semiconductor and strongly correlated) matter have been currently observed in high-quality organic crystals, including fractional quantum hall effect,[333,400] solid-state injection lasing,[25] high-temperature superconductivity[334,401−403] and Josephson effect.[404,405] The possibility to make a transistor based on molecular scale has been recently demonstrated,[406] which may lead to cheaper, faster, and much smaller computer chips, beyond the semiconductor limits.[407] The molecular electronics is a growing research field.[408−413]

Numerous high performance photonic devices fabricated from organic polymers and molecular crystals have been made,[20,21] including light emitting diodes (LEDs)[21,414−419] and electrochemical cells,[420] display panels,[421−423] photovoltaic cells,[424−426] photodetectors,[427−429] transistors,[430−432] light-emitting field-effect transistors,[26,433,434] biosensors,[435] imaging devices,[436,437] and solid-state lasers.[22,25,27,438,439] Organic photonic devices rely on the recombination of electrons and holes photogenerated or injected at the contact and a thorough understanding of the photogeneration[440−445] and charge transport processes[248,446] is necessary to improve operation of these devices. Conjugated molecules are promising for nonlinear optical applications as well.[14,15,31,447,448] Adding an electron-withdrawing and an electron-donating group enhances the nonlinear optical response even further.[10,12−14,18,19,303,308,309,449,450] Understanding the mechanisms leading to dramatic changes in optical polarizabilities with increasing chain length and donor/acceptor strength, and the limiting factors of these enhancements are the key for a rational design strategy of molecules possessing large optical polarizabilities.[266,451]

Conjugated molecules form important groups of natural pigments and play the major roles in fundamental biological phenomena. For example, carotenoids are found in all families of vegetables and animal kingdoms.[452−454] Among the innumerable biological molecules, this class has numerous biophysical applications. Carotenoids play important roles in pharmaceutical and food technology as well. In the photosynthetic apparatus, these molecules appear in antenna complexes that absorb the light and transfer excitations to the reaction centers.[454−456] In addition, they serve as antioxidants by quenching the chlorophyll triplet via energy transfer and preventing the formation of singlet oxygen. The photoisomerization of the closely related retinoids has various physiological functions (e.g., the primary process of vision[455,457] and proton pump). Chlorophylls and porphyrins are the other primary pigments of photosynthesis (Section IVD).[6,7] In addition, metallophthalocyanine complexes and porphyrin derivatives are reverse saturable absorbers,[24,330,331] efficient light-emitters,[458] and nonlinear materials.[459−462] These molecules exhibit improved excited-state absorption and optical limiting, have a large intersystem crossing rate indicated by transmittance and excited-state lifetime measurements. This makes these materials attractive for technology as well.

The study of conjugated molecules has become a research frontier that involves many challenges for theory, experiment, and synthesis. Exploring the electronic structure and spectroscopic properties of the molecular systems constitute an important part of the ongoing global progress. The theoretical and computational approaches such as CEO, which provide means to analyze electronic properties, establish molecular structure−functionality relations, and predict the trends, are useful for this research.

The CEO approach offers numerous computational advantages: instead of arbitrary truncation of molecular orbitals, the fast Krylov space algorithms (Lanczos, Davidson, and IDSMA) take into account all active space included in the TDHF approximation, making such calculations straightforward. Yet, the computational cost per excited state is very low and usually does not exceed that of the ground state. This makes excited-state structure calculations possible whenever SCF ground state computations are available. The electronic density matrix associated with the nonlinear optical response may be easily obtained by summing over the electronic oscillators coupled by relevant nonlinear dipole (see Section F). These oscillators may be grouped into a few effective degrees of freedom using the DSMA algorithm which expresses the molecular optical response in terms of dominant collective variables. Even though the sum-over-states method allows the calculation of any optical response including to strong fields once the eigenstates are known, the SOS approach rapidly becomes more complex with molecular size, since both tasks of calculating the eigenstates and performing the necessary summations over them are very expensive for large systems. The CEO approach carries less information but at considerably lower cost, making it readily applicable to the interesting crossover region between small molecules and bulk. The power of the oscillator picture are particularly apparent in the calculation of nonlinear optical properties.[87,151,300,301] Interference effects in the SOS approach result in a cancellation of large positive and negative contributions to optical susceptibilities,[15,32,33,76,463] limiting the accuracy and making approximate calculations risky (since innocent approximations may lead to huge errors). One manifestation of this problem is that individual terms (Liouville Space Paths)[76] do not have the correct scaling with size. The latter is only obtained once all of the terms are carefully combined. In the oscillator picture, these cancellations are built-in from the start and each separate contribution to the susceptibility scales properly (see Appendix F). The density matrix approach thus guarantees size-consistency providing an adequate real space description of the scaling and saturation of off-resonant linear and nonlinear polarizabilities as shown in Section IIID. For odd response functions such as γ, individual terms which scale as n^2 interfere to yield an n scaling, whereas for even response functions such as β in substituted molecules individual n scaling terms interfere to yield as overall n^0 scaling.[87,151,297,300−302]

Optical excitations move an electron from an occupied to an unoccupied orbital creating an electron−hole pair. The CEO quasiparticle description of the optical response is based on following the simultaneous and coupled dynamics of this pair as given by the two indices of the transition density matrix. The space of higher dimensionality (the pair) captures the essential physics of the optical excitations, and even the simplest (TDHF) factorization yields an adequate description. A real space CEO analysis which pinpoints the origin of each optical transition is obtained by displaying the electronic mode matrices. In semiconductors, the electron−hole pairs are loosely bound and form Wannier excitons.[40,464−467] In molecular

aggregates, each pair is tightly bound and can be considered as a single particle (Frenkel exciton).[270,271] Conjugated molecules are intermediate between these two extremes. The CEO thus offers a unified description of different materials and allows a direct comparison of their optical properties.[468] It is possible to go beyond the semiempirical Hamiltonians and the TDHF approximation and include additional variables, using a different ansatz for the wave function.[128−131,133,209,469] Formally the calculation of optical properties using sums over states is also unified and universal. However, very different approximate schemes and terminologies are used in the calculation of the eigenstates of various systems. This prohibits a clear comparison and obscures the origin of differences. The electronic oscillator picture may be applied to all correlated materials offering an intuitive and simple alternative to common molecular orbital descriptions.

The CEO approach provides a natural framework for predicting and guiding the design molecules with specific properties. Rather than asking which of the many-electron states are most relevant, we can explore how different regions of the molecule couple and affect each other. The electronic excitations of a large molecular system can thus be broken into separate chromophores, despite the delocalized nature of the underlying electronic states. Even when electron (and hole) exchange between segments is blocked, Coulomb interaction does allow the transfer of energy through the migration of electron−hole pairs (excitons). One can then address directly the effects of donor−acceptor substitutions and geometry (see Section IIIB). A new type of chemical intuition which focuses directly on the electronic charges and coherences and is not based on properties of many-electron eigenstates emerges naturally (see Sections III and IV). Much chemical intuition is based on the charge density.[61] The coherences make it possible to directly view how different parts of the molecule are coupled and how a perturbation at one point can affect the electronic motion at other regions. We further note that by treating the electronic degrees of freedom as oscillators we can couple them more naturally to nuclear degrees of freedom, which constitute another set of oscillators. The incorporation of nuclear notions is thus straightforward, and lends itself easily to semiclassical approximations.[75,470] The time-dependent density-matrix should then allow us to follow the dynamics of coherent intramolecular and intermolecular vibrations, solvent modes, and isomerization and account for vibronic structure and line broadening;[471] Interfacing with excited-state molecular dynamics simulations is thus most natural.[228,472,473] This approach allows modeling of complex vibronic phenomena during photoexcitation dynamics on femto- to nanosecond time scales in large molecular systems (up to hundreds of atoms size).[474] Nonadiabatic couplings can also be expressed using the transition density matrices.[78,475] The CEO was recently applied to electron energy loss and X-ray spectroscopy which requires the calculation of the entire wavevector and frequency-dependent electronic structure factor $S(\mathbf{k},\omega)$.[476,477]

VI. Acknowledgments

The research at Rochester is supported by the Chemical Sciences Division of the Office of Basic Energy Sciences of the U.S. Department of Energy, and by the National Science Foundation. The research at LANL is supported by the LDRD program of the U.S. Department of Energy. This support is gratefully acknowledged. S.M. wishes to thank the Alexander von Humboldt Foundation for a Senior Scientist fellowship while the review was being written. We wish to thank Dr. Vladimir Chernyak who was instrumental in developing the CEO method and Dr. Sergei Volkov for his critical comments. Drs. Akira Takahashi, Hong Xiang Wang, Thomas Wagerstreiter, Michael Hartmann, Guanhua Chen, and Eugene V. Tsiper made important contributions to the work surveyed in this article. The late Dr. Michael Zerner provided an invaluable help in combining the CEO with the ZINDO. We dedicate this article to his memory.

VII. Appendix A: The TDHF Equations of Motion of a Driven Molecule

The TDHF equations of motion follow the evolution of the reduced single-electron density matrix eq 1.4 representing the molecule driven by an external field $\rho(t) = \bar{\rho} + \delta\rho(t)$ where the ground-state density matrix $\bar{\rho}$ is the key input to these calculations. The diagonal element ρ_{nn} represents the charge at the nth atomic orbital, and

$$q_{\mathrm{A}} = \sum_{n\in\mathrm{A}} \bar{\rho}_{nn} - Z_{\mathrm{A}} \tag{A1}$$

is the net charge on the atom A. The off-diagonal elements ρ_{nm} ($n \neq m$) represent the electronic coherences between atomic orbitals. In particular, $\bar{\rho}_{n_A m_B}$ describe the chemical bonding strength (bond-order) between atoms A and B. The matrix elements of $\delta\rho_{nm}(t)$ represent the changes in these quantities induced by the external electric field.

We start with the Heisenberg equation of motion for $\rho_{nm}(t) = \langle c_n^\dagger c_m\rangle(t)$:

$$i\frac{\partial \rho_{\mathrm{nm}}}{\partial t} = \langle [c_{\mathrm{n}}^\dagger c_{\mathrm{m}}, H]\rangle \tag{A2}$$

where the Hamiltonian H is given by eq 2.1 and we set $\hbar = 1$. Equation A2 is exact but not closed since higher order products (two-electron density matrices $\rho^{(2)}_{nmn'm'}(t) = \langle c_n^\dagger\, c_m^\dagger c_{n'} c_{m'}\rangle(t)$) show up in the right-hand side. Writing equations of motion for these higher products will yield increasingly higher products. This is the famous hierarchy of many-body dynamics that is common to classical and quantum mechanics. To overcome this difficulty, one needs a truncation procedure. The simplest assumes that the many-body wave function is given by a single Slater determinant at all times. This yields the time-dependent Hartree−Fock factorization[77,81,83,87,156]

$$\langle c_n^\dagger\, c_m^\dagger c_n c_{m'}\rangle(t) = \langle c_n^\dagger c_{n'}\rangle\langle c_m^\dagger c_{m'}\rangle(t) + \langle c_n^\dagger c_{m'}\rangle\langle c_m^\dagger c_{n'}\rangle(t) \tag{A3}$$

Applying this approximation to eq A2 yields the following closed equations of motion for the single-electron density matrix $\rho(t)$.

$$i\frac{\partial\rho(t)}{\partial t} = i\frac{\partial\delta\rho(t)}{\partial t} = [F(\rho), \rho] - \mathcal{E}(t)\cdot[\mu, \rho] \quad \text{(A4)}$$

To zero order in the field, we recover the stationary solution eq 2.9.

This set of $K \times K$ matrix equations may be solved numerically for $\delta\rho(t)$ either in the frequency[151,153] or the time[478] domain. By restricting the number of equations to variables which contain only M occupied−unoccupied orbital pairs, we can develop a convenient algebra of electronic oscillators.[77,156] To that end, we first decompose $\delta\rho(t)$ into two components

$$\delta\rho(t) = \xi(t) + T(\xi(t)) \quad \text{(A5)}$$

where ξ represents the particle−hole (interband) and $T(\xi)$ represents the particle−particle and the hole−hole (intraband) parts.

Since the many-electron wave function is represented by a single Slater determinant, the total density matrix $\rho(t)$ must be a projector at all times:[76,77,83]

$$(\bar{\rho} + \delta\rho(t))^2 = \bar{\rho} + \delta\rho(t) \quad \text{(A6)}$$

This idempotent property of $\bar{\rho}$ allows us to project any single particle matrix ζ into the interband ($p-h$) subspace

$$\zeta_{p-h} = [[\zeta, \bar{\rho}], \bar{\rho}] \quad \text{(A7)}$$

Consequently, not all elements of the density matrix are independent. The number of degrees of freedom of $\delta\rho$ subject to the condition eq A6 is precisely the number of its particle-hole matrix elements,[77] and $T(\xi)$ can therefore be expressed in terms of ξ[96,219] using eq A6 and eq A5

$$T(\xi) = \left(\bar{\rho} - \frac{I}{2}\right)(I - \sqrt{I - 4\xi^2}) \quad \text{(A8)}$$

where I is the unit $K \times K$ matrix. Equation A8 can be expanded in powers of ξ

$$T(\xi) = (I - 2\bar{\rho})(\xi^2 + \xi^4 + 2\xi^6 + \cdots) \quad \text{(A9)}$$

An alternative expansion is[77,81]

$$T(\xi) = \frac{1}{2!}[[\xi, \bar{\rho}], \xi] + \frac{1}{4!}[[\xi, \bar{\rho}], [[\xi, \bar{\rho}], [[\xi, \bar{\rho}], \xi]]] + \cdots \quad \text{(A10)}$$

In eqs A9 and A10, all ξ are taken at time t, $\xi = \xi(t)$. Formally, interband and intraband subspaces of $K \times K$ density matrix have $2N(K - N)$ and $N^2 + (K - N)^2$ dimensions, respectively. These subspaces are clearly decomposed only in the MO representation. Equations A7−A10 provide a convenient way of separating interband and intraband subspaces in an arbitrary (e.g., site) basis set. The expressions in Appendices A−F (except equations in MO representation which include X, Y, p, and q) hold for an arbitrary representation and all entering matrices have $K \times K$ size.

Projecting eq A4 onto the interband subspace using eq A7, we obtain the following closed equations of motion for ξ.

$$i\frac{\partial\xi}{\partial t} - L\xi = R(\xi)_{p-h} - \mathcal{E}(t)\cdot[\mu, \bar{\rho}] \quad \text{(A11)}$$

where L is a linear operator in Liouville space (i.e., superoperator)[77,81,87,300] given by eq 2.19, and

$$R(\xi) = [F(\xi), \xi + T(\xi)] + [F(T(\xi)), \bar{\rho} + \xi] - \mathcal{E}\cdot[\mu, \xi + T(\xi)] \quad \text{(A12)}$$

is the nonlinear part of the equation projected onto the particle−hole subspace (eq A7). The Fock operator F and the Coulomb operator V were defined by eqs 2.11 and 2.12. The equations of motion of ξ (eq A11) have fewer variables than those of $\delta\rho$ (eq A4) but contain additional nonlinearities. However, ξ is the set of truly independent variables that are required to uniquely represent $\delta\rho$.

The time-dependent polarization which determines all optical properties is finally given by

$$P(t) = \mathrm{Tr}(\mu\rho(t)) = \mathrm{Tr}(\mu\xi(t)) + \mathrm{Tr}(\mu T(\xi(t))) \quad \text{(A13)}$$

Equations A11 and A8 constitute the basic TDHF equations.[77] They may be solved by expanding the density matrix in powers of the external field

$$\xi = \xi^{(1)} + \xi^{(2)} + \cdots, \quad T(\xi) = T^{(2)}(\xi) + T^{(3)}(\xi) + \cdots \quad \text{(A14)}$$

where $T^{(j)}(t)$ is expressed in terms of $\xi^{(j)}$ by comparing eq A9 (or eq A10) with eq A14:

$$\begin{aligned} T^{(1)}(t) &\equiv 0 \\ T^{(2)}(t) &= (I - 2\bar{\rho})(\xi^{(1)}(t))^2 \\ T^{(3)}(t) &= (I - 2\bar{\rho})(\xi^{(2)}(t)\xi^{(1)}(t) + \xi^{(1)}(t)\xi^{(2)}(t)) \\ T^{(4)}(t) &= (I - 2\bar{\rho})(\xi^{(3)}(t)\xi^{(1)}(t) + \xi^{(2)}(t)\xi^{(2)}(t) + \xi^{(1)}\xi^{(3)}(t)) \end{aligned} \quad \text{(A15)}$$

The polarization to jth order in the external field $\mathcal{E}(t)$ is calculated by taking the expectation value of the dipole operator μ with respect to the time-dependent density matrix

$$P^{(j)}(t) = \mathrm{Tr}(\mu\delta\rho^{(j)}(t)) \quad \text{(A16)}$$

with

$$\delta\rho^{(j)}(t) = \xi^{(j)}(t) + T^{(j)}(t) \quad \text{(A17)}$$

The original nonlinear eq A11 has thus been transformed into a hierarchy of linear inhomogeneous equations that may be readily solved. To jth order we have

$$i\frac{\partial\xi^{(j)}(t)}{\partial t} - L\xi^{(j)}(t) = \eta^{(j)}(t) \quad \text{(A18)}$$

where the inhomogeneous part $\eta^{(j)}(t)$ is given in terms of $\bar{\rho}$ and lower order $\xi^{(k)}$ $k < j$,

$$\eta^{(1)}(t) = -\mathcal{S}(t)[\mu, \bar{\rho}]$$

$$\eta^{(2)}(t) = [[([V(\delta\rho^{(1)}(t)), \delta\rho^{(1)}(t)] + [V(T^{(2)}(t)), \bar{\rho}] - \mathcal{S}(t)[\mu, \delta\rho^{(1)}(t)]), \bar{\rho}], \bar{\rho}]$$

$$\eta^{(3)}(t) = [[([V(\delta\rho^{(2)}(t)), \delta\rho^{(1)}(t)] + [V(\delta\rho^{(1)}(t)), \delta\rho^{(2)}(t)] + [V(T^{(3)}(t)), \bar{\rho}] - \mathcal{S}(t)[\mu, \delta\rho^{(2)}(t)]), \bar{\rho}], \bar{\rho}] \quad \text{(A19)}$$

The linear and nonlinear optical response is calculated by solving eq A18 either in the frequency or in the time domain. In the frequency, this involves diagonalizing the linearized Liouville operator L which formally requires a large memory ($\sim K^4$ where K is the total number of orbitals in the system). Time-domain calculations do not require a large memory ($\sim K^2$) and may be applied for larger systems.[478] However, evaluating the commutators in eqs 2.19 and A12 is time-consuming. These difficulties have so far limited the solution of eq A18 to basis set size of about 100 functions. Computationally efficient Krylov-space algorithms may be used to overcome this limitation.

VIII. Appendix B: Algebra of Electronic Oscillators

In this appendix, we review the main properties of the tetradic linear $M = N \times (K - N)$ dimensional space defined by the Liouville operator L.[77,81,87,300] We first introduce the following scalar product of any two interband matrices ξ and η which are the elements of this space.[77,81,300,479]

$$\langle \xi | \eta \rangle \equiv \mathrm{Tr}(\bar{\rho}[\xi^{\dagger}, \eta]) \quad \text{(B1)}$$

We have used the bracket to underline the similarity with Dirac's Hilbert space notation. Equation B1 obeys the following properties:

$$\langle \xi | \eta \rangle = \langle \eta^{\dagger} | \xi^{\dagger} \rangle^{*} = -\langle \eta | \xi \rangle \quad \text{(B2)}$$

This is an unusual scalar product. It can further be expressed through the particle−hole (X) and hole−particle (Y) components of the interband density matrix in MO representation as

$$\langle \xi | \eta \rangle \equiv (X_{\xi}, X_{\eta}) - (Y_{\xi}, Y_{\eta}) \quad \text{(B3)}$$

where $\xi = \left[\begin{smallmatrix} X_{\xi} \\ Y_{\xi} \end{smallmatrix}\right]$, $\eta = \left[\begin{smallmatrix} X_{\eta} \\ Y_{\eta} \end{smallmatrix}\right]$, and angular brackets denote standard (Hermitian) scalar product of two vectors. We also note that the commutator of $\bar{\rho}$ with an arbitrary interband matrix $\xi = \left[\begin{smallmatrix} X \\ Y \end{smallmatrix}\right]$ corresponds to transformation $\left[\begin{smallmatrix} X \\ Y \end{smallmatrix}\right] \rightarrow \left[\begin{smallmatrix} X \\ -Y \end{smallmatrix}\right]$.

The main reason for introducing this scalar product is that the Liouville operator L defined by eq 2.19 is Hermitian with respect to this scalar product:

$$\langle L\xi | \eta \rangle = \langle \xi | L\eta \rangle \quad \text{(B4)}$$

The operator adjoint to L,

$$L^{\dagger}\xi = [\xi, F] + V([\xi, \bar{\rho}]) \quad \text{(B5)}$$

is also Hermitian with respect to this scalar product i.e., $\langle L^{\dagger}\xi | \eta \rangle = \langle \xi | L^{\dagger}\eta \rangle$.[219]

The eigenmodes ξ_{ν} and eigenfrequencies Ω_{ν} of L satisfy eq 2.15 and come in conjugate pairs: each vector ξ_{ν} with frequency Ω_{ν} has a counterpart $\xi_{-\nu} = \xi_{\nu}^{\dagger}$ with frequency $\Omega_{-\nu} = -\Omega_{\nu}$. Since L is real, the electronic modes can be taken to be real as well. The electronic modes can be expressed through the particle−hole (X) and hole−particle (Y) components in the MO representation as

$$\xi_{\nu} = \begin{bmatrix} X_{\nu} \\ Y_{\nu} \end{bmatrix}, \xi_{\nu}^{\dagger} = \begin{bmatrix} Y_{\nu} \\ X_{\nu} \end{bmatrix}, \nu = 1, ..., M \quad \text{(B6)}$$

the magnitudes of X elements are usually much larger than Y, since the former includes both the first (CI singles) and the higher order electronic correlations, whereas the latter includes only the second and the higher order electronic correlations present in the RPA.

Similarly, the spectrum of $\hat{L}^{\dagger}$ consists of pairs of conjugated eigenvectors with eigenfrequencies $\pm\Omega_{\nu}$:

$$L^{\dagger}[\xi_{\nu}, \bar{\rho}] = \Omega_{\nu}[\xi_{\nu}, \bar{\rho}], \quad L^{\dagger}[\xi_{\nu}^{\dagger}, \bar{\rho}] = -\Omega_{\nu}[\xi_{\nu}^{\dagger}, \bar{\rho}], \quad \nu = 1, ..., M \quad \text{(B7)}$$

which correspond to $\left[\begin{smallmatrix} X_{\xi} \\ -Y_{\xi} \end{smallmatrix}\right]$ and $\left[\begin{smallmatrix} -Y_{\xi} \\ X_{\xi} \end{smallmatrix}\right]$ pairs of eigenvectors.

A classical mode picture of the optical response may be obtained by constructing the electronic oscillators defined by the coordinate-momentum variables

$$Q_{\nu} = \frac{\xi_{\nu} + \xi_{\nu}^{\dagger}}{\sqrt{2}} \qquad P_{\nu} = -i\frac{\xi_{\nu} - \xi_{\nu}^{\dagger}}{\sqrt{2}} \quad \text{(B8)}$$

In the MO representation P and Q are given by

$$Q_{\nu} = \frac{1}{\sqrt{2}}\begin{bmatrix} X_{\nu} + Y_{\nu} \\ X_{\nu} + Y_{\nu} \end{bmatrix} = \frac{1}{\sqrt{2}}\begin{bmatrix} q_{\nu} \\ q_{\nu} \end{bmatrix}$$

$$P_{\nu} = \frac{-i}{\sqrt{2}}\begin{bmatrix} X_{\nu} - Y_{\nu} \\ -X_{\nu} + Y_{\nu} \end{bmatrix} = \frac{-i}{\sqrt{2}}\begin{bmatrix} p_{\nu} \\ -p_{\nu} \end{bmatrix} \quad \text{(B9)}$$

where $q_{\nu} = X_{\nu} + Y_{\nu}$ and $p_{\nu} = X_{\nu} - Y_{\nu}$. We further define

$$T = A + B \qquad K = A - B, \quad \text{(B10)}$$

which are the stiffness and kinetic energy matrices, respectively. We found that the ξ $\xi^{\dagger}$ variables are more convenient for computing the optical response and the (P, Q) representation is useful for gaining a classical insight. The eigenvalue problem eq 2.15 in these variables becomes

$$Kq_{\nu} = \Omega_{\nu}p_{\nu} \quad Tp_{\nu} = \Omega_{\nu}q_{\nu} \quad \nu = 1, ..., M \quad \text{(B11)}$$

Similarly, P and Q satisfy the relation

$$-iLQ_{\nu} = \Omega_{\nu}P_{\nu} \quad iLP_{\nu} = \Omega_{\nu}Q_{\nu} \quad \nu = 1, ..., M \quad \text{(B12)}$$

We shall adopt the following normalization of the electronic modes:[77]

$$\langle \xi_\alpha | \xi_\beta \rangle = \delta_{\alpha\beta} \qquad \langle \xi_\alpha^\dagger | \xi_\beta \rangle = 0 \tag{B13}$$

$$\langle P_\alpha | Q_\beta \rangle = i\delta_{\alpha\beta} \qquad \langle P_\alpha | P_\beta \rangle = \langle Q_\alpha | Q_\beta \rangle = 0 \tag{B14}$$

In the MO representation this normalization reads:

$$(X_\alpha, X_\beta) - (Y_\alpha, Y_\beta) = \delta_{\alpha\beta} \qquad (p_\alpha, q_\beta) = \delta_{\alpha\beta} \tag{B15}$$

The electronic oscillator is a pair of conjugated electronic modes ($K \times K$ matrices ξ_ν and $\xi_\nu^\dagger$ or P_ν and Q_ν, which have $2M$ interband components X_ν and Y_ν or p_ν and q_ν in MO representation) with frequency Ω_ν. Any interband $K \times K$ matrix ζ can be expanded in the basis set of electronic oscillators as

$$\zeta = \sum_\nu \langle \xi_\nu^\dagger | \zeta \rangle \xi_\nu - \langle \xi_\nu | \zeta \rangle \xi_\nu^\dagger = \sum_\nu \langle Q_\nu | \zeta \rangle iP_\nu - \langle iP_\nu | \zeta \rangle Q_\nu, \nu = 1, ..., M \tag{B16}$$

In the following appendices, we will use several useful identities that hold for any interband matrices ξ and ζ and directly follow from eqs A6−A10 and B1:[77,89,219,81]

$$\xi = \rho\xi + \xi\rho \tag{B17}$$

$$\rho\xi^2 = \xi^2\rho \tag{B18}$$

$$[\xi, \rho] = (I - 2\rho)\xi \tag{B19}$$

$$\xi(I - 2\rho)\xi = -(I - 2\rho)\xi^2 \tag{B20}$$

$$\frac{1}{2}[[\xi, \rho], \xi] = (I - 2\rho)\xi^2 \tag{B21}$$

$$[[\xi, \rho], \zeta] = (I - 2\rho)(\xi\zeta + \zeta\xi) \tag{B22}$$

Finally, the effective single body Coulomb operator V obeys

$$\langle \xi | V(\zeta) \rangle = \langle V(\xi) | \zeta \rangle \tag{B23}$$

IX. Appendix C: The IDSMA Algorithm

The density-matrix-spectral-moments algorithm (DSMA)[81,89,300] is an approximate scheme for solving the TDHF equations that allows us to calculate $\xi^{(j)}$ from the source ($\eta^{(j)}$) by solving eq A18 without a direct diagonalization of L. This is accomplished by computing the set of electronic oscillators that dominate the expansion of $\eta^{(j)}$. Without loss of generality, we can take $\eta^{(j)}(t)$ to be real and express it in terms of our momentum variables as[81,300]

$$\eta^{(j)} = \sum_{\nu=1}^{M} \langle \xi_\nu^\dagger | \eta^{(j)} \rangle \xi_\nu - \langle \xi_\nu | \eta^{(j)} \rangle \xi_\nu^\dagger = \sum_{\nu=1}^{M} \langle Q_\nu | \eta^{(j)} \rangle iP_\nu = \sum_{\nu=1}^{M} \mu_\nu^{(j)} iP_\nu \tag{C1}$$

where $\eta^{(j)}$ can be viewed either in the frequency or in the time domain, and $\mu_\nu^{(j)} = \sqrt{2}\langle x_\nu | \eta^{(j)} \rangle = \langle Q_\nu | \eta^{(j)} \rangle$ are the real frequency (or time) dependent expansion coefficients. These electronic oscillators provide a convenient procedure for solving eq A18.[77]

The formal solution of eq A18 in the time and frequency domain is

$$\xi^{(j)}(t) = \int_0^t d\tau e^{-iL(t-\tau)} \eta^{(j)}(\tau) \qquad \xi^{(j)}(\omega) = \frac{1}{\omega - L}\eta^{(j)}(\omega) \tag{C2}$$

Substituting the expansion (C1) for $\eta^{(j)}$ in these equations and utilizing the eigenvector properties of the modes

$$e^{-iLt}\xi_\nu = e^{-i\Omega_\nu t}\xi_\nu \quad e^{-iLt}\xi_\nu^\dagger = e^{i\Omega_\nu t}\xi_\nu^\dagger$$
$$\frac{1}{\omega - L}\xi_\nu = \frac{1}{\omega - \Omega_\nu}\xi_\nu \quad \frac{1}{\omega - L}\xi_\nu^\dagger = \frac{1}{\omega + \Omega_\nu}\xi_\nu^\dagger \tag{C3}$$

we can recast the solution of eq A18 in terms of eigenmodes ξ_ν and $\xi_\nu^\dagger$ (or P_ν and Q_ν). For example, the jth order interband component of the reduced single-electron density matrix in the frequency domain is given by

$$\xi^{(j)}(\omega) = \sum_{\nu=1}^{M} \mu_\nu^{(j)}(\omega)\left[\frac{\Omega_\nu}{\Omega_\nu^2 - \omega^2}Q_\nu - \frac{i\omega}{\Omega_\nu^2 - \omega^2}P_\nu\right] \tag{C4}$$

Since only few electronic oscillators contribute significantly to the source in the expansion (C1), the summation can be truncated at some effective number of oscillators $M' \ll M$ without sacrificing accuracy.

The family of the density-matrix spectral moments is defined as $S_n \equiv L^n\eta$ which are the expansion coefficients in the short-time evolution of the density-matrix response function. These moments are used to construct the main DSMA equations[81,300]

$$S_n^{(j)} = \sum_{\nu=1}^{M'} \Omega_\nu^n \mu_\nu^{(j)} iP_\nu \qquad n = 0, 2, 4, ..., 2M' - 2 \tag{C5}$$

$$S_n^{(j)} = \sum_{\nu=1}^{M'} \Omega_\nu^n \mu_\nu^{(j)} Q_\nu \qquad n = 1, 3, 5, ..., 2M' - 1 \tag{C6}$$

where $S_0^{(j)} = \eta^{(j)}$ and $S_n^{(j)} = L^n S_0^{(j)}$, $n = 1, 2, ...$ In principle, the spectral moments S_n can be expressed using the electronic normal modes ξ_ν, but the choice of momentum-coordinate Hermitian variables has two advantages: First, it allows the separation of the total system of equations (C5, C6) into two independent subsystems (C5) and (C6), which is computationally preferable. Second, the matrix η, which is the input to the procedure, is Hermitian and expressed through momentum variables (eq C1). The higher moments S_n are, therefore, either momentum or coordinate type.

The scalar products $K_n^{(j)} \equiv \langle S_n^{(j)} | S_{n+1}^{(j)} \rangle$, $n = 1, 2, ...,$ $2M'$ provide a set of equations for the frequencies Ω_ν and effective oscillator strength $f_\nu^{(j)} = 2(\mu_\nu^{(j)})^2\Omega_\nu$ ($f_\nu^{(j)}$ and $\mu_\nu^{(j)}$ depend on the external field (eq A11). For example, for linear response we have $f_\nu^{(1)} \equiv -\mathcal{E}(t)f_\nu$ and $\mu_\nu^{(1)} \equiv -\mathcal{E}(t)\mu_\nu$. Here f_ν and μ_ν are the oscillator strength and the ground-state dipole, respectively.):

$$\sum_{\nu=1}^{M'} f_\nu^{(j)} \Omega_\nu^{2n} = K_n^{(j)} \qquad n = 0, 1, 2, ..., 2M' - 1 \tag{C7}$$

The set of DSMA equations (C5−C7) is now complete.

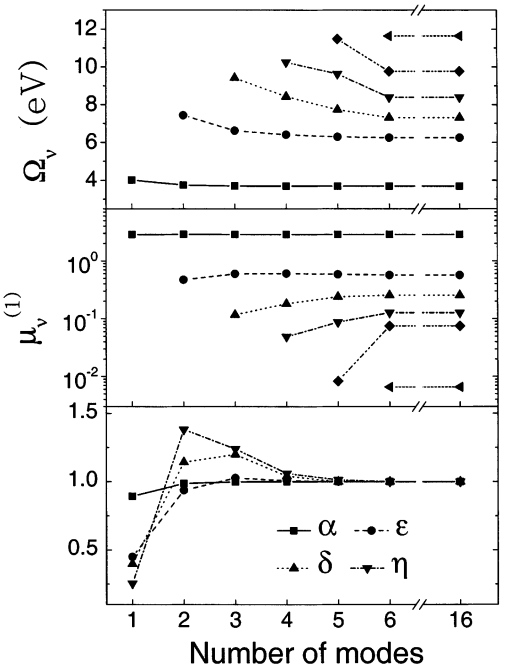

Figure 16. Variation of electronic oscillator frequencies Ω_ν, effective dipole moments $\mu_\nu^{(1)}$, and first (α), third (γ), fifth (ε), and seventh (η) off-resonant polarizabilities with the number of modes used for octatetraene ($N = 8$). The polarizabilities will be defined later in this Section. Here convergence of the DSMA to the full TDHF calculation ($M = 16$ is demonstrated. The magnitudes of polarizabilities are normalized at their converged values: $\alpha = 3.2 \times 10^{-23}$ esu, $\gamma = 6.6 \times 10^{-35}$ esu, $\varepsilon = 1.4 \times 10^{-46}$ esu, $\eta = 2.3 \times 10^{-59}$ esu. Reprinted with permission from ref 300. Copyright 1996 American Institute of Physics.

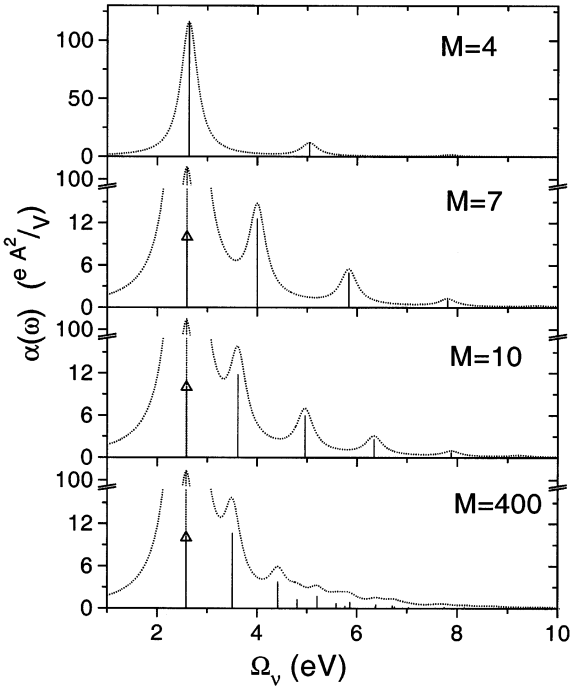

Figure 17. Convergence of the linear absorption (the imaginary part of α (eq 1.5)) with the number of modes used for $N = 40$ atom oligomer. The line width is $\Gamma = 0.2$ eV. Note, that the fundamental band at 2.57 eV with strength 109 eÅ²/V (1.57×10^{-21} esu) remains basically the same in all panels. Reprinted with permission from ref 300. Copyright 1996 American Institute of Physics.

To start our calculations, we compute the moments $S_n^{(j)}$ and $K_n^{(j)}$ by acting Liouville operator L (2.19) on the source $\eta^{(j)}$ and using the scalar product (B1). We then solve eqs C7 for the frequencies Ω_ν and oscillator strengths $f_\nu^{(j)}$. These nonlinear equations have a simple analytical solution.[89] Once we have Ω_ν and $\mu_\nu^{(j)}$, we solve eqs C5 and C6 for the modes P_ν and Q_ν. The most time-consuming part of the DSMA is the calculation of commutators. Typically only a small number of modes is required and the DSMA greatly reduces the numerical effort involved in solving the complete TDHF equations.

The procedure starts with a single mode approximation and by successively adding new modes improved approximations for frequencies and oscillator strengths of the dominant modes is obtained, until some convergence criteria are satisfied. The linear response $j = 1$ is calculated first. The resulting first-order modes are used to calculate the relevant modes for the second-order response ($j = 2$) and so forth. Because of truncation at M′ oscillators, the resulting electronic modes do not coincide with the TDHF modes. Equations B12 hold approximately, but the normalization relations (B14) are satisfied exactly. These effective electronic oscillators give the best approximation for the spectrum with a given number of features (M′).

The following examples use the PPP Hamiltonian to demonstrate the efficiency of the DSMA. Convergence as a function of the number of modes M′, M′ = 1−6 is shown in Figure 16 for octatetraene ($N = 8$). Only few (3−4) modes contribute significantly to the response, but to calculate them accurately we need to include some additional high-frequency modes with very small oscillator strengths. Using six modes, we reproduce the frequencies and the first-order effective dipoles $\mu_\nu^{(1)}$ ($\omega = 0$) to 10^{-8} of the values for the full TDHF (16-mode) calculation. The figure also shows that the polarizabilities converge much faster than the frequencies and dipoles of individual modes. The convergence of the linear absorption (the imaginary part of $\chi^{(1)}$ (eq 1.5)) with the number of modes for a $N = 40$ atom polyacetylene oligomers is displayed in Figure 17. Note that the strong band edge transition is reproduced well even at M′ = 4. The weaker transitions at higher frequencies require more modes. The convergence of the lowest three nonvanishing polarizabilities (α, γ, and ε) of polyacetylene chains with up to 40 carbon atoms as a function of the number of modes used is shown on Figure 18. The linear response is well represented by a single mode calculation, whereas the 8-mode approximation gives adequate values for high hyperpolarizabilities.

One advantage of the DSMA is that it immediately gives a global picture of the entire spectrum. However, the number of effective oscillators M′ cannot be increased at will to improve the accuracy. High moments scale as ($K_n \sim \Omega^{2n}$) and are dominated by the high-frequency tails. Therefore, increasing the number of oscillators does not refine the low and middle frequency range. We found that in practice M′ is limited to ≤ 10−14. Applications of the DSMA using the PPP Hamiltonian which only describes the

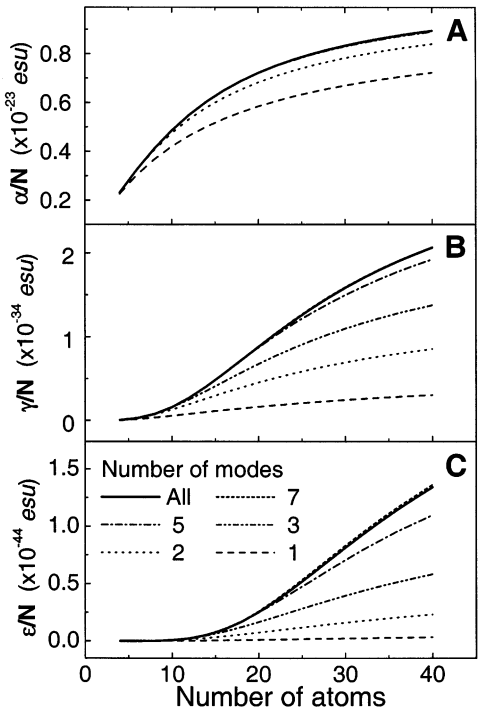

Figure 18. (A−C): convergence of the lowest three nonvanishing polarizabilities (α, γ, and ε) of polyacetylene chains (up to 40 carbon atoms) with the number of modes used for calculations. The polarizabilities will be defined later in this section. Here convergence of the DSMA is demonstrated. The results obtained with the full TDHF calculations (panels A and B) and with $M = 12$ modes (panel C are shown by solid lines. Note that $M = 7$ modes approximation gives good values for hyperpolarizabilities γ, and ε. Reprinted with permission from ref 89. Copyright 1996 Elsevier Science.

π-electron system allowed one to calculate accurately spectra of polyenes dominating by a few resonances. The INDO/S Hamiltonian includes also the valence electrons; therefore, the source is not limited to $\pi-\pi^*$ molecular excitations but also depends on a manifold of high-frequency atomic transitions. For molecules with many peaks in the spectra, the DSMA does not reproduce delicate spectral features such as excitations with a small oscillator strength.

Improved accuracy may be obtained by applying the DSMA iteratively. The DSMA automatically generates orthonormal effective oscillators (eqs B14), which satisfy the eigenvalue equation (B12) in an optimal way. Therefore, each of the effective DSMA modes is a superposition of the exact TDHF modes with similar frequencies. The entire spectrum is thus divided into several regions. Each effective oscillator is responsible for part of the spectrum and is dominated by fewer exact oscillators than the initial source. This property allows one to use any effective mode P_ν as a new fictitious source term $\eta = iP_\nu$ in the DSMA. The resulting oscillators are much closer to the exact ones. This procedure (i.e., using one of the new oscillators as a new fictitious source for the next DSMA level) can be repeated until some convergence criteria are satisfied. This is the iterative DSMA (IDSMA) procedure. In practice, this fictitious source is dominated by a single oscillator (P_1, Q_1) which converges to the exact one. To recover the next mode, the same iterative procedure can be applied with one principal difference: all input sources must be made orthogonal to the lower frequency modes. Thus by using

$$\eta_\perp = \eta - \sum_k^{\text{recovered}} \langle Q_k|\eta\rangle P_k \qquad \text{(C8)}$$

all the recovered modes are excluded from the source in the following calculations. We can continue this iterative process utilizing this orthogonalization procedure to refine several electronic modes. This yields an expansion of the original source and allows us to focus on desirable fine features of the spectrum at high resolution.

The static polarizabilities are readily obtained using eq A13

$$\chi^{(j)} = -\frac{1}{\mathcal{E}_o^k}\mathrm{Tr}(\mu\delta\rho^{(j)}(\omega = 0)) \qquad \text{(C9)}$$

where $\delta\rho^{(j)}(\omega = 0))$ is the jth order of the density matrix induced by the static electric field $\mathcal{E}_o$ and $\chi^{(1)} = \alpha(0)$, $\chi^{(2)} = \beta(0)$, $\chi^{(3)} = \gamma(0)$, etc. The resulting electronic oscillators may be used to construct frequency (time)-dependent optical response. Frequency-dependent response functions up to the third order are expressed using the electronic modes in Appendix F.

The DSMA has a close formal connection with other short-time algorithms widely used in different contexts such as Stieltjes imaging procedure, which approximates a continuous distribution given its low-order moments,[480−482] the Mori-Zwanzig algorithm of reduced dynamics[483,484] and the continued fraction representation of correlation functions.[485] In particular, we note the analogy with the analysis of optical line shapes in terms of spectral moments.[486] The moments can be easily calculated without going through a complex eigenvalue problem, and often very few moments provide for an adequate representation of the line shape.

In summary, the DSMA calculates the optical response by solving the TDHF equations for motion of the single-electron density matrix. The algorithm consists of several levels of increasing complexity. First, the entire optical response with low resolution is recovered at extremely low computational cost. All strong transitions are fully recovered, but the fine structure of spectrum is missing. The iterative DSMA provides more detailed information. The simplest version of this procedure was implemented to calculate the optical response of organic molecules. The band edge transition oscillator was calculated first. The remaining electronic oscillators were recovered sequentially with increasing frequency and were used to compute optical polarizabilities. This approach allows us to recover accurately the experimentally relevant low-frequency spectral region (up to ~8 eV) in conjugated molecular systems.[81,91,92]

X. Appendix D: Lanczos Algorithms

A. Lanczos Algorithm for Hermitian Matrices

The Hermitian Lanczos algorithm finds a few lowest eigenvalues of a Hermitian matrix H by

starting with an arbitrary vector v_0 and constructing linear combinations of vectors $v_m = H^m v_0$, $m = 0, 1, \ldots M'$. The coefficients in the linear combination of v_m are found using the Ritz variational procedure[214,215] which guarantees to yield the best approximation to the lowest eigenvalue of H that belongs to a Krylov subspace. This subspace ($\mathscr{K}_{M'}$) spanned by the vectors $v_0 \ldots v_{M'}$ approximates an invariant subspace of H with increasing accuracy as the number of vectors (M′) is increased.

A simple recursive procedure allows one to build a set of orthogonal vectors w_m spanning the same Krylov subspace. Finding each new vector w_{m+1} only requires the two previous vectors w_m and w_{m-1}:[215,218]

$$w_{m+1} = \beta_{m+1}^{-1}(Hw_m - \alpha_m w_m - \beta_m w_{m-1}), \quad m = 1, \ldots, M' \quad \text{(D1)}$$

At each step m, the pair of coefficients α_m and β_m is chosen to preserve orthonormality of w_{m+1} with respect to w_m and w_{m-1}. The recursion eq D1 ensures that w_m form an orthogonal set and that the Rayleigh-Ritz matrix $\tilde{H}_{mn} = (w_m, Hw_n)$ is symmetric tridiagonal, with the diagonal and subdiagonal given by the coefficients α_m and β_m, respectively.

The matrix $\tilde{H}$ can be viewed as the result of the orthogonal projection of the full matrix H onto the subspace $\mathscr{K}_{M'}$. It can be written in matrix form:

$$\tilde{H} = W_{M'}^{\dagger} H W_{M'} \quad \text{(D2)}$$

where $W_{M'}$ is the rectangular matrix whose columns are the vectors $w_1, \ldots, w_{M'}$. The lowest eigenvalue of $\tilde{H}$ gives approximation to the true lowest eigenvalue of H and the corresponding eigenvector y gives the coefficients of expansion of the eigenvector v of H in the basis of w_m, $v = W_{M'}y$. Indeed, if $\tilde{H}y = \lambda y$, then $(w_m, HW_{M'}y - \lambda W_{M'}y) = 0$, $m = 1, \ldots, M'$, i.e., the residual vector is orthogonal to $\mathscr{K}_{M'}$. Thus, the original eigenvalue problem $Hv_\nu = \Omega_\nu v_\nu$, $\nu = 1, \ldots, M$ has been reduced to eigenvalue problem $\tilde{H}y_\nu = \lambda_\nu y_\nu$, $\nu = 1, \ldots, M'$ in much smaller Krylov space spanned by w_m vectors, which contain an approximation for the original eigenvector. The latter could be found with desirable accuracy by increasing Krylov space dimensionality M′.

The recursive relation (D1) provides a great computational advantage to the Lanczos algorithm, making it applicable to very large matrices, since the required memory does not grow with the number of iterations. The problem of loss of global orthogonality due to computer round-off errors has been extensively studied[214] and is not addressed here.

B. Lanczos-algorithm for Non-Hermitian Matrices

The major difficulty with non-Hermitian matrices is that in general, no variational principle exists for their eigenvalues, and therefore the Ritz procedure is not applicable. In addition, the Lanczos recursion eq D1, which is based on the Hermiticity of H, does not yield an orthonormal set of vectors w_m when applied to a non-Hermitian matrix L. In search of efficient algorithms for RPA problem, the symplectic Lanczos algorithm was suggested by Mei[487] and improved by Benner.[488] This method exploits the analogy between the unitary transformations that preserve Hermiticity and the symplectic transformations that preserve the paired structure of eqs 2.15 and 2.18. The oblique Lanczos algorithm for general non-Hermitian matrices[214] was applied to the TDHF problem in ref 219. However, this method is not stable for some initial trial vectors and should be restarted once it diverges, since it is not based on the of variational principle.

However, even though the RPA-type matrix is non-Hermitian, its block paired structure (eq 2.18) provides some properties similar to the Hermitian matrices. In particular, there exists a variational principle that yields the lowest positive eigenvalue of eq 2.15 suggested by Thouless back in 1961:[210]

$$\Omega_{\min} = \min_{\{X, Y\}} \frac{[X, Y]\begin{pmatrix} A & -B \\ B & -A \end{pmatrix}\begin{bmatrix} X \\ Y \end{bmatrix}}{|(XX) - (YY)|} \quad \text{(D3)}$$

where X and Y span particle−hole and hole−particle components of the interband density matrix, respectively. The minimum always exists, since the HF stability condition eq 2.9 keeps the numerator positive. Note, that the denominator can be arbitrarily small, and therefore the expression has no maximum.

The oblique Lanczos algorithm formulated for RPA[219] was further improved using the Thouless variational principle (eq D3).[220,221] The resulting stable Lanczos procedure efficiently solves RPA eigenvalue problem and is described below. It it convenient to work in the space of coordinate-momentum variables $q = X + Y$ and $p = X - Y$ (eq B9) where the Thouless minimal principle eq D3 is given by

$$\Omega_{\min} = \min_{(pq)=1} \frac{(p, Tp)}{2} + \frac{(q, Kq)}{2}, \quad \text{(D4)}$$

which is the condition for the lowest frequency of a harmonic Hamiltonian system spanning all phase-space configuration $\{P, Q\}$ with normalization condition $(p, q) = 1$ (eq B15). The two terms in the rhs of eq D4 are the kinetic and potential energies of the system at the configuration $\{p, q\}$, respectively.

The minimum of eq D4 can be found using the generalized Lanczos recursion[220,221]

$$q_{m+1} = \beta_{m+1}^{-1}(Tp_m - \alpha_m q_m - \beta_m q_{m-1}) \quad \text{(D5)}$$

$$p_{m+1} = \eta_{m+1}^{-1}(K^{\dagger} q_m - \gamma_m p_m - \eta_m p_{m-1}), \quad m = 1, \ldots, M' \quad \text{(D6)}$$

which generates configuration space vectors $\{q_m, p_m\}$ that span the Krylov subspace of eq D3. The action of operators T and K on vectors p_m and q_m can be computed directly using eq 2.19. Coefficients α_m, β_m, γ_m, and η_m are chosen at each step m to ensure

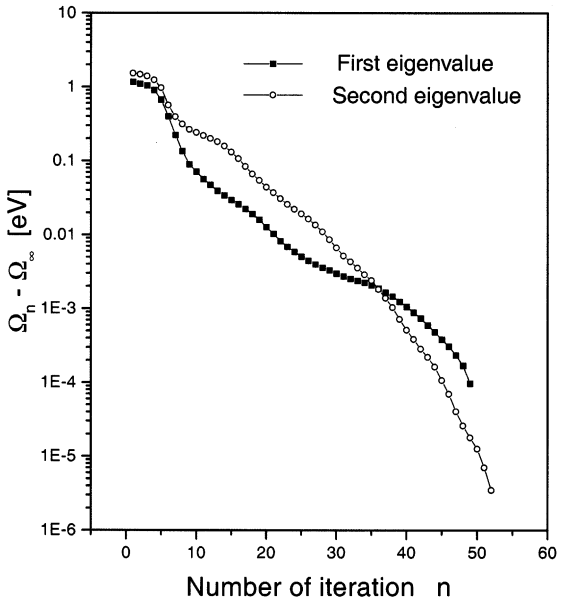

Figure 19. Convergence of the Lanczos algorithm for PPV-4 oligomer. Reprinted with permission from ref 219. Copyright 1996 American Institute of Physics.

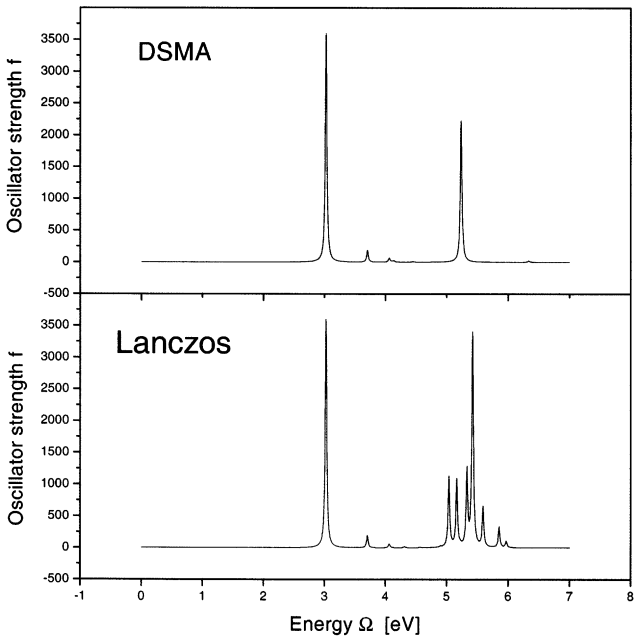

Figure 20. Linear absorption spectrum for PPV-4 oligomer calculated using the DSMA (top panel) and the Lanczos algorithm (bottom panel). Reprinted with permission from ref 219. Copyright 1996 American Institute of Physics.

orthogonality $(q_{m+1}, p_m) = (q_{m+1}, p_{m-1}) = (q_{m-1}, p_m) = (q_{m-1}, p_{m+1}) = 0$. The vectors p_m and q_m form thus a biorthogonal basis, $(q_n, p_m) = \delta_{mn}$, and the matrices $\tilde{K}_{ij} = (q_i, Kq_j)$ and $\tilde{T}_{ij} = (p_i, Tp_j)$ are symmetric tridiagonal, with the only nonzero matrix elements $\tilde{K}_{ii} = \alpha_i$, $\tilde{K}_{i,i-1} = \tilde{K}_{i-1,i} = \beta_i$, $\tilde{T}_{ii} = \eta_i$, and $\tilde{T}_{i,i-1} = \tilde{T}_{i-1,i} = \gamma_i$. Expanding $q = \sum_{m=1}^{M'} c_m q_m$ and $p = \sum_{m=1}^{M'} d_m p_m$ we obtain $2M' \times 2M'$ eigenvalue equation

$$\tilde{K}c_m = \tilde{\Omega}_m d_m \quad Td_m = \tilde{\Omega}_m c_m \quad \nu = 1, ..., M' \quad \text{(D7)}$$

which has the same structure as the original eigenproblem eq D7 but in the space of much lower dimensionality M′. The lowest positive eigenvalue Ω_{min} of eq D7 gives the approximation to the true RPA eigenfrequency. The accuracy increases exponentially with expanding Krylov space dimensionality M′ as illustrated in Figure 19. Similar to the Hermitian Lanczos method, we need to retain only three latest pairs $\{p_m, q_m\}$ of expansion vectors, which ensures minimal memory requirements for this procedure.

The diagonal part of L in the molecular-orbital representation is dominant because the major contribution of the transition frequencies comes from energy differences of occupied-unoccupied molecular orbital pairs. Thus, the diagonal approximation corresponds to the HOMO−LUMO approximation for the transition, and gives reasonable guess for the starting vectors $p^{(1)}$ and $q^{(1)}$. Once the lowest pair of eigenmodes $\{\xi_1, \xi_1^\dagger\}$ (or equivalently $\{p_1, q_1\}$) with $\Omega_1 > 0$ is found, one can work in the orthogonal subspace by choosing initial vectors $p^{(2)}$ and $q^{(2)}$ orthogonal to p_1 and q_1, respectively. All subsequent Lanczos expansion vectors $\{p_m^{(2)}, q_m^{(2)}\}$ will remain orthogonal to $\{p_1, q_1\}$ as follows from eq D4 (the oblique projection may be used to correct the loss of orthogonality at large M′.[214,220,221]) The Lanczos algorithm will thus converge to the second-lowest RPA eigenvalue. Alternatively, the deflection procedure[214,219] could be used for the same purpose. Suppose we have found the j lowest eigenmodes $\xi_{\pm1}$, $\xi_{\pm2}$, ..., $\xi_{\pm j}$. We introduce the deflected operator L_{def}:

$$L_{def}\xi \equiv L\xi + \sum_{\nu=1}^{j} \Delta\{\xi_\nu\langle\xi, \xi_\nu\rangle - \xi_\nu^\dagger\langle\xi, \xi_\nu^\dagger\rangle\} \quad \text{(D8)}$$

where the modes ξ_ν are normalized: $\langle\xi_\nu^\dagger|\xi_\nu\rangle = 1$ for $\nu > 0$. The operator L_{def} has the same eigenmodes as L; however, the eigenvalues of $\xi_{\pm\nu}$ for $\nu = 1, ..., j$ are shifted: $\Omega_{\pm\nu}^{(d)} = \pm(\Omega_\nu + \Delta)$. The next pair of eigenmodes of L, $\xi_{\pm(j+1)}$, thus corresponds to the lowest pair of L_{def}, provided Δ is large enough. Orthogonalization (or deflection) procedures thus allow one to find RPA eigenproblem (eqs 2.15 and 2.18) solutions one by one.

It is illustrative to compare the results of the IDSMA algorithm, which provide an approximate spectrum, and Lanczos algorithm, which provide accurate eigenstates. The PPV-4 oligomer has been computed using oblique Lanczos algorithm (50 modes) and IDSMA (9 modes for each of the three polarization directions).[219] The results shown in the top and bottom panel of Figure 20, respectively, are very close for both algorithms for low-energy spectrum (below 4 eV) where the peaks are well separated energetically. On the other hand, the higher energy (5−6 eV) spectrum has many closely lying modes resolved by the Lanczos algorithm. IDSMA approximates these peaks by a single effective oscillator. Lanczos and IDSMA are thus complementary since they provide "high" and "low" resolution spectra. In particular, the DSMA algorithm is extremely useful for computing off-resonant response because it allows one to take

into account integral effective oscillator contributions from the entire spectrum. In comparison, other algorithms, such as Lanczos and Davidson, are able to calculate contributions to the response only from a narrow spectral region.

XI. Appendix E: Davidson's Algorithm

A. Davidson's Preconditioning

The Hermitian Lanczos algorithm is the best method for approximating extreme eigenvalues, when no extra information about the matrix H is given besides the prescription for computing the matrix−vector products. In some problems, there exists some useful information about the internal structure of H, and preconditioning techniques can speed up the convergence. One of the most widely used methods of this class is the Davidson algorithm[216] that utilizes the information about the diagonal elements of H (e.g., CI Singles matrix $H = A$ in eq 2.18), and requires fewer iterations when the diagonal elements of H are dominant. Davidson derived his method though perturbation analysis for large scale CI calculations.[216] The idea of Davidson's preconditioning is simple. As in the Lanczos algorithm, the eigenvalue problem is solved by projecting the matrix onto a certain subspace $\mathcal{K}_{M'}$ that expands with the number of iterations. In the Lanczos algorithm, the space $\mathcal{K}_{M'}$ is augmented at each iteration step by the residual vector

$$r_{M'} = (H - \lambda_{M'} I) v_{M'} \tag{E1}$$

where $\lambda_{M'}$ and $v_{M'}$ are approximations for an exact eigenvalue and eigenvector, respectively, in the space $\mathcal{K}_{M'}$. In contrast, the Davidson algorithm augments the subspace $\mathcal{K}_{M'}$ by

$$\tilde{r}_{M'} = \frac{1}{D - \lambda_{M'} I}(H - \lambda_{M'} I) v_{M'} \tag{E2}$$

where D is the diagonal part of H (e.g., for $H = A$, $D_{ij} = \epsilon_i - \epsilon_j$ where ϵ_i and ϵ_j are the energies of unoccupied and occupied MOs in eq 2.8). In eqs E1 and E2 vectors $r_{M'}$ and $\tilde{r}_{M'}$, respectively, are intended to be a correction to $v_{M'}$.

To rationalize the merits of Davidson's preconditioning, we recall that the rate of convergence is approximately exponential in the gap ratio[489]

$$\Delta = \frac{\lambda_2 - \lambda_1}{\lambda_M - \lambda_2} \tag{E3}$$

where λ_1, λ_2, and λ_M are the smallest, second, and the largest eigenvalues of H. The convergence thus decreases if the desired eigenvalues are not well separated from the rest of the spectrum. To improve convergence, Lanczos algorithms with preconditioned conjugate gradient method has been developed.[490] In the Davidson expansion eq E2, $1/(D - \lambda_{M'} I)$ can be viewed as approximate inverse of $(H - \lambda_{M'} I)$ if H is dominated by its diagonal elements. Eventually, $\lambda_{M'}$ approaches a true eigenvalue λ and, therefore, the distribution of the eigenvalues of $\Lambda = (H - \lambda I)/(D - \lambda I)$ controls the asymptotic convergence of Davidson's method. We can easily see that the smallest eigenvalue of Λ is 0 and the other eigenvalues have the tendency to be compressed around 1, making the gap ratio eq E3 large and the Davidson's method substantially more efficient than Lanczos when H is dominated by its diagonal elements. We also note that the Davidson algorithm requires the knowledge of the entire basis of the subspace $\mathcal{K}_{M'}$ which imposes heavier memory requirements compared to Lanczos algorithm which only keeps three vectors from $\mathcal{K}_{M'}$.

B. Davidson's Algorithm for Non-Hermitian Matrices

Similarly to Lanczos method for solving the RPA problem eq 2.15, Davidson's algorithm needs to be modified to take into account the block paired structure of eq 2.18 and scalar product eq B1. The first RPA algorithm has been developed by Rettrup[208] and later improved by Olsen.[222] The method has been further refined in ref 79, combined with TDDFT technique, and incorporated into Gaussian 98 package.[142] We will follow ref 79 to describe this method.

We first note that in the space of coordinate-momentum variables q and p (eq B10), the RPA $M \times M$ eigenvalue problem (eq 2.18) can be presented as

$$KT[q] = \Omega^2[q] \tag{E4}$$

where T and K are the stiffness and kinetic energy matrices, respectively. The right and left eigenvectors of this non-Hermitian equation are q_ν and p_ν electronic modes which satisfy eq B11 with $(p_\nu, q_\nu) = 1$ normalization condition (eq B15). Alternatively eq 2.18 can be presented in the form of Hermitian eigenvalue problem:

$$K^{1/2} T K^{1/2}[q'] = \Omega^2[q'] \tag{E5}$$

where $[q'] = K^{-1/2}[q]$. Similarly to the Lanczos procedure, the Davidson's algorithm constructs the reduced analogue of eqs E4 (or E5) in $\mathcal{K}_{M'}$ subspace with $M' \ll M$.

To calculate the first k eigenvectors of L, the algorithm starts from selected trial vectors in the orthonormal subspace b_1, ..., $b_{M'}$, $M' > k$. We next generate configuration space vectors Kb_m and Tb_m, $m = 1$, ..., M' using eq 2.19 (the most intensive CPU step), and form matrices $\tilde{M}^+_{mn} = (b_m, Tb_n)$ and $\tilde{M}^-_{mn} = (b_m, Kb_n)$ $(m, n = 1, ..., M')$. The reduced analogues of eqs E4 and E5 are constructed by computing, respectively,

$$\tilde{M}^{(1)}_{mn} = \sum_k \tilde{M}^-_{mk} \tilde{M}^+_{kn} \tag{E6}$$

$$\tilde{M}^{(2)}_{mn} = \sum_{jk} (\tilde{M})^{-1/2}_{mj} (\tilde{M}^+_{jk}) (\tilde{M}^-_{kn})^{1/2} \tag{E7}$$

Diagonalizing matrix $M^{(1)}$ (or $M^{(2)}$) we obtain the reduced eigenvalues $\tilde{\Omega}_\nu$ which are the approximations

for eigenvalues of L. The approximate eigenvectors of our RPA problem $\tilde{p}_\nu$ and $\tilde{q}_\nu$ are then computed as

$$\tilde{p}_\nu = \sum_m^{M'} L_{m\nu} b_m, \quad \tilde{q}_\nu = \sum_m^{M'} R_{m\nu} b_m, \quad \nu = 1, ..., k \quad \text{(E8)}$$

where $L_{m\nu}$ and $R_{m\nu}$ are the left end right eigenvectors of matrix $M^{(1)}$ (or $M^{(2)}$), respectively. It was found numerically in ref 79 that eq E7 provides faster convergence than eq E6.

To improve the approximation, the dimensionality of $\mathscr{K}_{M'}$ needs to be extended. Following ref 79, we define $2k$ residual vectors

$$r_\nu^p = T[\tilde{q}_\nu] - \tilde{\Omega}_\nu \tilde{p}_\nu \quad r_\nu^q = K[\tilde{p}_\nu] - \tilde{\Omega}_\nu \tilde{q}_\nu \quad \nu = 1, ..., k \quad \text{(E9)}$$

and a set of perturbed vectors using Davidson's preconditioning:[216]

$$(W_\nu)_{ij} = \frac{1}{\tilde{\Omega}_\nu I - D_{ij}} (r_\nu)_{ij} \quad \nu = 1, ..., 2k \quad \text{(E10)}$$

where $D_{ij} = \epsilon_i - \epsilon_j$ (ϵ_i and ϵ_j are the energies of unoccupied and occupied MOs in eq 2.8) and indices i and j run over the particle and hole variables in M space. Finally, we orthogonalize the W_ν vectors among themselves and with respect to the previous expansion vectors b_1, ..., $b_{M'}$, and add them to the expansion set: b_1, ..., $b_{M'+2k}$ expanding M′ to M′ + $2k$. We then start with new expansion set and find new approximations for eigenvalues and eigenvectors of L and so on. This procedure is repeated until the desired convergence criteria are satisfied.

XII. Appendix F: Frequency and Time Dependent Nonlinear Polarizabilities

A. Equation of Motion for Electronic Oscillators and Anharmonicities

We start with the equation of motion for the interband component of the density matrix (eq A11)

$$i\frac{\partial \xi}{\partial t} = L\xi - \mathscr{E}(t)[\mu, \bar{\rho}] - \mathscr{E}(t)[\mu, \xi] - \mathscr{E}(t)[\mu, T(\xi)] + [V(\xi), \xi] + [V(\xi), T(\xi)] + [V(T(\xi)), \xi] + [V(T(\xi)), \bar{\rho}] \quad \text{(F1)}$$

where L is a Liouville operator (eq 2.19), V is a Coulomb operator (eq 2.5), ξ and $T(\xi)$ (eq A8) are interband and intraband parts of the time-dependent single-electron density matrix $\rho(t) = \bar{\rho} + \xi(t) + T(\xi(t))$, respectively. T can be expanded in a Taylor series which contains only even powers of ξ (eqs A9 and A10). For optical signals not higher than third order, it is sufficient to retain only the lowest (second order) term:

$$T(\xi) = \frac{1}{2}[[\xi, \bar{\rho}], \xi] = (I - 2\bar{\rho})\xi^2 \quad \text{(F2)}$$

We next expand $\xi(t)$ in terms of modes ξ_α (eq B16)

$$\xi(t) = \sum_{\alpha>0} (\xi_\alpha z_\alpha(t) + \xi_\alpha^\dagger z_\alpha^*(t)) \quad \alpha = 1, ..., M \quad \text{(F3)}$$

Each oscillator α is described by two conjugated modes ξ_α and $\xi_\alpha^\dagger$. Adopting the notation of refs 77, 207, and 491, we define $\xi_{-\alpha} = \xi_\alpha^\dagger$ and $\Omega_{-\alpha} = -\Omega_\alpha$, so that equation $L\alpha = \Omega_\alpha \xi_\alpha$ would hold for $\alpha = -M$ ..., M. z_α and its complex conjugate $z_{-\alpha} = z_\alpha^*$ constitute the complex oscillator amplitudes. Inserting the expansion eq F3 into eq F1 and using eq F2 gives the following equations for the complex amplitudes,

$$i\frac{\partial z_\alpha}{\partial t} = \Omega_\alpha z_\alpha - \mathscr{E}(t)\mu_{-\alpha} - \mathscr{E}(t)\sum_\beta \mu_{-\alpha,\beta} z_\beta - \mathscr{E}(t)\sum_{\beta\gamma} \mu_{-\alpha,\beta\gamma} z_\beta z_\gamma + \sum_{\beta\gamma} V_{-\alpha,\beta\gamma} z_\beta z_\gamma + \sum_{\beta\gamma\delta} V_{-\alpha,\beta\gamma\delta} z_\beta z_\gamma z_\delta \quad \text{(F4)}$$

The amplitudes for the adjoint (negative frequency) variables are simply the complex conjugates. This nonlinear equation may be solved by expanding $z(t)$ ($z^*(t)$) in powers of the external field $\mathscr{E}(t)$:

$$z(t) = z^{(1)}(t) + z^{(2)}(t) + z^{(3)}(t) + ... \quad \text{(F5)}$$

Similarly, using eqs A13 and F2 we obtain the optical polarization

$$P(t) = \sum_\beta \mu_\beta z_\beta + \frac{1}{2}\sum_{\beta\gamma} \mu_{\beta\gamma} z_\beta z_\gamma. \quad \text{(F6)}$$

In eqs F4 and F6, we only retained terms that contribute to the third-order optical response; $\alpha = 1$, ..., M, β, γ, $\delta = -M$, ..., M, and the coefficients in the rhs could be expressed using identities (B18) − (B23) in the form

$$\mu_\alpha = \mathrm{Tr}([\bar{\rho}, \xi_\alpha][\mu, \bar{\rho}]) = \mathrm{Tr}(\mu\xi_\alpha) \quad \text{(F7)}$$

$$\mu_{\alpha\beta} = \mathrm{Tr}([\bar{\rho}, \xi_\alpha][\mu, \xi_\beta]) = \mathrm{Tr}(\mu(I - 2\bar{\rho})(\xi_\alpha\xi_\beta + \xi_\beta\xi_\alpha)) \quad \text{(F8)}$$

$$\mu_{\alpha,\beta\gamma} = \mathrm{Tr}\left([\bar{\rho}, \xi_\alpha]\left[\mu, \frac{1}{2}[[\xi_\beta, \bar{\rho}], \xi_\gamma]\right]\right) = -\frac{1}{2}\mathrm{Tr}((\mu\xi_\alpha + \xi_\alpha\mu)(\xi_\beta\xi_\gamma + \xi_\gamma\xi_\beta)) \quad \text{(F9)}$$

$$V_{\alpha,\beta\gamma} = \frac{1}{2!}\sum_{\beta\gamma}^{\mathrm{perm}} \left(\mathrm{Tr}([\bar{\rho}, \xi_\alpha][V(\xi_\beta), \xi_\gamma]) + \mathrm{Tr}\left([\bar{\rho}, \xi_\alpha]\left[V\left(\frac{1}{2}[[\xi_\beta, \bar{\rho}], \xi_\gamma]\right), \bar{\rho}\right]\right)\right) = \frac{1}{2}\mathrm{Tr}((I - 2\bar{\rho}) \times ((\xi_\beta\xi_\gamma + \xi_\gamma\xi_\beta)V(\xi_\alpha) + (\xi_\alpha\xi_\beta + \xi_\beta\xi_\alpha)V(\xi_\gamma) + (\xi_\alpha\xi_\gamma + \xi_\gamma\xi_\alpha)V(\xi_\beta))) \quad \text{(F10)}$$

$$V_{\alpha,\beta\gamma\delta} = \frac{1}{3!}\sum_{\beta\gamma\delta}^{\text{perm}}\left(\mathrm{Tr}\left([\bar{\rho},\xi_\alpha]\left[V\left(\frac{1}{2}[\xi_\beta,\bar{\rho}],\xi_\gamma\right],\xi_\delta\right]\right) + \mathrm{Tr}\left([\bar{\rho},\xi_{-\alpha}]\left[V(\xi_\delta),\frac{1}{2}[[\xi_\beta,\bar{\rho}],\xi_\delta]\right]\right)\right) =$$

$$\frac{1}{6}\mathrm{Tr}((I-2\bar{\rho})(\xi_\alpha\xi_\delta+\xi_\delta\xi_\alpha)V((I-2\bar{\rho})(\xi_\beta\xi_\gamma+\xi_\gamma\xi_\beta))) +$$

$$\frac{1}{6}\mathrm{Tr}((I-2\bar{\rho})(\xi_\alpha\xi_\gamma+\xi_\gamma\xi_\alpha)V((I-2\bar{\rho})(\xi_\delta\xi_\beta+\xi_\beta\xi_\delta))) +$$

$$\frac{1}{6}\mathrm{Tr}((I-2\bar{\rho})(\xi_\alpha\xi_\beta+\xi_\beta\xi_\alpha)V((I-2\bar{\rho})(\xi_\delta\xi_\alpha+\xi_\gamma\xi_\delta))) - \frac{1}{6}\mathrm{Tr}((\xi_\alpha V(\xi_\beta)+V(\xi_\beta)\xi_\alpha)(\xi_\gamma\xi_\delta+\xi_\delta\xi_\gamma)) -$$

$$\frac{1}{6}\mathrm{Tr}((\xi_\alpha V(\xi_\gamma)+V(\xi_\gamma)\xi_\alpha)(\xi_\beta\xi_\delta+\xi_\delta\xi_\beta)) - \frac{1}{6}\mathrm{Tr}((\xi_\alpha V(\xi_\beta)+V(\xi_\delta)\xi_\alpha)(\xi_\beta\xi_\gamma+\xi_\gamma\xi_\beta)) \quad \text{(F11)}$$

Here $V_{\alpha,\beta\gamma}$ and $V_{\alpha,\beta\gamma\delta}$ have been symmetrized with respect to all permutations of indices β, γ and β, γ, δ, respectively. These anharmonicities describe coupling among electronic oscillators mediated by Coulomb V and dipole μ interactions (Note that the indices α, β, γ, and δ run over positive and negative modes). μ describes optical transitions between oscillators whereas V describes scattering between oscillators induced by the many-body Coulomb interaction. It is important to note that all the anharmonic coefficients can be calculated using the ground-state density matrix $\bar{\rho}$ as well as the eigenmodes ξ_ν of the linearized TDHF equation. Equations F6 and F4 map the task of computing the optical response of the original many-electron system onto finding the oscillators and the nonlinear couplings μ and V. We further note that the expressions for anharmonicities involving multiplications of electronic modes matrices are better suited for numerical computations than those involving commutators.

B. Definition of Nonlinear Response Functions

Optical polarizabilities are induced by the deviation of the reduced density matrix from its equilibrium value $\bar{\rho}$ expanded in powers of the external field $\mathscr{E}(t)$. Following refs 76 and 77, we define time domain response functions $R^{(j)}(t,\tau_1,...,\tau_j)$ up to the third order ($j = 1,2,3$):

$$P^{(1)}(t) = \int_{-\infty}^{t} d\tau \mathscr{E}(\tau) R^{(1)}(t,\tau) \quad \text{(F12)}$$

$$P^{(2)}(t) = \int_{-\infty}^{t}\int_{-\infty}^{t} d\tau_1 d\tau_2 \mathscr{E}(\tau_1)\mathscr{E}(\tau_2) R^{(2)}(t,\tau_1,\tau_2) \quad \text{(F13)}$$

$$P^{(3)}(t) = \int_{-\infty}^{t}\int_{-\infty}^{t}\int_{-\infty}^{t} d\tau_1 d\tau_2 d\tau_3 \mathscr{E}(\tau_1)\mathscr{E}(\tau_2)\mathscr{E}(\tau_3) R^{(3)}(t,\tau_1,\tau_2,\tau_3) \quad \text{(F14)}$$

The corresponding frequency domain polarizabilities $R^{(j)}(-\omega_s;\omega_1,...,\omega_j)$ ($j = 1,2,3$) are defined by

$$P^{(1)}(\omega_s) = \int_{-\infty}^{\infty}\frac{d\omega}{2\pi} R^{(1)}(-\omega_s;\omega)\mathscr{E}(\omega) \quad \text{(F15)}$$

$$P^{(2)}(\omega_s) = \int_{-\infty}^{\infty}\int_{-\infty}^{\infty}\frac{d\omega_1 d\omega_2}{2\pi\ 2\pi} R^{(2)}(-\omega_s;\omega_1,\omega_2)\mathscr{E}(\omega_1)\mathscr{E}(\omega_2) \quad \text{(F16)}$$

$$P^{(3)}(\omega_s) = \int_{-\infty}^{\infty}\int_{-\infty}^{\infty}\int_{-\infty}^{\infty}\frac{d\omega_1 d\omega_2 d\omega_3}{2\pi\ 2\pi\ 2\pi} R^{(3)} \times (-\omega_s;\omega_1,\omega_2,\omega_3)\mathscr{E}(\omega_1)\mathscr{E}(\omega_2)\mathscr{E}(\omega_3) \quad \text{(F17)}$$

Here $\mathscr{E}(\omega)$ is the Fourier transform of the time-dependent external field $\mathscr{E}(t)$ defined as

$$f(\omega) \equiv \int dt f(t) e^{i\omega t} \qquad f(t) \equiv \frac{1}{2\pi}\int d\omega f(\omega) e^{-i\omega t} \quad \text{(F18)}$$

The relations between response functions and polarizabilities are obtained by comparing eqs F12−F14 with eqs F15−F17 and using the Fourier transform eq F18:

$$R^{(1)}(-\omega_s;\omega) = \int_{-\infty}^{\infty} dt e^{i\omega_s t}\int_{-\infty}^{t} d\tau e^{-i\omega\tau} R^{(1)}(t,\tau) \quad \text{(F19)}$$

$$R^{(2)}(-\omega_s;\omega_1,\omega_2) = \int_{-\infty}^{\infty} dt e^{i\omega_s t}\int_{-\infty}^{t} d\tau_1 e^{-i\omega_1\tau_1}\int_{-\infty}^{t} d\tau_2 e^{-i\omega_2\tau_2} R^{(2)}(t,\tau_1,\tau_2) \quad \text{(F20)}$$

$$R^{(3)}(-\omega_s;\omega_1,\omega_2,\omega_3) = \int_{-\infty}^{\infty} dt e^{i\omega_s t}\int_{-\infty}^{t} d\tau_1 e^{-i\omega_1\tau_1}\int_{-\infty}^{t} d\tau_2 e^{-i\omega_2\tau_2} \times \int_{-\infty}^{t} d\tau_3 e^{-i\omega_3\tau_3} R^{(3)}(t;\tau_1,\tau_2,\tau_3). \quad \text{(F21)}$$

The linear, second, and third order polarizabilities are usually denoted α, β, and γ, respectively

$$R^{(1)}(\omega_s = \omega;\omega) = 2\pi\delta(-\omega_s+\omega)\alpha(\omega) \quad \text{(F22)}$$

$$R^{(2)}(\omega_s = \omega_1+\omega_2,\omega_1,\omega_2) = 2\pi\delta(-\omega_s+\omega_1+\omega_2)\beta(\omega_1,\omega_2) \quad \text{(F23)}$$

$$R^{(3)}(\omega_s = \omega_1+\omega_2+\omega_3;\omega_1,\omega_2,\omega_3) = 2\pi\delta(-\omega_s+\omega_1+\omega_2+\omega_3)\gamma(\omega_1,\omega_2,\omega_3) \quad \text{(F24)}$$

C. Linear Response

We use the linear response to illustrate the strategy of computing polarizabilities. We start with the equation of motion for $z_\alpha^{(1)}$ obtained from eq F4 using expansion eq F5:

$$i\frac{\partial z_\alpha^{(1)}}{\partial t} = \Omega_\alpha z_\alpha^{(1)} - \mathscr{E}(t)\mu_{-\alpha} \quad \alpha = 1,...,M \quad \text{(F25)}$$

The solution of this equation for $z_\alpha^{(1)}$ and its complex conjugate $z_\alpha^{*(1)}$ is

$$z_\alpha^{(1)} = i\int_{-\infty}^{t}\mathscr{E}(\tau)\mu_{-\alpha}G_\alpha(t-\tau) \quad \alpha > 0 \quad \text{(F26)}$$

$$z_\alpha^{*(1)} = z_{-\alpha}^{(1)} = -i\int_{-\infty}^{t}\mathscr{E}(\tau)\mu_\alpha G_\alpha^*(t-\tau) \quad \alpha > 0 \quad \text{(F27)}$$

where we introduce time-domain Green function

$$G_\alpha(t) = \theta(t)e^{-i\Omega_\alpha t} \quad G_{-\alpha}(t) = \theta(t)e^{-i\Omega_{-\alpha} t} = \theta(t)e^{i\Omega_\alpha t} \tag{F28}$$

and $\theta(t)$ is the Heavyside step function. Using the notation $S_\alpha = \mathrm{sign}(\alpha)$, eqs F4 and eqs F4 can be represented in a compact notation.

$$z_\alpha^{(1)} = iS_\alpha \int_{-\infty}^{t} \mathscr{E}(\tau)\mu_{-\alpha}G_\alpha(t-\tau) \quad \alpha = -M, ..., M \tag{F29}$$

where positive and negative α correspond to $z_\alpha^{(1)}$ and $z_\alpha^{*(1)}$, respectively.

Inserting eq F29 into eq F6 we finally obtain for the linear polarizability

$$P^{(1)}(t) = \sum_{\alpha=-M,...,M} z_\alpha^{(1)}\mu_\alpha = \sum_{\alpha=-M,...,M} iS_\alpha \int_{-\infty}^{t} \mathscr{E}(\tau)\mu_{-\alpha}\mu_\alpha G_\alpha(t-\tau) \tag{F30}$$

The linear response function (eq F12) is then

$$R^{(1)}(t,\tau) = i \sum_{\alpha=-M,...,M} iS_\alpha\mu_{-\alpha}\mu_\alpha G_\alpha(t-\tau) \tag{F31}$$

Using eqs F19 and F22, we obtain the linear polarizability

$$\alpha(\omega) = \sum_{\alpha=-M,...,M} \frac{S_\alpha\mu_{-\alpha}\mu_\alpha}{\Omega_\alpha - \omega} = \sum_{\alpha=1,...,M} \frac{2\Omega_\alpha|\mu_\alpha|^2}{\Omega_\alpha^2 - \omega^2} \tag{F32}$$

Here and below Ω_α is positive (negative) for all $\alpha > 0$ ($\alpha < 0$) according to the convention $\Omega_{-\alpha} = -\Omega_\alpha$. Finally, the expression for static linear polarizability can be obtained from eq F32 by setting $\omega = 0$:

$$\alpha(0) = \sum_{\alpha=1,...,M} \frac{2|\mu_\alpha|^2}{\Omega_\alpha} \tag{F33}$$

D. Second-Order Response

The equation of motion for $z_\alpha^{(2)}$ is

$$i\frac{\partial z^{(2)}}{\partial t} = \Omega_\alpha z_\alpha^{(2)} - \mathscr{E}(t)\sum_\beta \mu_{-\alpha,\beta} z_\beta^{(1)} + \sum_{\beta,\gamma} V_{-\alpha\beta\gamma} z_\beta^{(1)} z_\gamma^{(1)} \quad \alpha = 1, ..., M, \beta,\gamma = -M,..., M \tag{F34}$$

and its solution, which includes complex conjugate, is

$$z_\alpha^{(2)} = i\int_{-\infty}^{t} d\tau_1 S_\alpha G_\alpha(t-\tau_1)\Gamma_\alpha^{(2)}(\tau_1) \quad \alpha = -M, ..., M \tag{F35}$$

where

$$\Gamma_\alpha^{(2)}(\tau_1) = \sum_{\beta\gamma} V_{-\alpha\beta\gamma} \int_{-\infty}^{\tau_1}\int_{-\infty}^{\tau_1} d\tau_2 d\tau_3 \mathscr{E}(\tau_2) \times \mathscr{E}(\tau_3)\mu_{-\beta}\mu_{-\gamma}S_\beta S_\gamma G_\beta(\tau_1-\tau_2)G_\gamma(\tau_1-\tau_3) + i\mathscr{E}(\tau_1)\sum_\beta \mu_{-\alpha\beta}\int_{-\infty}^{\tau_1} \mathscr{E}(\tau_2)\mu_{-\beta}S_\beta G_\beta(\tau_1-\tau_2), \quad \alpha, \beta, \gamma = -M, ..., M \tag{F36}$$

Inserting eqs F29 and F35 into eq F6 and keeping all terms up to the second-order, we find that the second-order response function has three contributions:

$$R^{(2)}(t,\tau_1\tau_2) = R_{\mathrm{I}}^{(2)} + R_{\mathrm{II}}^{(2)} + R_{\mathrm{III}}^{(2)} \tag{F37}$$

where

$$R_{\mathrm{I}}^{(2)}(t,\tau_1\tau_2) = -\sum_{\alpha\beta}\mu_{-\alpha,\beta}\mu_\alpha\mu_{-\beta}S_\alpha S_\beta G_\alpha(t-\tau_1)G_\beta(\tau_1-\tau_2) \tag{F38}$$

$$R_{\mathrm{II}}^{(2)}(t,\tau_1\tau_2) = i\int_{\tau_2}^{t} d\tau \sum_{\alpha\beta\gamma} V_{-\alpha\beta\gamma}\mu_\alpha\mu_{-\beta}\mu_{-\gamma}S_\alpha S_\beta S_\gamma G_\alpha(t-\tau) \times G_\beta(\tau-\tau_1)G_\gamma(\tau-\tau_2) \tag{F39}$$

$$R_{\mathrm{III}}^{(2)}(t,\tau_1\tau_2) = -\sum_{\alpha\beta}\mu_{\alpha\beta}\mu_{-\alpha}\mu_{-\beta}S_\alpha S_\beta G(t-\tau_1)G(t-\tau_2) \tag{F40}$$

Using eq F20, we finally obtain the second-order polarizability which is symmetric with respect to ω_1 and ω_2 permutations

$$\beta(\omega_1,\omega_2) = -\sum_{\alpha\beta\gamma}\frac{V_{-\alpha,\beta\gamma}\mu_\alpha\mu_{-\beta}\mu_{-\gamma}S_\alpha S_\beta S_\gamma}{(\Omega_\alpha - \omega_1 - \omega_2)(\Omega_\beta - \omega_1)(\Omega_\gamma - \omega_2)} + \frac{1}{2}\sum_{\alpha\beta}\frac{\mu_{-\alpha\beta}\mu_\alpha\mu_{-\beta}S_\alpha S_\beta}{(\Omega_\alpha - \omega_1 - \omega_2)(\Omega_\beta - \omega_2)} + \frac{1}{2}\sum_{\alpha\beta}\frac{\mu_{-\alpha\beta}\mu_\alpha\mu_{-\beta}S_\alpha S_\beta}{(\Omega_\alpha - \omega_1 - \omega_2)(\Omega_\beta - \omega_1)} + \frac{1}{2}\sum_{\alpha\beta}\frac{\mu_{\alpha\beta}\mu_{-\alpha}\mu_{-\beta}S_\alpha S_\beta}{(S_\alpha\Omega_\alpha - \omega_1)(S_\beta\Omega_\beta - \omega_2)}, \quad \alpha, \beta, \gamma = -M, ..., M \tag{F41}$$

Here and below Ω_ν, $\nu = \alpha, \beta, \gamma$, is positive (negative) for all $\nu > 0$ ($\nu < 0$) according to the convention $\Omega_{-\nu} = -\Omega_\nu$. Finally, by setting ω_1 and ω_2 to zero and using identities $S_\nu\Omega_\nu = |\Omega_\nu|$ and $\mu_{-\nu} = \mu_\nu$ we obtain the second-order static polarizability:

$$\beta(0) = -\sum_{\alpha\beta\gamma}\frac{V_{\alpha,\beta\gamma}\mu_\alpha\mu_\beta\mu_\gamma}{|\Omega_\alpha\Omega_\beta\Omega_\gamma|} + \frac{3}{2}\sum_{\alpha\beta}\frac{\mu_{\alpha\beta}\mu_\alpha\mu_\beta}{|\Omega_\alpha\Omega_\beta|} \quad \alpha, \beta, \gamma = -M, ..., M \tag{F42}$$

E. Third-Order Response

The equation of motion for $z_\alpha^{(3)}$ is

$$i\frac{\partial z_\alpha^{(3)}}{\partial t} = \Omega_\alpha z_\alpha^{(3)} - [\mathcal{E}(t)\sum_\beta \mu_{-\alpha\beta} z_\beta^{(2)} + \mathcal{E}(t)\sum_{\beta\gamma} \mu_{-\alpha\beta\gamma} z_\beta^{(1)} z_\gamma^{(1)} - 2\sum_{\beta\gamma} V_{-\alpha\beta\gamma} z_\beta^{(1)} z_\gamma^{(2)} - \sum_{\beta\gamma\delta} V_{-\alpha\beta\gamma\delta} z_\beta^{(1)} z_\gamma^{(1)} z_\delta^{(1)}] \quad \alpha = 1, ..., M, \beta, \gamma, \delta = -M, ..., M \quad \text{(F43)}$$

and its solution, which includes the complex conjugate, is

$$z_\alpha^{(3)} = i\int_{-\infty}^{t} d\tau_1 S_\alpha G_\alpha(t-\tau_1)\Gamma_\alpha^{(3)}(\tau_1) \quad \alpha = -M, ..., M \quad \text{(F44)}$$

where

$$\Gamma_\alpha^{(3)}(\tau_1) = \mathcal{E}(\tau_1)\sum_\beta \mu_{-\alpha\beta} z_\beta^{(2)}(\tau_1) + \mathcal{E}(\tau_1)\sum_{\beta\gamma} \mu_{-\alpha\beta\gamma} z_\beta^{(1)}(\tau_1) z_\gamma^{(1)}(\tau_1) - 2\sum_{\beta\gamma} V_{-\alpha\beta\gamma} z_\beta^{(1)}(\tau_1) z_\gamma^{(2)}(\tau_1) - \sum_{\beta\gamma\delta} V_{-\alpha\beta\gamma\delta} z_\beta^{(1)}(\tau_1) z_\gamma^{(1)}(\tau_1) z_\delta^{(1)}(\tau_1) \quad \text{(F45)}$$

Here $\alpha, \beta, \gamma, \delta = -M, ..., M$ and $z^{(1)}(\tau_1)$ and $z^{(2)}(\tau_1)$ are given by eqs F29 and F35. Inserting eqs F29, F35, and F44 into eq F6 and keeping all terms up to third-order we obtain the following 8-term expression for the third-order response function:

$$R^{(3)}(t,\tau_1\tau_2\tau_3) = R_{\mathrm{I}} + R_{\mathrm{II}} + R_{\mathrm{III}} + R_{\mathrm{IV}} + R_{\mathrm{V}} + R_{\mathrm{VI}} + R_{\mathrm{VII}} + R_{\mathrm{VIII}} \quad \text{(F46)}$$

where

$$R_{\mathrm{I}}^{(3)}(t,\tau_1\tau_2\tau_3) = -i\sum_{\alpha\beta\gamma} \mu_{-\alpha\beta}\mu_{-\beta\gamma}\mu_\alpha\mu_{-\gamma} S_\alpha S_\beta S_\gamma G_\alpha \times (t-\tau_1)G_\beta(\tau_1-\tau_2)G_\gamma(\tau_2-\tau_3) \quad \text{(F47)}$$

$$R_{\mathrm{II}}^{(3)}(t,\tau_1\tau_2\tau_3) = -\sum_{\alpha\beta\gamma\delta} \mu_{-\alpha\beta} V_{-\beta\gamma\delta}\mu_\alpha\mu_{-\gamma}\mu_{-\delta} S_\alpha S_\beta S_\gamma S_\delta \times \int_{\tau_3}^{t} d\tau G_\alpha(t-\tau_1)G_\beta(\tau_1-\tau)G_\gamma(\tau-\tau_2)G_\delta(\tau-\tau_3) \quad \text{(F48)}$$

$$R_{\mathrm{III}}^{(3)}(t,\tau_1\tau_2\tau_3) = -i\sum_{\alpha\beta\gamma} \mu_{-\alpha\beta\gamma}\mu_\alpha\mu_{-\beta}\mu_{-\gamma} S_\alpha S_\beta S_\gamma G_\alpha \times (t-\tau_1)G_\beta(\tau_1-\tau_2)G_\gamma(\tau_1-\tau_3) \quad \text{(F49)}$$

$$R_{\mathrm{IV}}^{(3)}(t,\tau_1\tau_2\tau_3) = -2\sum_{\alpha\beta\gamma\delta} V_{-\alpha\beta\gamma}\mu_{-\gamma\delta}\mu_\alpha\mu_{-\beta}\mu_{-\delta} S_\alpha S_\beta S_\gamma S_\delta \times \int_{\tau_3}^{t} d\tau G_\alpha(t-\tau)G_\beta(\tau-\tau_1)G_\gamma(\tau-\tau_2)G_\delta(\tau_2-\tau_3) \quad \text{(F50)}$$

$$R_{\mathrm{V}}^{(3)}(t,\tau_1\tau_2\tau_3) = 2i\sum_{\alpha\beta\gamma\delta\eta} V_{-\alpha\beta\gamma} V_{-\gamma\delta\eta}\mu_\alpha\mu_{-\beta}\mu_{-\delta}\mu_{-\eta} S_\alpha S_\beta S_\gamma S_\delta S_\eta \times \int_{\tau_3}^{t} d\tau \int_{t_3}^{t} d\tau' G_\alpha(t-\tau)G_\beta(\tau-\tau_1)G_\gamma(\tau-\tau') \times G_\delta(\tau'-\tau_2)G_\eta(\tau'-\tau_3) \quad \text{(F51)}$$

$$R_{\mathrm{VI}}^{(3)}(t,\tau_1\tau_2\tau_3) = \sum_{\alpha\beta\gamma\delta} V_{-\alpha\beta\gamma\delta}\mu_\alpha\mu_{-\beta}\mu_{-\gamma}\mu_{-\delta} S_\alpha S_\beta S_\gamma S_\delta \times \int_{\tau_3}^{t} d\tau G_\alpha(t-\tau)G_\beta(\tau-\tau_1)G_\gamma(\tau-\tau_2)G_\delta(\tau-\tau_3) \quad \text{(F52)}$$

$$R_{\mathrm{VII}}^{(3)}(t,\tau_1\tau_2\tau_3) = -2i\sum_{\alpha\beta\gamma} \mu_{\alpha\beta}\mu_{-\beta\gamma}\mu_{-\alpha}\mu_{-\gamma} S_\alpha S_\beta S_\gamma G_\alpha(t-\tau_1)G_\beta(\tau-\tau_2) \times G_\gamma(\tau_2-\tau_3) \quad \text{(F53)}$$

$$R_{\mathrm{VIII}}^{(3)}(t,\tau_1\tau_2\tau_3) = -2\sum_{\alpha\beta\gamma\delta} \mu_{\alpha\beta} V_{-\beta\gamma\delta}\mu_{-\alpha}\mu_\gamma\mu_{-\delta} S_\alpha S_\beta S_\gamma S_\delta \times \int_{\tau_3}^{t} d\tau G_\alpha(t-\tau_1)G_\beta(t-\tau)G_\gamma(\tau-\tau_2)G_\delta(\tau-\tau_3) \quad \text{(F54)}$$

Using eqs F21 and F24, we obtain the following 8-term expression for the third-order polarizability (symmetrized with respect to ω_1, ω_2, and ω_3 permutations)

$$\gamma(\omega_1,\omega_2,\omega_3) = \frac{1}{3!}\sum_{\omega_1\omega_2\omega_3}^{\mathrm{perm}} (\gamma_{\mathrm{I}} + \gamma_{\mathrm{II}} + \gamma_{\mathrm{III}} + ... \gamma_{\mathrm{VIII}}) \quad \text{(F55)}$$

where

$$\gamma_{\mathrm{I}} = \sum_{\alpha\beta\gamma} \frac{\mu_{-\alpha\beta}\mu_{-\beta\gamma}\mu_\alpha\mu_{-\gamma} S_\alpha S_\beta S_\gamma}{(\Omega_\alpha - \omega_1 - \omega_2 - \omega_3)(\Omega_\beta - \omega_2 - \omega_3)(\Omega_\gamma - \omega_3)} \quad \text{(F56)}$$

$$\gamma_{\mathrm{II}} = \sum_{\alpha\beta\gamma\delta} \frac{-\mu_{-\alpha\beta} V_{-\beta\gamma\delta}\mu_\alpha\mu_{-\gamma}\mu_{-\delta} S_\alpha S_\beta S_\gamma S_\delta}{(\Omega_\alpha - \omega_1 - \omega_2 - \omega_3)(\Omega_\beta - \omega_2 - \omega_3)(\Omega_\gamma - \omega_2)(\Omega_\delta - \omega_3)} \quad \text{(F57)}$$

$$\gamma_{\mathrm{III}} = \sum_{\alpha\beta\gamma} \frac{\mu_{-\alpha\beta\gamma}\mu_\alpha\mu_{-\beta}\mu_{-\gamma} S_\alpha S_\beta S_\gamma}{(\Omega_\alpha - \omega_1 - \omega_2 - \omega_3)(\Omega_\beta - \omega_2 - \omega_3)(\Omega_\gamma - \omega_3)} \quad \text{(F58)}$$

$$\gamma_{\mathrm{IV}} = \sum_{\alpha\beta\gamma\delta} \frac{-2V_{-\alpha\beta\gamma}\mu_{-\gamma\delta}\mu_\alpha\mu_{-\beta}\mu_{-\delta} S_\alpha S_\beta S_\gamma S_\delta}{(\Omega_\alpha - \omega_1 - \omega_2 - \omega_3)(\Omega_\beta - \omega_1)(\Omega_\gamma - \omega_2 - \omega_3)(\Omega_\delta - \omega_3)} \quad \text{(F59)}$$

$$\gamma_{\mathrm{V}} = \sum_{\alpha\beta\gamma\delta\eta} \frac{2V_{-\alpha\beta\gamma} V_{-\gamma\delta\eta}\mu_\alpha\mu_{-\beta}\mu_{-\delta}\mu_{-\eta} S_\alpha S_\beta S_\gamma S_\delta S_\eta}{(\Omega_\alpha - \omega_1 - \omega_2 - \omega_3)(\Omega_\beta - \omega_1)(\Omega_\gamma - \omega_2 - \omega_3)(\Omega_\delta - \omega_2)(\Omega_\eta - \omega_3)} \quad \text{(F60)}$$

$$\gamma_{\mathrm{VI}} = \sum_{\alpha\beta\gamma\delta} \frac{-V_{-\alpha\beta\gamma\delta}\mu_\alpha\mu_{-\beta}\mu_{-\gamma}\mu_{-\delta} S_\alpha S_\beta S_\gamma S_\delta}{(\Omega_\alpha - \omega_1 - \omega_2 - \omega_3)(\Omega_\beta - \omega_1)(\Omega_\gamma - \omega_2)(\Omega_\delta - \omega_3)} \quad \text{(F61)}$$

$$\gamma_{\mathrm{VII}} = \sum_{\alpha\beta\gamma} \frac{\mu_{\alpha\beta}\mu_{-\beta\gamma}\mu_{-\alpha}\mu_{-\gamma}S_\alpha S_\beta S_\gamma}{(\Omega_\alpha - \omega_1)(\Omega_\beta - \omega_2 - \omega_3)(\Omega_\gamma - \omega_3)} \quad \text{(F62)}$$

$$\gamma_{\mathrm{VIII}} = \sum_{\alpha\beta\gamma\delta} \frac{-\mu_{\alpha\beta}V_{-\beta\gamma\delta}\mu_{-\alpha}\mu_{-\gamma}\mu_{-\delta}S_\alpha S_\beta S_\gamma S_\delta}{(\Omega_\alpha - \omega_1)(\Omega_\beta - \omega_2 - \omega_3)(\Omega_\gamma - \omega_2)(\Omega_\delta - \omega_3)} \quad \text{(F63)}$$

Here $\nu = \alpha, \beta, \gamma, \delta, \eta = -M, ..., M$ and Ω_ν is positive (negative) for all $\nu > 0$ ($\nu < 0$) according to the convention $\Omega_{-\nu} = -\Omega_\nu$. Note, that in eq F41 the permutations over ω_1 and ω_2 were written explicitly. Finally, by setting ω_1, ω_2, and ω_3 to zero and using identities $S_\nu\Omega_\nu = |\Omega_\nu|$ and $\mu_{-\nu} = \mu_\nu$ we obtain the third-order static polarizability:

$$\gamma(0) = \sum_{\alpha\beta\gamma} \frac{\mu_{\alpha\beta\gamma}\mu_\alpha\mu_\beta\mu_\gamma}{|\Omega_\alpha\Omega_\beta\Omega_\gamma|} + \sum_{\alpha\beta\gamma} \frac{2\mu_{\alpha\beta}\mu_{-\beta\gamma}\mu_\alpha\mu_\gamma}{|\Omega_\alpha\Omega_\beta\Omega_\gamma|} - \sum_{\alpha\beta\gamma\delta} \frac{4\mu_{\alpha\beta}V_{-\beta\gamma\delta}\mu_\alpha\mu_\gamma\mu_\delta}{|\Omega_\alpha\Omega_\beta\Omega_\gamma\Omega_\delta|} + \sum_{\alpha\beta\gamma\delta\eta} \frac{2V_{\alpha\beta\gamma}V_{-\gamma\delta\eta}\mu_\alpha\mu_\beta\mu_\delta\mu_\eta}{|\Omega_\alpha\Omega_\beta\Omega_\gamma\Omega_\delta\Omega_\eta|} - \sum_{\alpha\beta\gamma\delta} \frac{V_{\alpha\beta\gamma\delta}\mu_\alpha\mu_\beta\mu_\gamma\mu_\delta}{|\Omega_\alpha\Omega_\beta\Omega_\gamma\Omega_\delta|},$$
$$\alpha, \beta, \gamma, \delta, \eta = -M, ..., M \quad \text{(F64)}$$

XIII. References

(1) Birks, J. B. *Photophysics of Aromatic Molecules*; Wiley: New York, 1970.
(2) Michl, J.; Bonacic-Koutecky, V. *Electronic Aspects Of Organic Photochemistry*; Wiley: New York, 1990.
(3) Klessinger, M.; Michl, J. *Excited States and Photochemistry of Organic Molecules*; VCH: New York, 1995.
(4) Forrest, S. R. *Chem. Rev.* **1997**, *97*, 1793.
(5) McBranch, D. W.; Sinclair, M. B. In *The Nature of the Photoexcitations in Conjugated Polymers*; Sariciftci, N. S., Ed.; Word Scientific Publishing: Singapore, 1997.
(6) Zuber, H.; Brunisholz, R. A. *Photosynthesis: Physical Mechanism and Chemical Patterns*; Cambridge University Press: New York, 1980.
(7) Scheer, H. *Chlorophylls*; CRC Press: Boca Raton Ann Arbor, Boston London, 1991.
(8) Mukamel, S., Chemla, D. S. *Chem. Phys.* **1996**, *210*.
(9) *Proc. NATO Adv. Res. Workshop in Conjugated Polymeric Materials: Opportunities in Electronics, Optoelectronics, and Molecular Electronics*, Vol. 182 of *NATO ASI, Series E: Applied Sciences*; Bredás, J. L., Chance, R., Ed.; Kluver: Dordrecht, 1990.
(10) Bubeck, C. *Nonlinear Optical Material: Principles and Applications*; Degiorgio, V., Flytzanis, C., Eds.; IOS Press: Amsterdam, 1995; p 359.
(11) Albota, M.; Beljonne, D.; Brédas, J. L.; Ehrlich, J. E.; Fu, J. Y.; Heikal, A. A.; Hess, S. E.; Kogej, T.; Levin, M. D.; Marder, S. R.; McCord Maughon, D.; Perry, J. W.; Rockel, H.; Rumi, M.; Subramaniam, C.; Webb, W. W.; Wu, X. L.; Xu, C. *Science* **1998**, *281*, 1653.
(12) Puccetti, G.; Blanchard-Desce, M.; Ledoux, I.; Lehn, J. M.; Zyss, J. *J. Phys. Chem.* **1993**, *97*, 9385.
(13) Blanchard-Desce, M.; Wortmann, R.; Lebus, S.; Lehn, J.; Kramer, P. *Chem. Phys. Lett.* **1995**, *243*, 526.
(14) Kanis, D. R.; Ratner, M. A.; Marks, T. J. *Chem. Rev.* **1994**, *94*, 195.
(15) Brédas, J. L.; Adant, C.; Tackx, P.; Persoons, A.; Pierce, B. M. *Chem. Rev.* **1994**, *94*, 243.
(16) Brédas, J. L.; Cornil, J.; Beljonne, D.; Santos, D. A.dos; Shuai, Z. G. *Acc. Chem. Res.* **1999**, *32*, 267.
(17) Marder, S. R.; Torruellas, W. E.; Blanchard-Desce, M.; Ricci, V.; Stegeman, G. I.; Gilmour, S.; Brédas, J. L.; Li, J.; Bublitz, G. U.; Boxer, S. G. *Science* **1997**, *276*, 1233.
(18) Blanchard-Desce, M.; Runser, C.; Fort, A.; Barzoukas, M.; Lehn, J. M.; Bloy, V.; Alain, V. *Chem. Phys.* **1995**, *199*, 253.
(19) Blanchard-Desce, M.; Lehn, J. M.; Barzoukas, M.; Ledoux, I.; Zyss, J. *Chem. Phys.* **1994**, *181*, 281.
(20) Heeger, A. J. *Rev. Mod. Phys.* **2001**, *73*, 681.
(21) Friend, R. H.; Gymer, R. W.; Holmes, A. B.; Burroughes, J. H.; Marks, R. N.; Taliani, C.; Bradley, D. D. C.; Santos, D. A.dos; Brédas, J. L.; Logdlund, M.; Salaneck, W. R. *Nature* **1999**, *397*, 121.
(22) Frolov, S. V.; Gellermann, W.; Ozaki, M.; Yoshino, K.; Vardeny, Z. V. *Phys. Rev. Lett.* **1997**, *78*, 729.
(23) Proc. Int. Conf. on Synth. Met. ICSM 96; *Synth. Met.* **1997**, *84*.
(24) Pachter, R.; Crane, R.; Adams, W. W. *Mater. Res. Soc. Symp. Proc.* **1995**, *374*, 39.
(25) Schon, J. H.; Kloc, C.; Dodabalapur, A.; Batlogg, B. *Science* **2000**, *289*, 599.
(26) Schon, J. H.; Dodabalapur, A.; Kloc, C.; Batlogg, B. *Science* **2000**, *290*, 963.
(27) Baldo, M. A.; Thompson, M. E.; Forrest, S. R. *Nature* **2000**, *403*, 750.
(28) Fano, U.; Theodosiou, C. E.; Dehmer, J. L. *Rev. Mod. Phys.* **1976**, *48*, 49.
(29) Ward, J. F. *Rev. Mod. Phys.* **1965**, *37*, 1.
(30) Orr, B. J.; Ward, J. F. *Mol. Phys.* **1971**, *20*, 513.
(31) *Nonlinear Optical Properties of Organic Molecules and Crystals*; Zyss, J., Chemla, D. S., Eds.; Academic Press: Florida, 1987; Vol. 1 and 2.
(32) Rodenberger, D. C.; Heflin, J. R.; Garito, A. F. *Nature* **1992**, *359*, 309.
(33) Heflin, J. R.; Wong, K. Y.; Zamanikhamiri, O.; Garito, A. F. *Phys. Rev. B* **1988**, *38*, 1573.
(34) Kirtman, B.; Toto, J. L.; Robins, K. A.; Hasan, M. *J. Chem. Phys.* **1995**, *102*, 5350.
(35) Tato, T. T.; Toto, J. L.; Demelo, C. P.; Hasan, M.; Kirtman, B. *Chem. Phys. Lett.* **1995**, *244*, 59.
(36) Sekino, H.; Bartlett, R. J. *J. Chem. Phys.* **1986**, *85*, 976.
(37) Soos, Z. G.; Mukhopadhyay, D.; Ramasesha, S. *Nonlin. Opt. Mater.* **1996**, *628*, 189.
(38) Soos, Z. G.; Ramasesha, S.; Galvao, D. S. *Phys. Rev. Lett.* **1993**, *71*, 1609.
(39) Soos, Z. G. *Mol. Cryst. Liq. Cryst.* **1994**, *256*, 35.
(40) Haug, H.; Koch, S. W. *Quantum Theory of the Optical and Electronic Properties of Semiconductors*, 3rd ed; World Scientific: Singapore, 1994.
(41) Kirova, N.; Brazovskii, S.; Bishop, A. R. *Synth. Met.* **1999**, *100*, 29.
(42) Brazovskii, S.; Kirova, N.; Bishop, A. R. *Opt. Mater.* **1998**, *9*, 465.
(43) Gartstein, Y. N.; Rice, M. J.; Conwell, E. M. *Phys. Rev. B* **1995**, *52*, 1683.
(44) Rice, M. J.; Gartstein, Y. N. *Phys. Rev. Lett.* **1994**, *73*, 2504.
(45) Ivanov, I.; Gherman, B. F.; Yaron, D. *Synth. Met.* **2001**, *116*, 111.
(46) Pople, J. A.; Gill, P. M. W.; Johnson, B. G. *Chem. Phys. Lett.* **1992**, *199*, 557.
(47) Becke, A. D. *Phys. Rev. A* **1988**, *38*, 3098.
(48) Gross, E. K. U.; Dobson, J. F.; Petersilka, M. In *Density Functional Theory*; Nalewajski, R. F., Ed.; Springer: Berlin, 1996, Vol. 181.
(49) Casida, M. E. In *Recent Advances in Density-Functional Methods*, Vol. 3 of *Part I*; Chong, D. A., Ed.; World Scientific: Singapore, 1995.
(50) Jamorski, C.; Casida, M. E.; Salahub, D. R. *J. Chem. Phys.* **1996**, *104*, 5134.
(51) Trickey, S. B. *Adv. Quantum Chem.* **1990**, *21*.
(52) Hohenberg, P.; Kohn, W. *Phys. Rev. B* **1964**, *136*, 864.
(53) Kohn, W.; Sham, L. J. *Phys. Rev. A* **1965**, *137*, 1697.
(54) McWeeny, R.; Sutcliffe, B. T. *Methods of Molecular Quantum Mechanics*; Academic Press: New York, 1976.
(55) Davidson, E. R. *Reduced Density* Matrices *in Quantum Chemistry*; Academic Press: New York, 1976.
(56) Löwdin, P.-O. *Phys. Rev.* **1955**, *97*, 1474.
(57) Löwdin, P.-O. *Adv. Phys.* **1956**, *5*, 1.
(58) Löwdin, P.-O. *Rev. Mod. Phys.* **1962**, *34*, 80.
(59) Mulliken, R. S. *J. Chem. Phys.* **1955**, *23*, 1833, 1841, 2338, 2343.
(60) Szabo, A.; Ostlund, N. S. *Modern Quantum Chemistry: Introduction to Advanced Electronic Structure Theory*; McGraw-Hill: New York, 1989.
(61) Bader, R. F. W. *Atoms in Molecules: A Quantum Theory*; Oxford: New York, 1990.
(62) Nesbet, R. K. *Phys. Rev. A* **2000**, *6204*, 701.
(63) Nesbet, R. K. *Int. J. Quantum Chem.* **2001**, *85*, 405.
(64) Weiner, B.; Trickey, S. B. *Adv. Quantum Chem.* **1999**, *35*, 217.
(65) Weiner, B.; Trickey, S. B. *J. Mol. Str.-Theochem* **2000**, *501*, 65.
(66) Micha, D. A. *Int. J. Quantum Chem.* **2000**, *80*, 394.
(67) Gross, E. K. U.; Dobson, J. F.; Petersilka, M. *Density Functional Theory II* **1996**, *181*, 81.
(68) *Density Matrixes and Density Functions, Proc. A. J. Coleman Symp.*; Erdahl, R., Smith, V. H., Eds.; D. Reidel Publishing: Dordrecht, 1987.
(69) Coleman, A. J.; Yukalov, V. I. *Reduced Density Matrices*; Springer, New York, 2000.
(70) Valdemoro, C.; Tel, L. M.; PerezRomero, E. *Adv. Quantum Chem.* **1997**, *28*, 33.

(71) Nakata, M.; Ehara, M.; Yasuda, K.; Nakatsuji, H. *J. Chem. Phys.* **2000**, *112*, 8772.
(72) Mazziotti, D. A. *J. Chem. Phys.* **2000**, *112*, 10125.
(73) Rohlfing, M.; Louie, S. G. *Phys. Rev. Lett.* **1998**, *80*, 3320.
(74) Linderberg, J.; Öhrn, Y. *Propagators in Quantum Chemistry*; Academic Press: London, 1973.
(75) Deumens, E.; Diz, A.; Longo, R.; Öhrn, Y. *Rev. Mod. Phys.* **1994**, *66*, 917.
(76) Mukamel, S. *Principles of Nonlinear Optical Spectroscopy*; Oxford: New York, 1995.
(77) Chernyak, V.; Mukamel, S. *J. Chem. Phys.* **1996**, *104*, 444.
(78) Chernyak, V.; Mukamel, S. *J. Chem. Phys.* **2000**, *112*, 3572.
(79) Stratmann, R. E.; Scuseria, G. E.; Frisch, M. J. *J. Chem. Phys.* **1998**, *109*, 8218.
(80) Wiberg, K. B.; Stratmann, R. E.; Frisch, M. J. *Chem. Phys. Lett.* **1998**, *297*, 60.
(81) Tretiak, S.; Chernyak, V.; Mukamel, S. *J. Am. Chem. Soc.* **1997**, *119*, 11408.
(82) Thouless, D. J. *The Quantum Mechanics of Many-Body Systems*; Academic Press: New York, 1972.
(83) Ring, P.; Schuck, P. *The Nuclear Many-Body Problem*; Springer-Verlag: New York, 1980.
(84) Blaizot, J.-P.; Ripka, G. *Quantum Theory of Finite Systems*; The MIT Press: Cambridge Massachusetts, 1986.
(85) Sekino, H.; Bartlett, R. J. *Int. J. Quantum Chem.* **1992**, *43*, 119.
(86) Sekino, H.; Bartlett, R. J. *J. Chem. Phys.* **1993**, *98*, 3022.
(87) Takahashi, A.; Mukamel, S. *J. Chem. Phys.* **1994**, *100*, 2366.
(88) Takahashi, A.; Mukamel, S. *J. Chem. Phys.* **1995**, *103*, 7144.
(89) Tretiak, S.; Chernyak, V.; Mukamel, S. *Chem. Phys. Lett.* **1996**, *259*, 55.
(90) Tretiak, S.; Chernyak, V.; Mukamel, S. *J. Phys. Chem. B* **1998**, *102*, 3310.
(91) Mukamel, S.; Tretiak, S.; Wagersreiter, T.; Chernyak, V. *Science* **1997**, *277*, 781.
(92) Bazan, G. C.; Oldham, W. J.; Lachicotte, R. J.; Tretiak, S.; Chernyak, V.; Mukamel, S. *J. Am. Chem. Soc.* **1998**, *120*, 9188.
(93) Tretiak, S.; Middleton, C.; Chernyak, V.; Mukamel, S. *J. Phys. Chem. B* **2000**, *104*, 4519.
(94) Tretiak, S.; Middleton, C.; Chernyak, V.; Mukamel, S. *J. Phys. Chem. B* **2000**, *104*, 9540.
(95) Tretiak, S.; Saxena, A.; Martin, R. L.; Bishop, A. R. *J. Phys. Chem. B* **2000**, *104*, 7029.
(96) Tretiak, S., Ph.D. Thesis, University of Rochester, Rochester, NY, 1998.
(97) Casida, M. E.; Jamorski, C.; Casida, K. C.; Salahub, D. R. *J. Chem. Phys.* **1998**, *108*, 4439.
(98) Bauernschmitt, R.; Ahlrichs, R.; Hennrich, F. H.; Kappes, M. M. *J. Am. Chem. Soc.* **1998**, *120*, 5052.
(99) Dirac, P. A. *Proc. Camb. Philos. Soc.* **1930**, *26*, 376.
(100) Ferrel, R. A. *Phys. Rev.* **1957**, *107*, 1631.
(101) Zyrianov, P. S.; Eleonskii, V. M. *Sov. Phys. JETP* **1956**, *3*, 620.
(102) Goldstone, J.; Gottfried, K. *Nuovo Cimento* **1959**, *13*, 849.
(103) Enrenreich, H.; Cohen, M. H. *Phys. Rev.* **1959**, *115*, 786.
(104) Rowe, D. J. *Rev. Mod. Phys.* **1968**, *40*, 153.
(105) Pines, D.; Bohm, D. *Phys. Rev.* **1952**, *85*, 338.
(106) Lindhard, J. *Kgl. Danske Videnskab. Selskab., Mater.-Fys. Medd.* **1954**, *28*.
(107) Linderberg, J.; Thulstrup, E. W. *J. Chem. Phys.* **1968**, *49*, 710.
(108) Linderberg, J.; Öhrn, Y. *J. Chem. Phys.* **1968**, *49*, 716.
(109) Reinhardt, W. P.; Doll, J. D. *J. Chem. Phys.* **1969**, *50*, 2767.
(110) Reinhardt, W. P.; Smith, J. B. *J. Chem. Phys.* **1973**, *58*, 2148.
(111) Sasai, M.; Fukutome, H. *Prog. Theor. Phys.* **1985**, *73*, 1.
(112) Fukutome, H. *J. Mol. Struct.-Theochem* **1989**, *57*, 337.
(113) Dunning, T. H.; McKoy, V. *J. Chem. Phys.* **1967**, *47*, 1735.
(114) Dunning, T. H.; McKoy, V. *J. Chem. Phys.* **1967**, *48*, 5263.
(115) Shibuya, T.-I.; Mckoy, V. *J. Chem. Phys.* **1971**, *54*, 1738.
(116) Shibuya, T.-I.; McKoy, V. *J. Chem. Phys.* **1970**, *53*, 3308.
(117) Rose, J.; Shibuya, T.-I.; McKoy, V. *J. Chem. Phys.* **1973**, *58*, 74.
(118) Howell, J. M.; Jorgensen, P. *J. Am. Chem. Soc.* **1973**, *95*, 2813.
(119) Jorgensen, P.; Öhrn, Y. *Chem. Phys. Lett.* **1973**, *18*, 261.
(120) Linderberg, J.; Jorgensen, P.; Oddershede, J.; Ratner, M. *J. Chem. Phys.* **1972**, *56*, 6213.
(121) Oddershede, J.; Jorgensen, P.; Beebe, N. H. F. *J. Phys. B* **1978**, *11*, 1.
(122) Čížek, J.; Paldus, J. *Phys. Rev. A* **1971**, *3*, 525.
(123) Paldus, J.; Čížek, J. *Chem. Phys. Lett.* **1969**, *3*, 1.
(124) Fukutome, H. *Prog. Theor. Phys.* **1974**, *52*, 115.
(125) Fukutome, H. *Prog. Theor. Phys.* **1974**, *52*, 1766.
(126) Fukutome, H. *Prog. Theor. Phys.* **1975**, *53*, 1320.
(127) Shibuya, T.-I.; Rose, J.; McKoy, V. *J. Chem. Phys.* **1973**, *58*, 500.
(128) Shibuya, T.-I.; McKoy, V. *Phys. Rev. A* **1970**, *2*, 2208.
(129) Jorgensen, P.; Oddershede, J.; Ratner, M. A. *Chem. Phys. Lett.* **1975**, *32*, 111.
(130) Oddershede, J.; Jorgensen, P. *J. Chem. Phys.* **1977**, *66*, 1541.
(131) Paldus, J.; Čížek, J. *J. Chem. Phys.* **1974**, *60*, 149.
(132) Linderberg, J.; Öhrn, Y. *Int. J. Quantum Chem.* **1977**, *12*, 161.
(133) Öhrn, Y.; Linderberg, J. *Int. J. Quantum Chem.* **1979**, *15*, 343.
(134) Jorgensen, P.; Oddershede, J.; Albertsen, P.; Beebe, N. H. F. *J. Chem. Phys.* **1978**, *68*, 2533.
(135) Jorgensen, P.; Oddershede, J.; Beebe, N. H. F. *J. Chem. Phys.* **1978**, *68*, 2527.
(136) Oddershede, J.; Jorgensen, P.; Beebe, N. H. F. *J. Chem. Phys.* **1975**, *63*, 2996.
(137) Linderberg, J.; Prato, D. *Int. J. Quantum Chem.* **1974**, *8*, 901.
(138) Jorgensen, P. *Annu. Rev. Phys. Chem.* **1975**, *26*, 359.
(139) Baker, J. D.; Zerner, M. C. *J. Phys. Chem.* **1991**, *95*, 8614.
(140) Baker, J. D.; Zerner, M. C. *Chem. Phys. Lett.* **1990**, *175*, 192.
(141) Parkinson, W. A.; Zerner, M. C. *Chem. Phys. Lett.* **1987**, *139*, 563.
(142) Frisch, M. J.; Trucks, G. W.; Schlegel, H. B.; Scuseria, G. E.; Robb, M. A.; Cheeseman, J. R.; Zakrzewski, V. G.; Montgomery, J. A., Jr.; Stratmann, R. E.; Burant, J. C.; Dapprich, S.; Millam, J. M.; Daniels, A. D.; Kudin, K. N.; Strain, M. C.; Farkas, O.; Tomasi, J.; Barone, V.; Cossi, M.; Cammi, R.; Mennucci, B.; Pomelli, C.; Adamo, C.; Clifford, S.; Ochterski, J.; Petersson, G. A.; Ayala, P. Y.; Cui, Q.; Morokuma, K.; Malick, D. K.; Rabuck, A. D.; Raghavachari, K.; Foresman, J. B.; Cioslowski, J.; Ortiz, J. V.; Baboul, A. G.; Stefanov, B. B.; Liu, G.; Liashenko, A.; Piskorz, P.; Komaromi, I.; Gomperts, R.; Martin, R. L.; Fox, D. J.; Keith, T.; Al-Laham, M. A.; Peng, C. Y.; Nanayakkara, A.; Challacombe, M.; Gill, P. M. W.; Johnson, B.; Chen, W.; Wong, M. W.; Andres, J. L.; Gonzalez, C.; Head-Gordon, M.; Replogle, E. S.; Pople, J. A. *Gaussian 98 (Revision A.11)* (Gaussian, Inc., Pittsburgh, PA, 2002).
(143) Stewart, J. J. P. *MOPAC 2002* (Schrödinger Inc. and Fujitsu Limited, Portland, OR 97201, 2000).
(144) Schmidt, M. W.; Baldridge, K. K.; Boatz, J. A.; Elbert, S. T.; Gordon, M. S.; Jensen, J. H.; Koseki, S.; Matsunaga, N.; Nguyen, K. A.; Su, S. J.; Windus, T. L.; Dupuis, M.; Montgomery, J. A. *J. Comput. Chem.* **1993**, *14*, 1347.
(145) Zerner, M. C. *ZINDO, A Semiempirical Quantum Chemistry Program*; Quantum Theory Project, University of Florida, Gainesville, FL, 1996.
(146) Ortiz, J. V. *J. Chem. Phys.* **2000**, *112*, 56.
(147) Zakrzewski, V. G.; Dolgounitcheva, O.; Ortiz, J. V. *Int. J. Quantum Chem.* **1999**, *75*, 607.
(148) Sekino, H.; Bartlett, R. J. *J. Chem. Phys.* **1991**, *94*, 3665.
(149) Mukamel, S.; Wang, H. X. *Phys. Rev. Lett.* **1992**, *69*, 65.
(150) Wang, H. X.; Mukamel, S. *Chem. Phys. Lett.* **1992**, *192*, 417.
(151) Mukamel, S.; Takahashi, A.; Wang, H. X.; Chen, G. H. *Science* **1994**, *266*, 250.
(152) Chen, G. H.; Mukamel, S. *J. Phys. Chem.* **1996**, *100*, 11080.
(153) Wagersreiter, T.; Mukamel, S. *J. Chem. Phys.* **1996**, *104*, 7086.
(154) Wagersreiter, T.; Mukamel, S. *Chem. Phys.* **1996**, *210*, 171.
(155) Wagersreiter, T.; Mukamel, S. *J. Chem. Phys.* **1996**, *105*, 7995.
(156) Hartmann, M.; Chernyak, V.; Mukamel, S. *Phys. Rev. B* **1995**, *52*, 2528.
(157) Hartmann, M.; Mukamel, S. *J. Chem. Phys.* **1993**, *99*, 1597.
(158) Chernyak, V.; Mukamel, S. *J. Chem. Phys.* **1995**, *103*, 7640.
(159) Pople, J. A.; Segal, G. A. *J. Chem. Phys.* **1965**, *43*, S136.
(160) Pople, J. A.; Beveridge, D. L.; Dobosh, P. *J. Chem. Phys.* **1967**, *47*, 2026.
(161) Ridley, J.; Zerner, M. *Theor. Chim. Acta* **1973**, *32*, 111.
(162) Karlsson, G.; Zerner, M. C. *Int. J. Quantum Chem.* **1973**, *7*, 35.
(163) Zerner, M. C.; Loew, G. H.; Kirchner, R. F.; Mueller-Westerhoff, U. T. *J. Am. Chem. Soc.* **1980**, *102*, 589.
(164) Roothaan, C. C. J. *Rev. Mod. Phys.* **1960**, *32*, 179.
(165) Sobolewski, A. L.; Domcke, W. *J. Phys. Chem. A* **1999**, *103*, 4494.
(166) Domcke, W.; Koppel, H.; Cederbaum, L. S. *Mol. Phys.* **1981**, *43*, 851.
(167) Ridley, J. E.; Zerner, M. C. *Theor. Chim. Acta* **1976**, *42*, 223.
(168) Bacon, A. D.; Zerner, M. C. *Theor. Chim. Acta* **1979**, *53*, 21.
(169) Neto, J. D. D.; Zerner, M. C. *Int. J. Quantum Chem.* **2001**, *81*, 187.
(170) Canuto, S.; Coutinho, K.; Zerner, M. C. *J. Chem. Phys.* **2000**, *112*, 7293.
(171) Voityuk, A. A.; Zerner, M. C.; Rosch, N. *J. Phys. Chem. A* **1999**, *103*, 4553.
(172) Baker, J. D.; Zerner, M. C. *J. Phys. Chem.* **1991**, *95*, 2307.
(173) Anderson, W. P.; Cundari, T. R.; Zerner, M. C. *Int. J. Quantum Chem.* **1991**, *39*, 31.
(174) Baker, J. D.; Zerner, M. C. *J. Phys. Chem.* **1990**, *94*, 2866.
(175) Anderson, W. P.; Cundari, T. R.; Drago, R. S.; Zerner, M. C. *Inorg. Chem.* **1990**, *29*, 1.
(176) Cory, M. G.; Kostlmeier, S.; Kotzian, M.; Rosch, N.; Zerner, M. C. *J. Chem. Phys.* **1994**, *100*, 1353.
(177) Kotzian, M.; Rosch, N.; Zerner, M. C. *Theor. Chim. Acta* **1992**, *81*, 201.
(178) Culberson, J. C.; Knappe, P.; Rosch, N.; Zerner, M. C. *Theor. Chim. Acta* **1987**, *71*, 21.
(179) Stavrev, K. K.; Zerner, M. C.; Meyer, T. J. *J. Am. Chem. Soc.* **1995**, *117*, 8684.
(180) Kanis, D. R.; Ratner, M. A.; Marks, T. J.; Zerner, M. C. *Chem. Mater.* **1991**, *3*, 19.
(181) Cornil, J.; Beljonne, D.; Calbert, J. P.; Brédas, J. L. *Adv. Mater.* **2001**, *13*, 1053.
(182) Tretiak, S.; Saxena, A.; Martin, R. L.; Bishop, A. R. *J. Chem. Phys.* **2001**, *115*, 699.

(183) Tretiak, S.; Saxena, A.; Martin, R. L.; Bishop, A. R. *Chem. Phys. Lett.* **2000**, *331*, 561.
(184) Cory, M. G.; Zerner, M. C.; Xu, X. C.; Shulten, K. *J. Phys. Chem. B* **1998**, *102*, 7640.
(185) Karelson, M. M.; Zerner, M. C. *J. Phys. Chem.* **1992**, *96*, 6949.
(186) Onsager, L. *J. Am. Chem. Soc.* **1936**, *58*, 1486.
(187) Kirkwood, J. G. *J. Chem. Phys.* **1934**, *2*, 351.
(188) Bottcher, C. J. F. *Theory of Electric Polarization*; Elsevier: Amsterdam, 1973).
(189) Cammi, R.; Mennucci, B. *J. Chem. Phys.* **1999**, *110*, 9877.
(190) Amovilli, C.; Barone, V.; Cammi, R.; Cances, E.; Cossi, M.; Mennucci, B.; Pomelli, C. S.; Tomasi, J. *Adv. Quantum Chem.* **1999**, *32*, 227.
(191) Tawa, G. J.; Martin, R. L.; Pratt, L. R. *Int. J. Quantum Chem.* **1997**, *64*, 143.
(192) Pratt, L. R.; Tawa, G. J.; Hummer, G.; Garcia, A. E.; Corcelli, S. A. *Int. J. Quantum Chem.* **1997**, *64*, 121.
(193) Moore, E. E.; Yaron, D. *J. Chem. Phys.* **1998**, *109*, 6147.
(194) Moore, E.; Gherman, B.; Yaron, D. *J. Chem. Phys.* **1997**, *106*, 4216.
(195) Klamt, A.; Schuurmann, G. *J. Chem. Soc., Perkin Trans. 2* **1993**, *5*, 799.
(196) Stavrev, K. K.; Tamm, T.; Zerner, M. C. *Int. J. Quantum Chem.* **1996**, *60*, 373.
(197) Broo, A.; Pearl, G.; Zerner, M. C. *J. Phys. Chem. A* **1997**, *101*, 2478.
(198) Diercksen, G. H. F.; Karelson, M.; Tamm, T.; Zerner, M. C. *Int. J. Quantum Chem.* **1994**, *28*, 339.
(199) Karelson, M.; Tamm, T.; Zerner, M. C. *J. Phys. Chem.* **1993**, *97*, 11901.
(200) Szafran, M.; Karelson, M. M.; Katritzky, A. R.; Koput, J.; Zerner, M. C. *J. Comput. Chem.* **1993**, *14*, 371.
(201) Karelson, M.; Tamm, T.; Katritzky, A. R.; Szafran, M.; Zerner, M. C. *Int. J. Quantum Chem.* **1990**, *37*, 1.
(202) Karelson, M. M.; Katritzky, A. R.; Zerner, M. C. *Int. J. Quantum Chem.* **1986**, *20*, 521.
(203) Cammi, R.; Mennucci, B.; Tomasi, J. *J. Am. Chem. Soc.* **1998**, *120*, 8834.
(204) Cammi, R.; Mennucci, B.; Tomasi, J. *J. Phys. Chem. A* **2000**, *104*, 4690.
(205) Cammi, R.; Mennucci, B.; Tomasi, J. *J. Phys. Chem. A* **1999**, *103*, 9100.
(206) Champagne, B.; Mennucci, B.; Cossi, M.; Cammi, R.; Tomasi, J. *Chem. Phys.* **1998**, *238*, 153.
(207) Tretiak, S.; Chernyak, V.; Mukamel, S. *Int. J. Quantum Chem.* **1998**, *70*, 711.
(208) Rettrup, S. *J. Comput. Phys.* **1982**, *45*, 100.
(209) Linderberg, J. *Phys. Scripta* **1980**, *21*, 373.
(210) Thouless, D. J. *J. Nucl. Phys.* **1961**, *22*, 78.
(211) Löwdin, P.-O. *J. Chem. Phys.* **1950**, *18*, 365.
(212) Löwdin, P.-O. *Adv. Quantum Chem.* **1970**, *5*, 185.
(213) Ericsson, T.; Ruhe, A. *Math. Comput.* **1980**, *35*, 1251.
(214) Saad, Y. *Numerical Methods for Large Eigenvalue Problems*; Manchester, University Press: 1992.
(215) Parlett, B. N. *Symmetric Eigenvalue Problem*; Prentice Hall, Englewood Cliffs, 1980.
(216) Davidson, E. R. *J. Comput. Phys.* **1975**, *17*, 87.
(217) Weiss, H.; Ahlrichs, R.; Häser, M. *J. Chem Phys.* **1993**, *99*, 1262.
(218) Cullum, J.; Willoughby, R. A. *J. Comput. Phys.* **1981**, *44*, 329.
(219) Chernyak, V.; Schulz, M. F.; Mukamel, S.; Tretiak, S.; Tsiper, E. V. *J. Chem. Phys.* **2000**, *113*, 36.
(220) Tsiper, E. V. *J. Phys. B* **2001**, *34*, L401.
(221) Tsiper, E. V. *JETP Lett.* **1999**, *70*, 751.
(222) Olsen, J.; Jensen, H. J. A.; Jorgensen, P. *J. Comput. Phys.* **1988**, *74*, 265.
(223) Lehoucq, R. B.; Sorensen, D. C. *Siam J. Matr. Anal. Appl.* **1996**, *17*, 789.
(224) Kosloff, R. *Annu. Rev. Phys. Chem.* **1994**, *45*, 145.
(225) Leforestier, C.; Bisseling, R. H.; Cerjan, C.; Feit, M. D.; Friesner, R.; Guldberg, A.; Hammerich, A.; Jolicard, G.; Karrlein, W.; Meyer, H. D.; Lipkin, N.; Roncero, O.; Kosloff, R. *J. Comput. Phys.* **1991**, *94*, 59.
(226) Golub, G. H.; Loan, C. F. V. *Matrix Computation*; John Hopkins University Press: Baltimore, Maryland, 1983.
(227) Chaitin-Chatelin, F.; Ahues, M. *Eigenvalues of Matrices*; Wiley: Chichester, New York, 1993.
(228) Tommasini, M.; Zerbi, G.; Chernyak, V.; Mukamel, S. *J. Phys. Chem. A* **2001**, *105*, 7057.
(229) Ruhe, A. *Siam J. Sci. Comput.* **1998**, *19*, 1535.
(230) Ruhe, A. *Bit* **1994**, *34*, 165.
(231) Ruhe, A. *Lin. Algebra Appl.* **1994**, *198*, 283.
(232) Ruhe, A. *Lin. Algebra Appl.* **1984**, *58*, 391.
(233) Reed, A. E.; Curtiss, L. A.; Weinhold, F. *Chem. Rev.* **1988**, *88*, 899.
(234) Reed, A. E.; Weinstock, R. B.; Weinhold, F. *J. Chem. Phys.* **1985**, *83*, 735.
(235) White, S. R. *Phys. Rev. B* **1993**, *48*, 10345.
(236) Löwdin, P.-O.; Shull, H. *Phys. Rev.* **1956**, *101*, 1730.
(237) Kirkwood, J. C.; Scheurer, C.; Chernyak, V.; Mukamel, S. *J. Chem. Phys.* **2001**, *114*, 2419.
(238) Schulz, M.; Tretiak, S.; Chernyak, V.; Mukamel, S. *J. Am. Chem. Soc.* **2000**, *122*, 452.
(239) Wilson, E. B.; Decius, J. C.; Cross, P. C. *Molecular Vibrations*; McGraw-Hill: New York, 1955.
(240) Hellwarth, R. W. *Prog. Quantum Electron.* **1977**, *5*, 1.
(241) Placzek, G. *The Rayleigh and Raman Scattering*, Vol. 256(L) of *UCRL Transl.* (U.S. Department of Commerce, Washington, D. C., 1962).
(242) Hagler, T. W.; Pakbaz, K.; Voss, K. F.; Heeger, A. J. *Phys. Rev. B* **1991**, *44*, 8652.
(243) Halliday, D. A.; Burn, P. L.; Friend, R. H.; Bradley, D. D. C.; Holmes, A. B.; Kraft, A. *Synth. Met.* **1993**, *55*, 954.
(244) Sakamoto, A.; Furukawa, Y.; Tasumi, M. *J. Phys. Chem.* **1992**, *96*, 3870.
(245) Tian, B.; Zerbi, G.; Schenk, R.; Mullen, K. *J. Chem. Phys.* **1991**, *95*, 3191.
(246) Rauscher, U.; Bässler, H.; Bradley, D. D. C.; Hennecke, M. *Phys. Rev. B* **1990**, *42*, 9830.
(247) Cornil, J.; Beljonne, D.; Friend, R. H.; Brédas, J. L. *Chem. Phys. Lett.* **1994**, *223*, 82.
(248) Kohler, A.; Santos, D. A.dos; Beljonne, D.; Shuai, Z.; Brédas, J. L.; Holmes, A. B.; Kraus, A.; Mullen, K.; Friend, R. H. *Nature* **1998**, *392*, 903.
(249) Huser, T.; Yan, M.; Rothberg, L. J. *Proc. Natl. Acad. Sci. U.S.A.* **2000**, *97*, 11187.
(250) Yan, M.; Rothberg, L. J.; Papadimitrakopoulos, F.; Galvin, M. E.; Miller, T. M. *Phys. Rev. Lett.* **1994**, *72*, 1104.
(251) Beljonne, D.; Cornil, J.; Silbey, R.; Millie, P.; Brédas, J. L. *J. Chem. Phys.* **2000**, *112*, 4749.
(252) Comoretto, D.; Marabelli, F.; Tognini, P.; Stella, A.; Cornil, J.; Santos, D. A.dos; Brédas, J. L.; Moses, D.; Dellepiane, G. *Synth. Met.* **2001**, *124*, 53.
(253) Beljonne, D.; Shuai, Z.; Cornil, J.; Santos, D. A.dos; Brédas, J. L. *J. Chem. Phys.* **1999**, *111*, 2829.
(254) Bradley, D. D. C.; Friend, R. H.; Lindenberger, H.; Roth, S. *Polymer* **1986**, *27*, 1709.
(255) Chandross, M.; Mazumdar, S.; Jeglinski, S.; Wei, X.; Vardeny, Z. V.; Kwock, E. W.; Miller, T. M. *Phys. Rev. B* **1994**, *50*, 14702.
(256) Frolov, S. V.; Bao, Z.; Wohlgenannt, M.; Vardeny, Z. V. *Phys. Rev. Lett.* **2000**, *85*, 2196.
(257) Brédas, J. L.; Chance, R. R.; Baughman, R. H.; Silbey, R. *J. Chem. Phys.* **1982**, *76*, 3673.
(258) Speiser, S. *Chem. Rev.* **1996**, *96*, 1953.
(259) Balzani, V.; Scandola, F. *Supramolecular Photochemistry*; Ellis Harwood: New York, 1991.
(260) Bublitz, G. U.; Ortiz, R.; Runser, C.; Fort, A.; Barzoukas, M.; Marder, S. R.; Boxer, S. G. *J. Am. Chem. Soc.* **1997**, *119*, 2311.
(261) Ern, J.; Bens, A. T.; Martin, H. D.; Mukamel, S.; Schmid, D.; Tretiak, S.; Tsiper, E.; Kryschi, C. *Chem. Phys.* **1999**, *246*, 115.
(262) Ricci, V., Master's thesis, Department of Electrical Engineering, University of Central Florida, 1995.
(263) Gorman, C. B.; Marder, S. R. *Proc. Natl. Acad. Sci. U.S.A.* **1993**, *90*, 11297.
(264) Soos, Z. G.; Ramasesha, S.; Galvao, D. S.; Kepler, R. G.; Etemad, S. *Synth. Met.* **1993**, *54*, 35.
(265) Marder, S. R.; Gorman, C. B.; Meyers, F.; Perry, J. W.; Bourhill, G.; Brédas, J. L.; Pierce, B. M. *Science* **1994**, *265*, 632.
(266) Marder, S. R.; Kippelen, B.; Jen, A. K. Y.; Peyghambarian, N. *Nature* **1997**, *388*, 845.
(267) Marder, S. R.; Perry, J. W.; Tiemann, B. G.; Gorman, C. B.; Gilmour, S.; Biddle, S. L.; Bourhill, G. *J. Am. Chem. Soc.* **1993**, *115*, 2524.
(268) Meyers, F.; Marder, S. R.; Pierce, B. M.; Brédas, J. L. *J. Am. Chem. Soc.* **1994**, *116*, 10703.
(269) Balakina, M. Y.; Li, J.; Geskin, V. M.; Marder, S. R.; Brédas, J. L. *J. Chem. Phys.* **2000**, *113*, 9598.
(270) Pope, M.; Swenberg, C. E. *Electronic Processes in Organic Crystals*; Clarendon Press, Oxford University Press: New York, 1982.
(271) Silinsh, E. A.; Cápek, V. *Organic Molecular Crystals*; AIP Press: American Institute of Physics, New York, 1994.
(272) Champagne, B.; André, J. M. *Int. J. Quantum Chem.* **1990**, *24*, 859.
(273) Champagne, B.; André, J. M. *Int. J. Quantum Chem.* **1992**, *42*, 1009.
(274) Champagne, B.; Mosley, D. H.; Fripiat, J. G.; André, J. M. *Int. J. Quantum Chem.* **1993**, *46*, 1.
(275) Champagne, B.; Mosley, D. H.; Vracko, M.; André, J. M. *Phys. Rev. A* **1995**, *52*, 178.
(276) Champagne, B.; André, J. M.; Öhrn, Y. *Int. J. Quantum Chem.* **1996**, *57*, 811.
(277) Otto, P. *Int. J. Quantum Chem.* **1994**, *52*, 353.
(278) Otto, P. *Phys. Rev. B* **1992**, *45*, 10876.
(279) Kirtman, B.; Gu, F. L.; Bishop, D. M. *J. Chem. Phys.* **2000**, *113*, 1294.
(280) Otto, P.; Gu, F. L.; Ladik, J. *Synth. Met.* **1998**, *93*, 161.

(281) Hasan, M.; Kim, S. J.; Toto, J. L.; Kirtman, B. *J. Chem. Phys.* **1996**, *105*, 186.
(282) Otto, P.; Gu, F. L.; Ladik, J. *J. Chem. Phys.* **1999**, *110*, 2717.
(283) Jacquemin, D.; Champagne, B.; Perpete, E. A.; Luis, J. M.; Kirtman, B. *J. Phys. Chem. A* **2001**, *105*, 9748.
(284) Luis, J. M.; Duran, M.; Kirtman, B. *J. Chem. Phys.* **2001**, *115*, 4473.
(285) Luis, J. M.; Duran, M.; Champagne, B.; Kirtman, B. *J. Chem. Phys.* **2000**, *113*, 5203.
(286) Champagne, B.; Kirtman, B. *Chem. Phys.* **1999**, *245*, 213.
(287) Castiglioni, C.; DelZoppo, M.; Zerbi, G. *Phys. Rev. B* **1996**, *53*, 13319.
(288) DelZoppo, M.; Castiglioni, C.; Gerola, V.; Zuliani, P.; Zerbi, G. *J. Opt. Soc. Am. B* **1998**, *15*, 308.
(289) Tommasini, M.; Castiglioni, C.; Zerbi, G. *J. Mol. Str.-Theochem* **2000**, *500*, 323.
(290) Agrawal, G. P.; Cojan, C.; Flytzanis, C. *Phys. Rev. B* **1978**, *17*, 776.
(291) Gubler, U.; Bosshard, C.; Gunter, P.; Balakina, M. Y.; Cornil, J.; Brédas, J. L.; Martin, R. E.; Diederich, F. *Opt. Lett.* **1999**, *24*, 1599.
(292) Geskin, V. M.; Brédas, J. L. *J. Chem. Phys.* **1998**, *109*, 6163.
(293) Shuai, Z.; Brédas, J. L.; Saxena, A.; Bishop, A. R. *J. Chem. Phys.* **1998**, *109*, 2549.
(294) Perry, J. W.; Marder, S. R.; Meyers, F.; Lu, D.; Chen, G.; Goddard, W. A.; Brédas, J. L.; Pierce, B. M. *ACS Symp. Series* **1995**, *601*, 45.
(295) Flytzanis, C.; Huttler, J. In *Contemporary Nonlinear Optics*; Agrawal, G. P., Boyd, R. W., Eds.; Academic Press: San Diego, 1992.
(296) Mathy, A.; Ueberhofen, K.; Schenk, R.; Gregorius, H.; Garay, R.; Mullen, K.; Bubeck, C. *Phys. Rev. B* **1996**, *53*, 4367.
(297) Tretiak, S.; Chernyak, V.; Mukamel, S. *Phys. Rev. Lett.* **1996**, *77*, 4656.
(298) Samuel, I. D. W.; Ledoux, I.; Dhenaut, C.; Zyss, J.; Fox, H. H.; Schrock, R. R.; Silbey, R. J. *Science* **1994**, *265*, 1070.
(299) Ledoux, I.; Samuel, I. D. W.; Zyss, J.; Yaliraki, S. N.; Schattenmann, F. J.; Schrock, R. R.; Silbey, R. J. *Chem. Phys.* **1999**, *245*, 1.
(300) Tretiak, S.; Chernyak, V.; Mukamel, S. *J. Chem. Phys.* **1996**, *105*, 8914.
(301) Tretiak, S.; Chernyak, V.; Mukamel, S. *Chem. Phys. Lett.* **1998**, *287*, 75.
(302) Tretiak, S.; Chernyak, V.; Mukamel, S. *Chem. Phys.* **1999**, *245*, 145.
(303) Alain, V.; Redoglia, S.; Blanchard-Desce, M.; Lebus, S.; Lukaszuk, K.; Wortmann, R.; Gubler, U.; Bosshard, C.; Gunter, P. *Chem. Phys.* **1999**, *245*, 51.
(304) Albert, I. D. L.; Marks, T. J.; Ratner, M. A. *J. Am. Chem. Soc.* **1997**, *119*, 3155.
(305) Albert, I. D. L.; Marks, T. J.; Ratner, M. A. *J. Am. Chem. Soc.* **1997**, *119*, 6575.
(306) Morley, J. O.; Pavlides, P.; Pugh, D. *J. Chem. Soc., Faraday Trans. 2* **1989**, *85*, 1789.
(307) Morley, J. O.; Pugh, D. *J. Mol. El.* **1989**, *5*, 123.
(308) Morley, J. O.; Docherty, V. J.; Pugh, D. *J. Chem. Soc., Perkin Trans. 2* **1987**, *9*, 1351.
(309) Morley, J. O. *J. Chem. Soc., Faraday Trans.* **1991**, *87*, 3009.
(310) Santos, D. A.dos; Kogej, T.; Brédas, J. L.; Boutton, C.; Hendrickx, E.; Houbrechts, S.; Clays, K.; Persoons, A.; Xhang, J. X.; Dubois, P.; Jerome, R. *J. Mol. Str.* **2000**, *521*, 221.
(311) Oudar, J. L.; Chemla, D. S. *J. Chem. Phys.* **1977**, *66*, 2664.
(312) Oudar, J. L. *J. Chem. Phys.* **1977**, *67*, 446.
(313) Beratan, D. N.; Onuchic, J. N.; Perry, J. W. *J. Phys. Chem.* **1987**, *91*, 2696.
(314) Matsuzawa, N.; Dixon, D. A. *Int. J. Quantum Chem.* **1992**, *44*, 497.
(315) Pullerits, T.; Sundström, V. *Acc. Chem. Res.* **1996**, *29*, 381.
(316) Sundström, V.; Pullerits, T.; Grondelle, R.van *J. Phys. Chem. B* **1999**, *103*, 2327.
(317) Fleming, G. R.; Grondelle, R.van *Phys. Today* **1994**, *47*, 48.
(318) Hu, X. C.; Damjanovic, A.; Ritz, T.; Schulten, K. *Proc. Natl. Acad. Sci. U.S.A.* **1998**, *95*, 5935.
(319) Special Issue on Light-Harvesting Physics Workshop. *J. Phys. Chem. B* **1997**, *101*.
(320) Sundström, V.; Grondelle, R.van In *Anoxygenic Photosynthetic Bacteria*; Blankenship, R. E., Madiga, M. T., Baner, C. E., Eds.; Kluwer Academic: Dordrecht, 1995; p 349.
(321) Grondelle, R.van; Dekker, J. P.; Gillbro, T.; Sundström, V. *Biochim. Biophys. Acta* **1994**, *1187*, 1.
(322) Bradforth, S. E.; Jinenez, R.; Mourik, F.van; Grondelle, R.van; Fleming, G. R. *J. Phys. Chem.* **1995**, *99*, 16179.
(323) *Iron porphyrins*; Lever, A. B. P., Ed.; Addison-Wesley Press, Reading, MA, 1983.
(324) *Porphyrins: Excited States and Dynamics*; Gouterman, M., Rentzepis, P. M., Straub, K. D., Eds.; American Chemical Society: Washington, DC, 1986.
(325) Edwards, W. D.; Zerner, M. C. *Int. J. Quantum Chem.* **1983**, *23*, 1407.
(326) Thompson, M. A.; Zerner, M. C.; Fajer, J. *J. Phys. Chem.* **1990**, *94*, 3820.
(327) Tretiak, S.; Middleton, C.; Chernyak, V.; Mukamel, S. In *Photoinduced Charge Transfer*; Rothberg, L. J., Ed.; World Scientific: New Jersey, 2000.
(328) Koepke, J.; Hu, X. C.; Muenke, C.; Schulten, K.; Michel, H. *Structure* **1996**, *4*, 581.
(329) Tretiak, S.; Chernyak, V.; Mukamel, S. *Chem. Phys. Lett.* **1998**, *297*, 357.
(330) Nguyen, K. A.; Day, P. N.; Pachter, R. *J. Phys. Chem. A* **1999**, *103*, 9378.
(331) Nguyen, K. A.; Pachter, R. *J. Chem. Phys.* **2001**, *114*, 10757.
(332) Tsiper, E. V.; Soos, Z. G. *Phys. Rev. B* **2001**, *6419*, 5124.
(333) Schon, J. H.; Kloc, C.; Batlogg, B. *J. Phys.-Condensed Matter* **2001**, *13*, L163.
(334) Schon, J. H.; Kloc, C.; Batlogg, B. *Nature* **2000**, *406*, 702.
(335) Easter, D. C.; Whetten, R. L.; Wessel, J. E. *J. Chem. Phys.* **1991**, *94*, 3347.
(336) Easter, D. C.; Khoury, J. T.; Whetten, R. L. *J. Chem. Phys.* **1992**, *97*, 1675.
(337) Yeretzian, C.; Hansen, K.; Beck, R. D.; Whetten, R. L. *J. Chem. Phys.* **1993**, *98*, 7480.
(338) Syage, J. A.; Evans, M. D. *Spectroscopy* **2001**, *16*, 14.
(339) Syage, J. A. *J. Chem. Phys.* **1996**, *105*, 1007.
(340) Foley, S.; Berberan-Santos, M. N.; Fedorov, A.; McGarvey, D. J.; Santos, C.; Gigante, B. *J. Phys. Chem. A* **1999**, *103*, 8173.
(341) Berberan-Santos, M. N.; Choppinet, P.; Fedorov, A.; Jullien, L.; Valeur, B. *J. Am. Chem. Soc.* **1999**, *121*, 2526.
(342) Tretiak, S.; Zhang, W. M.; Chernyak, V.; Mukamel, S. *Proc. Natl. Acad. Sci. U.S.A.* **1999**, *96*, 13003.
(343) Ghiggino, K. P.; Yeow, E. K. L.; Haines, D. J.; Scholes, G. D.; Smith, T. A. *J. Photochem. Photobiol. A* **1996**, *102*, 81.
(344) Clayton, A. H. A.; Scholes, G. D.; Ghiggino, K. P.; PaddonRowm M. N. *J. Phys. Chem.* **1996**, *100*, 10912.
(345) Schiedt, J.; Knott, W. J.; Le Barbu, K.; Schlag, E. W.; Weinkauf, R. *J. Chem. Phys.* **2000**, *113*, 9470.
(346) Spirko, V.; Engvist, O.; Soldan, P.; Selzle, H. L.; Schlag, E. W.; Hobza, P. *J. Chem. Phys.* **1999**, *111*, 572.
(347) Hobza, P.; Selzle, H. L.; Schlag, E. W. *Chem. Rev.* **1994**, *94*, 1767.
(348) Canuto, S.; Zerner, M. C. *J. Am. Chem. Soc.* **1990**, *112*, 2114.
(349) The term "Davydov splitting" usually refers to the splitting of degenerate states in molecular aggregates and crystals in which intermolecular interactions are electrostatic, and are described by the Frenkel exciton Hamiltonian. In contrast, the coupling between electronic modes in dimers includes electrostatic as well as exchange interactions, which result in interchromophore electronic coherence. These may not be described by Frenkel exciton Hamiltonian.
(350) Kasha, M.; Rawls, H. R.; El-Bayoumi, M. A. *Pure Appl. Chem.* **1965**, *11*, 371.
(351) Rashba, E. I.; Sturge, M. D. *Excitons*; North-Holland, Amsterdam, 1982.
(352) Broude, V. B.; Rashba, E. I.; Sheka, E. F. *Spectroscopy of Molecular Excitons*; Springer, Berlin, 1985.
(353) Spano, F. C. *J. Chem. Phys.* **2001**, *114*, 5376.
(354) Spano, F. C. *Synth. Met.* **2001**, *116*, 339.
(355) Spano, F. C. *Chem. Phys. Lett.* **2000**, *331*, 7.
(356) Siddiqui, S.; Spano, F. C. *Chem. Phys. Lett.* **1999**, *308*, 99.
(357) Jenekhe, S. A.; Osaheni, J. A. *Science* **1994**, *265*, 765.
(358) Conwell, E. *Trends Pol. Sci.* **1997**, *5*, 218.
(359) Wang, S. J.; Bazan, G. C.; Tretiak, S.; Mukamel, S. *J. Am. Chem. Soc.* **2000**, *122*, 1289.
(360) Minami, T.; Tretiak, S.; Chernyak, V.; Mukamel, S. *J. Lumin.* **2000**, *87*−*9*, 115.
(361) Scholes, G. D.; Ghiggino, K. P.; Oliver, A. M.; Paddonrow, M. N. *J. Am. Chem. Soc.* **1993**, *115*, 4345.
(362) Scholes, G. D.; Ghiggino, K. P.; Oliver, A. M.; Paddonrow, M. N. *J. Phys. Chem.* **1993**, *97*, 11871.
(363) Mukhopadhyay, D.; Hayden, G. W.; Soos, Z. G. *Phys. Rev. B* **1995**, *51*, 9476.
(364) Bartholomew, G. P.; Bazan, G. C. *Acc. Chem. Res.* **2001**, *34*, 30.
(365) Iwata, S.; Fuke, K.; Sasaki, M.; Nagakura, S.; Otsubo, T.; Misumi, S. *J. Mol. Spectrosc.* **1973**, *46*, 1.
(366) Wang, P.; Collison, C. J.; Rothberg, L. J. *J. Photochem. Photobiol. A* **2001**, *144*, 63.
(367) Jakubiak, R.; Collison, C. J.; Wan, W. C.; Rothberg, L. J.; Hsieh, B. R. *J. Phys. Chem. A* **1999**, *103*, 2394.
(368) Yan, M.; Rothberg, L. J.; Kwock, E. W.; Miller, T. M. *Phys. Rev. Lett.* **1995**, *75*, 1992.
(369) Cornil, J.; Santos, D. A.dos; Crispin, X.; Silbey, R.; Brédas, J. L. *J. Am. Chem. Soc.* **1998**, *120*, 1289.
(370) Cornil, J.; Beljonne, D.; Shuai, Z.; Hagler, T. W.; Campbell, I.; Bradley, D. D. C.; Brédas, J. L.; Spangler, C. W.; Mullen, K. *Chem. Phys. Lett.* **1995**, *247*, 425.
(371) Ispasoiu, R. G.; Balogh, L.; Varnavski, O. P.; Tomalia, D. A.; Goodson, T. *J. Am. Chem. Soc.* **2000**, *122*, 11005.
(372) Miller, L. L.; Duan, R. G.; Tully, D. C.; Tomalia, D. A. *J. Am. Chem. Soc.* **1997**, *119*, 1005.

(373) KukowskaLatallo, J. F.; Bielinska, A. U.; Johnson, J.; Spindler, R.; Tomalia, D. A.; Baker, J. R. *Proc. Natl. Acad. Sci. U.S.A.* **1996**, *93*, 4897.
(374) Nishioka, T.; Tashiro, K.; Aida, T.; Zheng, J. Y.; Kinbara, K.; Saigo, K.; Sakamoto, S.; Yamaguchi, K. *Macromolecules* **2000**, *33*, 9182.
(375) Stewart, G. M.; Fox, M. A. *J. Am. Chem. Soc.* **1996**, *118*, 4354.
(376) BarHaim, A.; Klafter, J.; Kopelman, R. *J. Am. Chem. Soc.* **1997**, *119*, 6197.
(377) Junge, D. M.; McGrathy, D. V. *J. Am. Chem. Soc.* **1999**, *121*, 4912.
(378) Swallen, S. F.; Zhu, Z. G.; Moore, J. S.; Kopelman, R. *J. Phys. Chem. B* **2000**, *104*, 3988.
(379) Shortreed, M. R.; Swallen, S. F.; Shi, Z. Y.; Tan, W. H.; Xu, Z. F.; Devadoss, C.; Moore, J. S.; Kopelman, R. *J. Phys. Chem. B* **1997**, *101*, 6318.
(380) Brocorens, P.; Zojer, E.; Cornil, J.; Shuai, Z.; Leising, G.; Mullen, K.; Brédas, J. L. *Synth. Met.* **1999**, *100*, 141.
(381) Swallen, S. F.; Kopelman, R.; Moore, J. S.; Devadoss, C. *J. Mol. Str.* **1999**, *486*, 585.
(382) Gust, D.; Moore, T. A.; Moore, A. L. *Acc. Chem. Res.* **2001**, *34*, 40.
(383) Kopelman, R.; Shortreed, M.; Shi, Z. Y.; Tan, W. H.; Xu, Z. F.; Moore, J. S.; Bar Haim, A.; Klafter, J. *Phys. Rev. Lett.* **1997**, *78*, 1239.
(384) Devadoss, C.; Bharathi, P.; Moore, J. S. *J. Am. Chem. Soc.* **1996**, *118*, 9635.
(385) Morrison, R. T.; Boyd, R. N. *Organic Chemistry*; Allyn and Bacon: Boston, 1973.
(386) Poliakov, E. Y.; Chernyak, V.; Tretiak, S.; Mukamel, S. *J. Chem. Phys.* **1999**, *110*, 8161.
(387) Chernyak, V.; Poliakov, E. Y.; Tretiak, S.; Mukamel, S. *J. Chem. Phys.* **1999**, *111*, 4158.
(388) Krueger, B. P.; Scholes, G. D.; Fleming, G. R. *J. Phys. Chem. B* **1998**, *102*, 5378.
(389) Förster, T. *Naturwissenschaften* **1946**, *33*, 166.
(390) Pullerits, T.; Hess, S.; Herek, J. L.; Sundström, V. *J. Phys. Chem. B* **1997**, *101*, 10560.
(391) Meier, T.; Chernyak, V.; Mukamel, S. *J. Phys. Chem. B* **1997**, *101*, 7332.
(392) Meier, T.; Zhao, Y.; Chernyak, V.; Mukamel, S. *J. Chem. Phys.* **1997**, *107*, 3876.
(393) Sauer, K.; Cogdell, R. J.; Prince, S. M.; Freer, A.; Isaacs, N. W.; Scheer, H. *Photochem. Photobiol.* **1996**, *64*, 564.
(394) Krueger, B. P.; Scholes, G. D.; Jimenez, R.; Fleming, G. R. *J. Phys. Chem. B* **1998**, *102*, 2284.
(395) Krueger, B. P.; Scholes, G. D.; Fleming, G. R. *J. Phys. Chem. B* **1998**, *102*, 9603.
(396) Ihalainen, J. A.; Linnanto, J.; Myllyperkio, P.; Stokkum, I. H. M.van; Ucker, B.; Scheer, H.; Korppi-Tommola, J. E. I. *J. Phys. Chem. B* **2001**, *105*, 9849.
(397) Linnanto, J.; Korppi-Tommopa, J. E. I.; Helenius, V. M. *J. Phys. Chem. B* **1999**, *103*, 8739.
(398) Somsen, O. J. G.; Chernyak, V.; Frese, R. N.; Grondelle, R.van; Mukamel, S. *J. Phys. Chem. B* **1998**, *102*, 8893.
(399) Heeger, A. J.; Kivelson, S.; Schrieffer, J. R.; Su, W. P. *Rev. Mod. Phys.* **1988**, *60*, 781.
(400) Schon, J. H.; Kloc, C.; Batlogg, B. *Science* **2000**, *288*, 2338.
(401) Schon, J. H.; Kloc, C.; Siegrist, T.; Steigerwald, M.; Svensson, C.; Batlogg, B. *Nature* **2001**, *413*, 831.
(402) Schon, J. H.; Kloc, C.; Batlogg, B. *Science* **2001**, *293*, 2432.
(403) Schon, J. H.; Kloc, C.; Batlogg, B. *Nature* **2000**, *408*, 549.
(404) Schon, J. H. *Appl. Phys. Lett.* **2001**, *79*, 2208.
(405) Schon, J. H.; Kloc, C.; Hwang, H. Y.; Batlogg, B. *Science* **2001**, *292*, 252.
(406) Schon, J. H.; Meng, H.; Bao, Z. N. *Science* **2001**, *294*, 2138.
(407) Havemann, R. H.; Hutchby, J. A. *Proc. IEEE* **2001**, *89*, 586.
(408) Ratner, M. *Nature* **2000**, *404*, 137.
(409) Segal, D.; Nitzan, A.; Davis, W. B.; Wasielewski, M. R.; Ratner, M. A. *J. Phys. Chem. B* **2000**, *104*, 3817.
(410) Chen, J.; Reed, M. A.; Rawlett, A. M.; Tour, J. M. *Science* **1999**, *286*, 1550.
(411) Reed, M. A.; Zhou, C.; Muller, C. J.; Burgin, T. P.; Tour, J. M. *Science* **1997**, *278*, 252.
(412) Broo, A.; Zerner, M. C. *Chem. Phys.* **1995**, *196*, 423.
(413) Broo, A.; Zerner, M. C. *Chem. Phys.* **1995**, *196*, 407.
(414) Braun, D.; Heeger, A. J. *Appl. Phys. Lett.* **1991**, *58*, 1982.
(415) Burn, P. L.; Holmes, A. B.; Kraft, A.; Bradley, D. D. C.; Brown, A. R.; Friend, R. H.; Gymer, R. W. *Nature* **1992**, *356*, 47.
(416) Burroughes, J. H.; Bradley, D. D. C.; Brown, A. R.; Marks, R. N.; Mackay, K.; Friend, R. H.; Burns, P. L.; Holmes, A. B. *Nature* **1990**, *347*, 539.
(417) Cao, Y.; Parker, I. D.; Yu, G.; Zhang, C.; Heeger, A. J. *Nature* **1999**, *397*, 414.
(418) Gustafsson, G.; Cao, Y.; Treacy, G. M.; Klavetter, F.; Colaneri, N.; Heeger, A. J. *Nature* **1992**, *357*, 477.
(419) Shen, Z. L.; Burrows, P. E.; Bulovic, V.; Forrest, S. R.; Thompson, M. E. *Science* **1997**, *276*, 2009.
(420) Pei, Q. B.; Yu, G.; Zhang, C.; Yang, Y.; Heeger, A. J. *Science* **1995**, *269*, 1086.
(421) Sirringhaus, H.; Tessler, N.; Friend, R. H. *Science* **1998**, *280*, 1741.
(422) Ho, P. K. H.; Thomas, D. S.; Friend, R. H.; Tessler, N. *Science* **1999**, *285*, 233.
(423) Dodabalapur, A.; Bao, Z.; Makhija, A.; Laquindanum, J. G.; Raju, V. R.; Feng, Y.; Katz, H. E.; Rogers, J. *Appl. Phys. Lett.* **1998**, *73*, 142.
(424) Yu, G.; Gao, J.; Hummelen, J. C.; Wudl, F.; Heeger, A. J. *Science* **1995**, *270*, 1789.
(425) Granstrom, M.; Petritsch, K.; Arias, A. C.; Lux, A.; Andersson, M. R.; Friend, R. H. *Nature* **1998**, *395*, 257.
(426) Mende, L.; Fechtenkotter, A.; Mullen, K.; Moons, E.; Friend, R. H.; MacKenzie, J. D. *Science* **2001**, *293*, 1119.
(427) Yu, G.; Pakbaz, K.; Heeger, A. J. *Appl. Phys. Lett.* **1994**, *64*, 3422.
(428) Yu, G.; Zhang, C.; Heeger, A. J. *Appl. Phys. Lett.* **1994**, *64*, 1540.
(429) Halls, J. J. M.; Walsh, C. A.; Greenham, N. C.; Marseglia, E. A.; Friend, R. H.; Moratti, S. C.; Holmes, A. B. *Nature* **1995**, *376*, 498.
(430) Katz, H. E.; Bao, Z. N.; Gilat, S. L. *Acc. Chem. Res.* **2001**, *34*, 359.
(431) Crone, B.; Dodabalapur, A.; Gelperin, A.; Torsi, L.; Katz, H. E.; Lovinger, A. J.; Bao, Z. *Appl. Phys. Lett.* **2001**, *78*, 2229.
(432) Sheraw, C. D.; Zhou, L.; Huang, J. R.; Gundlach, D. J.; Jackson, T. N.; Kane, M. G.; Hill, I. G.; Hammond, M. S.; Campi, J.; Greening, B. K.; Francl, J.; West, J. *Appl. Phys. Lett.* **2002**, *80*, 1088.
(433) Yang, Y.; Heeger, A. J. *Nature* **1994**, *372*, 344.
(434) Schon, J. H.; Meng, H.; Bao, Z. *Nature* **2001**, *413*, 713.
(435) Wang, D. L.; Gong, X.; Heeger, P. S.; Rininsland, F.; Bazan, G. C.; Heeger, A. J. *Proc. Natl. Acad. Sci. U.S.A.* **2002**, *99*, 49.
(436) Heeger, A. J.; Heeger, D. J.; Langan, J.; Yang, Y. *Science* **1995**, *270*, 1642.
(437) Sirringhaus, H.; Kawase, T.; Friend, R. H.; Shimoda, T.; Inbasekaran, M.; Wu, W.; Woo, E. P. *Science* **2000**, *290*, 2123.
(438) Hide, F.; Diaz-Garcia, M. A.; Schwartz, B. J.; Andersson, M. R.; Pei, Q. B.; Heeger, A. J. *Science* **1996**, *273*, 1833.
(439) Tessler, N.; Denton, G. J.; Friend, R. H. *Nature* **1996**, *382*, 695.
(440) Wohlgenannt, M.; Tandon, K.; Mazumdar, S.; Ramasesha, S.; Vardeny, Z. V. *Nature* **2001**, *409*, 494.
(441) Osterbacka, R.; An, C. P.; Jiang, X. M.; Vardeny, Z. V. *Science* **2000**, *287*, 839.
(442) Wilson, J. S.; Dhoot, A. S.; Seeley, A. J. A. B.; Khan, M. S.; Kohler, A.; Friend, R. H. *Nature* **2001**, *413*, 828.
(443) Sirringhaus, H.; Brown, P.; Friend, R. H.; Nielsen, M. M.; Bechgaard, K.; LangeveldVoss, B. M. W.; Spiering, A. J. H.; Janssen, R. A. J.; Meijer, E. W.; Herwig, P.; Leeuw, D. M.de *Nature* **1999**, *401*, 685.
(444) Soos, Z. G.; Galvao, D. S.; Etemad, S. *Adv. Mater.* **1994**, *6*, 280.
(445) Shuai, Z.; Beljonne, D.; Silbey, R.; Brédas, J. L. *Phys. Rev. Lett.* **2000**, *84*, 131.
(446) Baughman, R. H.; Brédas, J. L.; Chance, R. R.; Elsenbaumer, R. L.; Shacklette, L. W. *Chem. Rev.* **1982**, *82*, 209.
(447) Toury, T.; Zyss, J.; Chernyak, V.; Mukamel, S. *J. Phys. Chem. A* **2001**, *105*, 5692.
(448) Rodenberger, D. C.; Heflin, J. R.; Garito, A. F. *Phys. Rev.* **1995**, *51*, 3234.
(449) Barzoukas, M.; Blanchard-Desce, M. *J. Chem. Phys.* **2000**, *113*, 3951.
(450) Beljonne, D.; Brédas, J. L.; Cha, M.; Torruellas, W. E.; Stegeman, G. I.; Hofstraat, J. W.; Horsthuis, W. H. G.; Mohlmann, G. R. *J. Chem. Phys.* **1995**, *103*, 7834.
(451) Barzoukas, M.; Blanchard-Desce, M. *J. Chem. Phys.* **2000**, *112*, 2036.
(452) Straub, O. *Key to Carotenoids*; Basel, Boston, 1987.
(453) *Carotenoids*; Britton, G., Liaaen-Jensen, S., Pfander, H., Eds.; Basel, Boston: Birkheauser, 1995.
(454) Bungard, R. A.; Ruban, A. V.; Hibberd, J. M.; Press: M. C.; Horton, P.; Scholes, J. D. *Proc. Natl. Acad. Sci. U.S.A.* **1999**, *96*, 1135.
(455) Koyama, Y.; Mukai, Y. *Biomolecular Spectroscopy*, Part B; Clark, R. J. H., Hester, R. E., Eds.; John Wiley & Sons Ltd, New York, 1993.
(456) Young, A.; Britton, G. *Carotenoids in Photosynthesis*; George, Ed; Chapman and Hall, London, 1993.
(457) Mathies, R. A.; Cruz, C. H. B.; Pollard, W. T.; Shank, C. V. *Science* **1988**, *240*, 777.
(458) Iqbal, R.; Moratti, S. C.; Holmes, A. B.; Yahioglu, G.; Milgrom, L. R.; Cacialli, F.; Morgado, J.; Friend, R. H. *J. Mater. Sci.* **2000**, *11*, 97.
(459) Diazgarcia, M. A.; Ledoux, I.; Duro, J. A.; Torres, T.; Agullolopez, F.; Zyss, J. *J. Phys. Chem.* **1994**, *98*, 8761.
(460) Diazgarcia, M. A.; Ledoux, I.; Fernandezlazaro, F.; Sastre, A.; Torres, T.; Agullolopez, F.; Zyss, J. *J. Phys. Chem.* **1994**, *98*, 4495.
(461) DiBella, S.; Fragala, I.; Marks, T. J.; Ratner, M. A. *J. Am. Chem. Soc.* **1996**, *118*, 12747.

(462) Cory, M. G.; Hirose, H.; Zerner, M. C. *Inorg. Chem.* **1995**, *34*, 2969.
(463) Yaron, D. *Phys. Rev. B* **1996**, *54*, 4609.
(464) Kira, M.; Hoyer, W.; Stroucken, T.; Koch, S. W. *Phys. Rev. Lett.* **2001**, *8717*, 6401.
(465) Meier, T.; Koch, S. W.; Phillips, M.; Wang, H. L. *Phys. Rev. B* **2000**, *62*, 12605.
(466) Lindberg, M.; Binder, R.; Koch, S. W. *Phys. Rev. A* **1992**, *45*, 1865.
(467) Lindberg, M.; Koch, S. W. *Phys. Rev. B* **1988**, *38*, 3342.
(468) Greene, B. I.; Orenstein, J.; Schmitt-Rink, S. *Science* **1990**, *247*, 679.
(469) Axt, V. M.; Mukamel, S. *Rev. Mod. Phys.* **1998**, *70*, 145.
(470) Chernyak, V.; Mukamel, S. *J. Phys. Chem. A* **2000**, *104*, 4263.
(471) Zerbi, G.; Galbiati, E.; Gallazzi, M. C.; Castiglioni, C.; Del Zoppo, M.; Schenk, R.; Mullen, K. *J. Chem. Phys.* **1996**, *105*, 2509.
(472) Tsiper, E. V.; Chernyak, V.; Tretiak, S.; Mukamel, S. *Chem. Phys. Lett.* **1999**, *302*, 77.
(473) Tsiper, E. V.; Chernyak, V.; Tretiak, S.; Mukamel, S. *J. Chem. Phys.* **1999**, *110*, 8328.
(474) Tretiak, S.; Saxena, A.; Martin, R. L.; Bishop, A. R. Photoexcited conformational dynamics of conjugated molecules. *Phys. Rev. Lett.* **2002**, *89*, 97402.
(475) Tommasini, M.; Chernyak, V.; Mukamel, S. *Int. J. Quantum Chem.* **2001**, *85*, 225.
(476) Chernyak, V.; Volkov, S. N.; Mukamel, S. *Phys. Rev. Lett.* **2001**, *86*, 995.
(477) Chernyak, V.; Minami, T.; Mukamel, S. *J. Chem. Phys.* **2000**, *112*, 7953.
(478) Yokojima, S.; Meier, T.; Mukamel, S. *J. Chem. Phys.* **1997**, *106*, 3837.
(479) Chernyak, V.; Mukamel, S. *J. Chem. Phys.* **1999**, *111*, 4383.
(480) Langhoff, P. W.; Corcoran, C. T.; Sims, J. S.; Weinhold, F.; Glover, R. M. *Phys. Rev. A* **1976**, *14*, 1042.
(481) Martin, R. L.; Daasch, W. R.; Davidson, E. R. *J. Chem. Phys.* **1979**, *71*, 2375.
(482) Martin, R. L.; Cohen, J. S. *Phys. Lett. A* **1985**, *110*, 95.
(483) Mori, H. *Prog. Theor. Phys.* **1965**, *34*, 399.
(484) Zwanzig, R. *Lect. Theor. Phys.* **1961**, *3*, 106.
(485) Grosso, G.; Parravicini, G. P.; Testa, A. *Phys. Rev. B* **1985**, *32*, 627.
(486) Ernst, R. R.; Bodenhausen, G.; Wokaun, A. *Principles of Nuclear Magnetic Resonance in One and Two Dimensions*; Clarendon Press: London, 1987.
(487) Mei, G., Master's Thesis, Nanjing Aeronautical Inst., Nanjing, China, 1986.
(488) Benner, P.; Fassbender, H. *Linear Algebra Appl.* **1997**, *263*, 75.
(489) Morgan, R. B.; Scott, D. S. In *Lasers, Molecules, and Methods*; Hirschfelder; J. O., Wyatt, R. E., Coalson, R. D., Eds.; John Wiley and Sons: New York, 1989.
(490) Paige, C. C.; Saunders, M. A. *SIAM J. Numer. Anal.* **1975**, *12*, 617.
(491) Meier, T.; Tretiak, S.; Chernyak, V.; Mukamel, S. *Phys. Rev. B* **1997**, *55*, 4960.
(492) Dewar, M. J. S.; Zoebisch, E. G.; Healy, E. F.; Stewart, J. J. P. *J. Am. Chem. Soc.* **1985**, *107*, 3902.
(493) Oldham, W. J.; Miao, Y. J.; Lachicotte, R. J.; Bazan, G. C. *J. Am. Chem. Soc.* **1998**, *120*, 419.
(494) Oelze, J. *Methods Microbiol.* **1985**, *18*, 257.
(495) Sauer, K.; Smith, J. R. L.; Schultz, A. J. *J. Am. Chem. Soc.* **1966**, *88*, 2681.
(496) Andersson, P. O.; Gillbro, T.; Ferguson, L.; Cogdell, R. J. *Photochem. Photobiol.* **1991**, *54*, 353.
(497) Krueger, B. P.; Yom, J.; Walla, P. J.; Fleming, G. R. *Chem. Phys. Lett.* **1999**, *310*, 57.

CR0101252